RUHR UNIVERSITÄT BOCHUM

RUB

UNIVERSITY OF TWENTE.

Ruhr-University Bochum

Master Thesis

Modelling and Experiments of Ultrasound Propagation in Porous Material: an Application to Bones

Stefan Emmerich

Mechanical Engineering

March 3, 2014

Supervisors

Prof. Dr.-Ing. H.Steeb

Continuum Mechanics
Ruhr-University Bochum

Prof. Dr. rer.-nat. S. Luding

Multi Scale Mechanics
University of Twente

Stefan Emmerich, Matr.-Nr. 108008218432,
Ruhr-University Bochum, Mechanical Engineering
Supervisors:
Prof. Dr.-Ing. H.Steeb, Ruhr-University Bochum
Prof. Dr. rer.-nat. S. Luding, University of Twente
Bochum, March 3, 2014

Abstract

The bone disease Osteoporosis reduces the connection of the solid structures in bone and increases porosity, which leads to a higher crack probability. An early detection of the disease can help to prevent bone cracks. In this thesis experiments and simulations on wave propagation are connected to investigate sample properties with the goal to understand how to model bone-like media. Ultrasound wave properties are dependent on the structure and properties of a sample and therefore useful to detect e.g. Osteoporosis.
The ultrasound wave characteristics dependent on the structure and the properties of a sample, are obtained experimentally and used as input for the simulations. With a one-dimensional particle chain wave propagation is simulated. This model is solved analytically. The back calculated wave velocity and attenuation is validated by comparison with the experimental results.
First, a solid sample of aluminium is modeled and validated. The wave velocities are matched very precise, staying in a specific range of discretization. The frequency and attenuation spectra were not matched, because the wave excitation are different in simulations and experiments.
However, the method is applied to a bone-like media, a scaffold of PCL. A case study with respect to porosity and structure is made. A dependency of wave velocity and attenuation on porosity and structure is found. Additional, a mass disorder is introduced to mimic real bone sample. A decrease in wave velocity and a frequency filtering is obtained.
Further works can examine how to obtain the shape of the frequency spectrum, found by experimental setups. For this, numerical investigations with the discrete element method are possible. Then, the match of simulations and experiments regarding on real bone can be targeted.

Notations

Material

Δd	thickness of the sample
ν	Poisson's ratio
Φ	porosity
ρ	bulk density
Σ	one dimensional stress
ε	one dimensional strain
E	Young's modulus
f	one dimensional force
S	shear modulus

Simulation

ΔT_{st}	time step
ω_{max}	cut off frequency
k_s	spring stiffness
m_p	particle mass
N_I^s	number of sample interfaces
N_I^{total}	number of total interfaces
N_p^s	number of particles of the sample layer

N_p^w number of particles of one water layer

r_p particle radius

r_{disorder} disorder parameter

T_{sim} Simulation time

V_p Volume of one particle

Waves

$\alpha(\omega)$ attenuation

Δt Time difference between two arrival times

$\hat{\mathbf{U}}$ amplitude of generalized displacement vector

λ wave length

$\mathbf{U}$ generalized displacement vector

ω angular frequency

τ transmission coefficient

A Fourier amplitude

c_p pressure wave velocity

c_p^w wave velocity in water

f frequency

I acoustic intensity

k wave number

p pressure amplitude

v_{group} group velocity

v_{phase} phase velocity

Z acoustic impedance

Mathematics

$\cdot$	scalar product/ matrix product
∇	nabla operator
$\otimes$	dyadic product
∂	partial derivation
σ	standard deviation

Contents

Chapter 1

Introduction

This short introduction gives a motivation on why wave propagation in bone is studied. It then defines the thesis goal and gives an overview about the current state of art.

1.1 Motivation

Bone is one of the more complex media. It is very important for living organisms, e.g. human beings, because it carries the weight and stabilizes the body. However, bone can be weakened by diseases. For example, Osteoporosis Osteoporosis reduces the density of the bone and weakens the structure. Higher crack probability is one of the consequences. Osteoporosis can be investigated with different techniques, e.g. Dual energy X-ray Absorptiometry (DXA) (cf. e.g. [36],). With this technique the decrease in bone density is analyzed. It is not possible to analyze the damage of connectivity of the structure or propagation of the damage structure. With ultrasound investigations it is possible to recognize the change of density and structure, because wave velocity and attenuation both depend on the material properties. For example the wave velocity and the density for a continuum model are linked by the bar equation (cf. [16]). Fundamentals of ultrasound

propagation can for example be looked up in [8], [20], [32]. Regarding bone the relation between material and ultrasound properties is not easy anymore and it can not linked by an easy equation. For example, the wave velocity is dependent on the propagation direction, which means that bone is a anisotropic media. Anisotropic behavior is not covered in the bar equation. Therefore, more sophisticated models or numerical investigations are needed.

1.2 Thesis goal and overview

The goal of this thesis is the study of wave propagation in bone and bone-like media. Wave propagation from continua to disordered structure, e.g. bone is introduced, to develop a better initial understanding. For this, fundamentals about bone material are introduced, too. A way how to simulate wave propagation for increasing complexity is then described. An analytically solution of a simple one dimensional particle chain is used to study wave propagation theoretically. The method is calibrated by experiments conducted at the laboratories of the Biomedical Photonic Imaging Group at the Universiteit Twente. An overview about the relation between experiments and simulations is given in figure 1.1. First, the simulation parameters are adjusted by using experimental values,

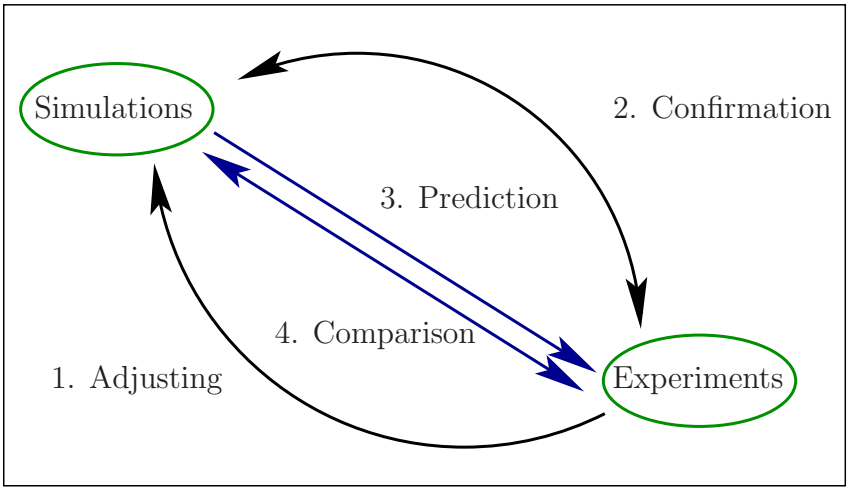

Figure 1.1: Relation between experiments and simulations

wave velocity and density, as input parameters for the simulations. For each material that is modeled, the parameters have to be adjusted independently. The experiments have to be independent for the different media, too. In step 2 the simulation technique is confirmed. For this, the experimental results, e.g. frequency spectrum are compared with the simulation results and the error is considered in a qualitative and quantitative way. Solid continuum specimens with regular microstructure are used in steps 1 and 2 to simplify the procedures. Initially, the influence of microstructure on the experimental and simulation results is assumed as not known. With the confirmed simulation technique, more complex structures can be modeled (step 3). The predictions can then be compared with experimental results to show their accuracy and usability (step 4). For step 3 and 4 simulations and experiments independent from steps 1 and 2 are used. Of course, different experimental and simulation techniques are possible. In this thesis through transmission experiments are used (cf. [18], [16], [29]). For the simulations, here, the above mentioned simple technique is used that can be calibrated by through transmission experiments. Of course, other simulation models exist, e.g. the Biot's theory, the finite element method. The most noted model is Biot's theory (cf. e.g. [16], [17], [23], [13]), which predicts three propagating waves in bones, two compressional waves (P-waves) and one shear wave (S-wave). The two different P-waves develop to the in-phase movement coupling and out-of-phase movement coupling of the fluid and the solid-structure. The Biot-model requires up to 14 material parameters to describe the material and wave properties. This can be a disadvantage, because some material parameters can often only be obtained in very precise and expensive experimental setups. With simple through transmission experiments not all parameters can be obtained. Further on, Biot's theory requires a longer wave length than the pore size, so that it is not valid for high frequencies (cf. [18]).
A numerical model could improve the understanding of the wave propagation, because the solution at any time and any place is available. That means, that the wave propagation can be also studied inside the sample at any point. It can reveal the wave propagation dependent on time and space. If once the simulation technique is validated, no more expensive simulations are needed. Depending on the numerical model, e.g. the distinct

element model (DEM) (cf. e.g. [**?**] and [10]) different material behavior like viscosity and linear elasticity can be applied on the micro-scale. The DEM is a particle interaction method, that can be solved e.g. by the implicit euler iteration. Comparing the DEM with dynamic finite-element-method (FEM), both have the advantage to be able to model in principle any geometry. However, for the FEM a mesh generation algorithm is needed (cf. [5] and [3]). For example if a bone is modeled completely in three dimensions, the DEM has the advantage that the particles can be placed very easily to fill out the round shapes, but for the DEM it can be difficult to define a good mesh in these rounds. There are special FEM-applications for wave propagation, but the effort of a finely meshed model is needed, with a resolution on the micro-scale (cf. [14], [7]). Further there is a distinction between compressible and incompressible analysis, dependent on the material. Another advantage of the DEM in contrary to the FEM would be that it is much easier to implement heterogeneity in the than in the FEM. If the media is than partially saturated, the FEM can not describe it, but with the DEM it is possible. Here the DEM method is used as an example of a particle method in general. No matter what are the disadvantages and advantages of the numerical model, it should make it possible to observe different material properties easily once the model is set up. Furthermore, micro- and macro-properties can be observed as functions of the input parameters very easily. This results in parameter studies, which are fast and budget-friendly in contrast to experiments.

As mentioned above, here a one dimensional particle chain is used to simulate wave propagation. This model can be solved analytically, which is a great advantage compared with numerical methods. The study is limited to an easy case; advantages and disadvantages are further discussed in chapter 4.

After defining the fundamentals in chapter 2 and the description of the experiments in chapter 3, the simulation technique is introduced in chapter 4. Before the experiment is validated, several analysis techniques are studied and the most precise for the wave velocity, the frequency spectrum and the attenuation are chosen. The simulation technique is then validated in chapter 6 and results for a structured and a bone like sample are predicted in chapter 7. Unfortunately, experimental results to confirm the predictions are

missing so far.

Chapter 2

Fundamentals

First, the fundamentals of bone structure and bone material are introduced. Then the needed information about wave propagation and the Fourier transformation is introduced. The steps from continuum media to real samples, especially bone are described. In the last step a model to describe real porous media, the stratified model, is explained.

2.1 Bone structure

Here, in a fundamental way the bone structure is explained and its properties are introduced. The fundamental knowledge is necessary to understand wave propagation in bone.

It is worth distinguishing between different scales of bone, because at each scale level different structures, materials and properties can be found. If one looks at the complete bone, shown in figure 2.1, two different main structures can be found ([34], [44]). Trabecular (cancellous bone) bone has a less stiff structure with a high porosity, while the second structure, the cortical bone is stiff and less porous. Porosity and microstructure distinguish between cortical and trabecular bone. Except for the ends, in the special case

of a long bone, the outer layer consists of cortical bone (cf. fig. 2.1). In the middle and at the ends trabecular bone can be found. In the special case of a flat bone, re-occurring layers of cortical bone at the outer and a thin trabecular structure can be found inside. Although for different bone-types the mesostructure can vary, the differences disappear if one goes deeper into the bone. Both, cortical and trabecular bone consist of the same kind of material, mainly mineralized collagen (submicroscale). However, how they are ordered and structured is different. Additionally, the porous structure of trabecular bone is filled with bone marrow, which is needed for biological reasons. Cortical bone, sizes

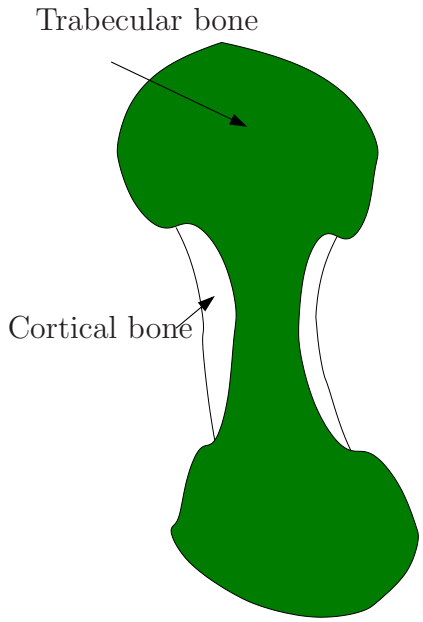

Figure 2.1: Scheme of a long bone, macroscale

from 500 μm to 10 mm, is a well organized system of osteons, resorption cavaties and interstitial lamella. The size of an osteon is about $10-500$ μm. The Osteons and resorption cavaties are densely packed, but their round structure leads to free spaces between them. These spaces are filled with interstitial lamella, which are parts of old osteons. Osteons consists of long cylindrical lamella which enclose a haversian canal. In the haversian canal blood is transported through fine blood vessels. Additionally nerves are going through the Osteons. Both, blood vessels and nerves are needed for biological reasons and do not have any mechanical influence. Due to the orientation of the osteons, e.g. in the long direction of a long bone, anisotropy is induced. This means, that bone has different elastic

properties in the direction of the osteons than in the perpendicular direction. However, the orientation of osteons is not fully investigated, but it does not seem to be a perfectly structured homogeneous system.

Trabecular bone is not well ordered. It is a randomly arranged structure of trabecular bone structure, whose pores are filled with bone marrow. Bone marrow is a fluid, whose properties are similar to water. The main mechanical difference between water and marrow is the higher viscosity of the marrow. The combination of the random solid and the fluid lead to two pressure waves in ultrasound experiments, a fast and a slow wave. The fast wave relates to the in-phase movement of the solid and the fluid, while the slow wave corresponds to the out-of-phase movement (cf. [36], [31], [23], [18], [28]). Like for cortical bone, anisotropic behavior can be found in trabecular bone, too (cf. [23]).

Looking at the mechanical properties of pure solid trabecular and solid cortical bone, it is often assumed for the case of simplicity that they have the same, because predictions using the nanoindentation and finite element analysis state it (cf. [34]). However, in [29] and [24] it was pointed out, that there are differences. Especially, the interfaces between cortical and trabecular bone are of interest. Therefore, more reliable investigations are needed. If one zooms in from the macro-scale, for example in the micro- or nano-scale, finer structures can be seen. However, the influence of their orientation and structures on the macro-scale are not part of this thesis. More information regarding bone structure can be found e.g. in [41], [44], [34], [15], [35], [29].

In summary, cortical and trabecular bone are very complex due to their structure and different scale levels. The high porosity of the trabecular bone and the stiff cortical bone lead to a very effective combination of less weight and high stiffness as well as high flexibility. Bone is anisotropic due to its structure orientation at micro- and mesoscale. Table 2.1 shows some mechanical and structure properties of a long bone for cortical and trabecular bone. The data-range was taken from several investigations based on different techniques e.g. tensile testing, three point bending, ultrasound testing (cf. [34], [29]). The Young's modulus E is given in longitudinal direction of a long bone. Please note, that the properties porosity Φ, E and shear modulus S are different for different bone types,

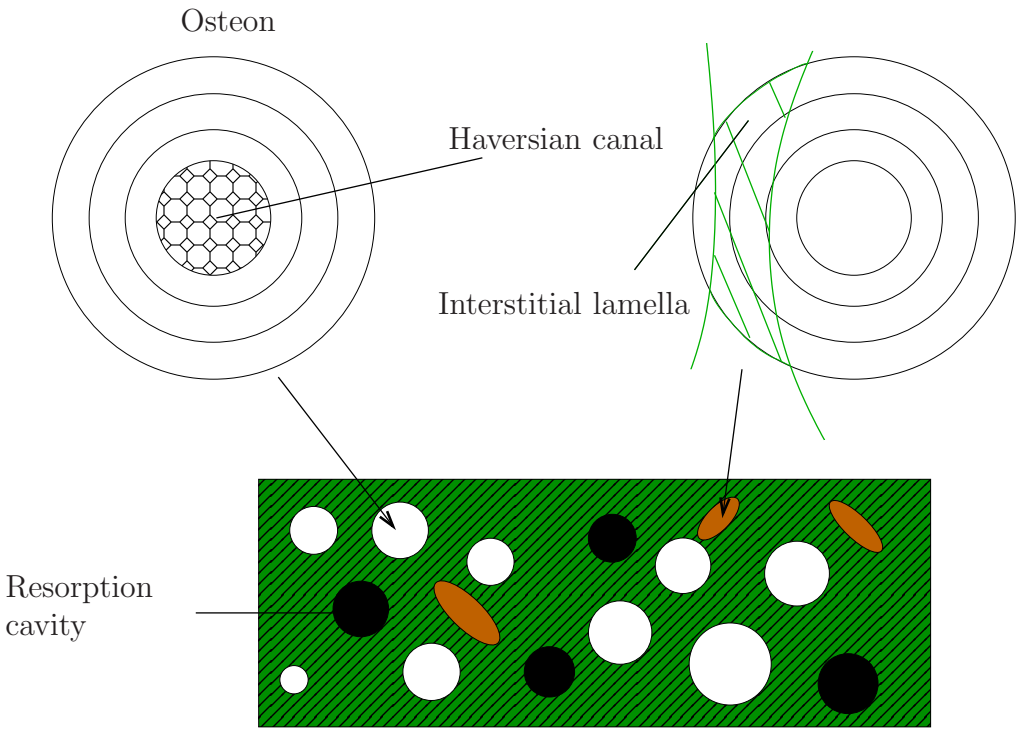

Figure 2.2: Cortical bone and its structure

e.g. long bone and flat bone, and that they differ strongly e.g. with age, individual human and diseases. Furthermore, the values are not independent, for example the Young's modulus is dependent on the density. After the properties and the structure of bone are

	ρ $[kg/m^3]$	Φ	E [GPa]	S [GPa]
Cortical bone	1960	0.2	15-25	8-20
Trabecular bone	100-1000	0.65	20	3.4

Table 2.1: Mechanical and structural properties of cortical and trabecular bone

introduced, the investigation scale has to be defined. In this thesis, experiments at the macroscale are conducted. The goal is to mimic the experiments by simulations. However, if one would look only at the bone as a solid, the influence of the smaller scales are ignored and the description is wrong. For example defining the Young's modulus at the mesoscale or microscale, they would differ from the one defined at the macroscale. Thus, the right properties have to be chosen. With a stratified model (cf. [16]), it is possible to induce porosity to the macroscale, without considering too many complex structures of the smaller scales. The stratified model is explained in detail in section 2.4.

Anyway, with the ultrasound through-transmission measurement technique, it is possible to get information about the wave velocity and the frequency spectrum (cf. [24], [42]). Both parameters are highly influenced by the structure and the material itself, so that it is suited to use the ultrasound technique. In the next chapter, fundamentals about wave propagation are explained.

2.2 Wave propagation

Here, the fundamentals of wave propagation are explained. A sound-wave is a pressure change that propagates through a medium. It can be described by wave parameters and material properties that may change over the spatial dimension, as e.g. wave velocity, frequency, amplitude and direction. In general, two types of wave forms exist, pressure waves (P-wave) and shear waves (S-wave). The pressure (compressive) of the P-wave changes in the direction of wave propagation, while the 'pressure' (shear stress) of the S-wave changes perpendicular to the propagation direction. The wave properties that can be measured, for example in experiments, depend on the material and on the wave itself. If a through transmission experiment is used, the wave can be measured as a displacement signal, that is converted by the detector into a voltage signal. The voltage signal can then be captured by an oscilloscope. The time, that is needed for the wave to travel the distance between the emitter and the detector, depends on the wave velocity and is called time of flight or arrival time. The amplitude of the received signal is related to the weakening of the wave, or in other words the loss of energy. This loss can be divided into two main causes, interface effects and attenuation. Interface effects include mainly the influences of reflections and refraction. Refraction is the change in propagation direction. Attenuation is mainly caused by the absorption of energy by the material due to viscosity, electrical influences, etc., as well as by scattering. The causes of loss of energy are in detail described in subsection 2.2.2. Furthermore, the wave velocity is influenced by the structure and micro-structure and the material (e.g. density). By measurements

of the wave properties one can determine to material properties, e.g. the bar equation written in [16].

2.2.1 Wave velocity

Considering wave velocity, one can use two definitions, the phase and the group velocity. The phase velocity is used when only a wave with a single frequency is present. The frequency f describes the number of repetitions of periodic displacements per unit time. The frequency range of sound is divided into several sections. The hearing range for humans is for example between 12 Hz and 20 kHz. For ultrasound the frequency range is above 20 kHz, which is out of the range of human hearing.

$$v_{\text{phase}} = f\lambda \tag{2.1}$$

λ is the wavelength and describes the length of one period of a wave. The phase velocity can further be transformed to wave number space using the relation between the frequency f and the angular frequency ω

$$\omega = 2\pi f \tag{2.2}$$

and the definition of the wave number k, which describes the magnitude of the wave vector $\mathbf{k}$.

$$k = \frac{2\pi}{\lambda} \tag{2.3}$$

For the one-dimensional case the wave length k describes the period of a wave, while k is the number of waves in a unit distance. Finally, we arrive at the following equation, which defines the phase wave velocity as the ratio between the frequency and the wave number.

$$v_{\text{phase}} = \frac{\omega}{k} \tag{2.4}$$

However, if one wants to describe a wave which is influenced by dispersion, that means that the wave velocity is dependent on the frequency, one can use the definition of the group velocity to describe the envelope (cf. eq. 2.5).

$$v_{\text{group}} = c_p = \frac{\partial \omega}{\partial k} \tag{2.5}$$

The group velocity is used when not only a single frequency is present, too. Furthermore in this thesis, the group velocity of the pressure wave is referred to as wave velocity c_p. Mathematically, one can describe wave propagation using a wave equation, which describes the displacement in a continuum at a certain time point:

$$\frac{\partial^2 \mathbf{U}(\mathbf{x}, t)}{\partial t^2} = v^2 \nabla(\mathbf{U}(\mathbf{x}, t)) \tag{2.6}$$

A solution of the wave equation is the harmonic wave ([22], [8]).

$$\mathbf{U}(\mathbf{x}, t) = \hat{\mathbf{U}}[i \exp(\omega t - \mathbf{k} \cdot \mathbf{x})] \tag{2.7}$$

$\hat{\mathbf{U}}$ is the amplitude of the wave, which may change over the spatial domain. This magnitude is related to attenuation. Its causes are not included in equation 2.7, but will be discussed in the next subsection.

2.2.2 Attenuation

Attenuation is the weakening of the wave due to material properties, e.g. viscosity. Other effects as e.g. interface reflections do also cause weakening of the wave, but are not considered as attenuation, because they are not dependent only on one material. It can be caused by absorption or scattering and follows a power law, also for bone issues (cf. [37]):

$$p = p_0 e^{-\alpha x} \tag{2.8}$$

Here, attenuation is described for the pressure amplitude p. α is the attenuation coefficient and x is the traveling distance of the wave. p_0 is the initial pressure. Attenuation can also be expressed for the acoustic intensity

$$I = \frac{p^2}{2Z} \quad , \tag{2.9}$$

where Z is the acoustic impedance of the material, which is defined as

$$Z = \rho c_p \quad , \tag{2.10}$$

where, ρ is the bulk density of the material.

Scattering is the spreading of the wave over the spatial domain. It is created, when an (ultrasonic) wave interacts with boundaries along its main propagation direction. For this case, the local physical properties have to be different, e.g. elasticity or density. This leads to another wave, the scattered wave, because the direction of the scatter movement is different from the main wave movement. Usually, many scattered waves are created due to heterogeneity. Scattering occurs when the wavelength is comparable to the size of the heterogeneity. Otherwise, when the wavelength is smaller than the heterogeneity, reflection occurs and if it is much longer, none of these effects happen.

Absorption is dependent on the material parameters, for example a high viscous material has a higher absorption effect than a pure elastic material. Other effects are non linearity and chemical effects that lead to absorption.

Further on, the signal amplitude can decrease due to interface effects. If a wave hits a surface with a non perpendicular angle, one part of the wave is reflected. The transmitted wave is refracted (the propagation direction of the wave changes), which leads to a loss in amplitude (loss of energy) depending on the angle. With the assumption of normal incidence (no diffraction occurs), the amplitude transmission coefficient τ can be calculated:

$$\tau = \frac{4Z_1Z_2}{(Z_1 + Z_2)^2} \tag{2.11}$$

The transmitted wave energy is not equal the wave energy before the wave hit the interface, because some energy is passed to the reflected wave. Index 1 denotes the first material and index 2 the second material. The reflection coefficient can be calculated to be $1 - \tau$. In this case, a perfectly smooth interfaces is considered. This idealization is typically not valid for real samples. The roughness has to be considered, too. Additionally, a shear wave component can be created in the case for a fluid-solid interface (mode conversion). Regarding bone, many additional effects that influence the wave propagation can be found. For example, bone marrow is a viscous material, that causes attenuation. Bone is also a porous media. Thus, interfaces due to the pore structure create reflections, refractions and additionally diffractions. Diffraction is the phenomena when a wave changes its direction while passing a sharp edge or an opening. Further on, the wave spreads due to this effect. For trabecular bone, the scattering effect has a high contribution to attenuation. The combination of bone marrow and trabecular structure creates many scattered waves. The describing parameters are randomization and differences in local elasticity and local density. The wave speed is determined by the structure of the material and the materials properties and may be influenced by the dispersion relation (cf. equ 2.5).

2.2.3 Fourier Transformation

Wave propagation can be studied in two different domains, the time domain and the frequency domain. The transformation of the signal from the time domain to the frequency domain can be done using the Fourier transformation, or the fast Fourier transformation (FFT) (cf. [39], [12], [18]). For discrete signals the discrete fast fourier method (DFFT) can be used, as implemented in MATLAB. The related command is `fft()`. The FFT looks for frequencies in the signal, by decomposing the periodic signal into a sum of sine-waves. The corresponding amplitudes of each sine-wave are then the output of the FFT. If the FFT is applied not to the time domain, but to the spatial dimension, the displacements in the chain are transformed to the wavenumber amplitudes. Applying the

FFT to both dimensions, the time and the space, the dispersion relation is created, that is the relation between the wavenumber and the frequency. The dispersion relation is one characteristic for a propagating waves. For example the linear trend for small frequencies of the dispersion relation can be looked up in [25].
The inversion of the FFT is done by the inverse fast fourier transformation (IFFT). For the calculation of the FFT, Matlab was used. The implemented code reads as

$$\mathbf{F}(\omega) = \sum_{j=1}^{N} \mathbf{f}(j)\omega_N^{(j-1)(\omega-1)} \quad , \tag{2.12}$$

where $\mathbf{F}(k)$ contains then the transformed amplitudes. $\mathbf{f}$ is the vector to transform and ω_N is defined as the N'th root of unity.

$$\omega_N = \exp^{(-2\pi i)/N} \tag{2.13}$$

Calculating the FFT in both directions of a matrix, which is the case to obtain the dispersion relation, the Matlab's function `fft2()` is used (see eq. 2.14).

$$\mathbf{F_2} = FFT(FFT(\mathbf{f_2}'))' \tag{2.14}$$

Here, f_2 is the full matrix containing the displacements for each particle at each time.

2.3 From continuum media (solids and liquids) to bone

In pure continuum solids, for example aliminium, dense and stiff structures can be found. The atoms are packed in a structured and regular way, where the atoms are strongly connected. The connection strength is dependent on the solid. For aluminium, this connection type is called metallic bonding. The electrons are free to move around, while the positively charged ions are fixed in the matrix. Typical matrices are face centered cubic or body centered cubic. In contrast to solids, liquids are less densely packed. Water molecules for example are connected by hydrogen bonds, which are weaker than metallic bonds. The differences in bond strength create different resistance to waves. The metallic bonding can resist shear stress, whereas the hydrogen bonds can not resist a shear stress strongly. Therefore, in metals the shear wave can propagate whereas it can not in water. In water only pressure waves propagate. The wave velocity of a wave is influenced strongly by elasticity properties and the density. A simple relation is the bar equation, e.g. found in [16]. Therefore, because the density of liquids are smaller than of solids, the P-wave in solids is typically faster than in liquids.

Anyway, here the focus is on pressure waves. In general, one pressure wave exists in a pure solid or liquid. Since wave propagation is the displacement of molecules, it can be described by a particle chain, where the particles are connected, e.g. by springs. This chain is considered in more detail in chapter 4. For a pure homogeneous solid, the chain can consist then of the same particles and springs. If a particle is displaced, this displacement starts to propagate through the chain. Using the restriction to one dimensional chains, shear waves cannot be described, since they need at least two degrees of freedom in space. For liquids, the same method can be used. A one dimensional chain consisting of identical particles and springs, that simulate a liquid, can transmit the displacement of one particle to another.

Increasing the complexity, a regular structured media can be considered. For that, higher

losses due to more interfaces are expected. At each interface inside the sample reflection can occur that weakens the signal. Dependent on how the structure is build, diffraction can also be created when a wave is bend by traveling through holes. If the structure is highly porous, diffraction can decrease the signal strongly. In porous samples P- and S-waves can travel, even though the S-waves cannot travel in liquids. The S-wave can use the solid matrix to travel. The wave velocity is here determined not just by the density and the elasticity, but also by the structure of the sample. A smaller wave velocity is expected with higher complexity of the structure. This effect of structure is assumed to occur on both wave types. The combination of solid and fluid should lead to two P-waves, due to in- and out-of-phase movement of the displacements in the liquid and the solid. Therefore, a structured sample can already be handled as a bone-like media, because many properties like porosity, and different media can be set. Effects, like viscosity and creation of two P-waves are also available.

For real media, a disorder can be introduced to a structured media, by e.g. disordering structure and/ or the discretization (for example the particle radius of a particle chain). Thus, it is not assumed that a real sample has a perfectly structure and micro-properties, as, at least consistent for natural grown materials, like bone. In the next subsection a way how to describe the complex bone-like media and bone is introduced with the goal to apply it to simulations.

2.4 Stratified model

The stratified model (cf. [16]) is used to simulate a porous media, e.g. bone. In general, it can be used for any kind of structured media. The media is divided into parts of the solid structure (matrix) and of the media that fills the pores. In figure 2.3 the ratio of solid to pores is shown. A media is structured in several layers of two materials after Schoenberg's Theory. The striped layers represent the solid phases with equal length of $(1 - \Phi)$H. Thus, the length of the solid layer is dependent only on the porosity Φ.

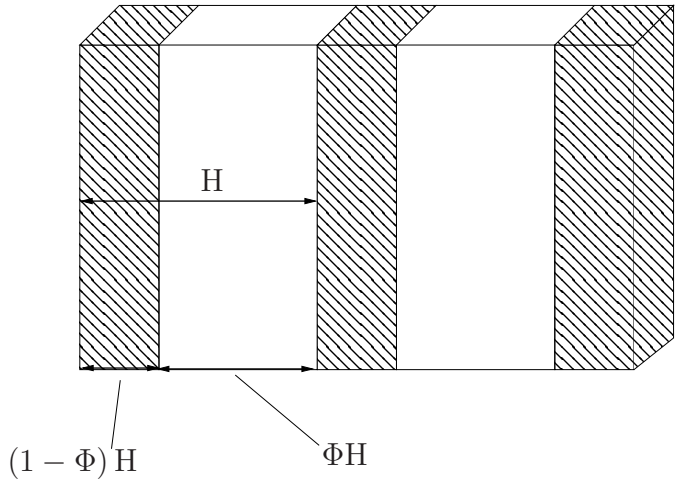

Figure 2.3: Stratified model in three dimensions

The blank layer represents the pores of the medium. In sum, the solid layer length and the porous layer length equals H. This model simplifies a porous media with a complex structure to a less complex and well ordered structure. Schoenberg developed a dispersion relation shown in equation 2.15.

$$\left(\frac{s_3^2}{<\rho>}\right) - \left[\frac{\beta(V_f^{-2} - s_1^2)}{\rho_f} + \frac{(1-\beta)(V_s^{-2} - s_1^2)}{\rho_s(1 - V_{pl}^2 s_1^2)}\right] = 0 \tag{2.15}$$

Instead of a velocity vector, a slowness vector $\mathbf{s}$ is used. Its magnitude is inverse to the magnitude of the phase wave velocity. s_1 is the component parallel to the layered structure and s_3 normal to the structure. V_l is the plate velocity, ρ_f is the density of the medium filling the pores, ρ_s is the density of the solid phase, β the porosity and V_s, V_f the wave velocities of the solid and the fluid phase. More details can be looked up in [16]. The number of layers is not simply definable, because for example the wave velocity was shown to be dependent on it. To avoid scattering, the wavelength should be longer than the period H. Layering the sample has a great advantage for bone investigations, because it is possible to create to waves, a fast and a slow pressure wave. The fast and the slow P-waves were explained for the bone issue and here it follows the same way. The coupled movement of the solid layers with the porous layers lead to the fast wave, while the decoupled movement of both create the slow wave. Anisotropy is also covered by this model. Investigating a wave in the direction of the layers, would lead to a different wave

velocity obtained by a wave investigation in the perpendicular direction. The effect on the frequency propagation is not known and therefore has to be investigated. It is expected, that the attenuation is dependent on the number of interfaces, since the interfaces create transmission losses.

Chapter 3

Experiments

In this chapter the experimental setup is described. The way how to obtain the wave velocity, the frequency spectrum and the attenuation values are described. The investigated specimens are aluminium and PMMA samples. The experimental setup is calibrated itself and the results are used to calibrate the simulation model in chapter (4). With the experimental setup, it is possible to obtain information about the complete sample, but not explicitly about the microstructure. With the simulation model it is possible to study the influence of parameters at different scales and to control the sample structure.

3.1 Experimental Setup

The experiments are conducted at the laboratories of the Biomedical Photonic Imaging Group, Universiteit Twente, together with or by M. Kuniyil Ajith Singh.
The through transmission experiments, shown in figure 3.1, consist of a ultrasound transmitter and a receiver, a pulser, a digital oscilloscope and a water tank. The immersion ultrasound transmitter by Panametrics (V309) has a central frequency of 5 MHz. Instead of using an ultrasound transmitter, a needle hydrophone (BLLMCX074 Precision Acous-

tic Ltd., Dorchester, Needle diameter 1 mm) is used. This has the advantage, that a larger bandwidth can be detected. The range is declared as between 200 kHz to 50MHz. The specimen and the ultrasound transmitter/receiver are held in a water tank. The transducer is driven by a pulser/receiver (Panameterics 5077PR). To determine the frequency output, the frequency range was set to $5 - 6$ MHz. Thus, the main peak of 5 MHz of the transducer cannot be matched exactly. The wave-form, that is produced by the pulser, is a negative rectangular pulse. The pulse-width corresponds to the frequency range from 5 MHz to 6 MHz. The sample is also placed in the water tank, in between the transducers, so that the shape of the ultrasonic transducer/receiver does not have to fit to the sample shape. The data received by the needle hydrophone is captured with 500 MS/s by the data acquisition card by Acqiris (8 bit). Additionally, the water temperature is measured with an USB based thermocouple sensor, because the wave velocity of water depends on the temperature. The measured temperature for all experiments is 20°C. Comparable

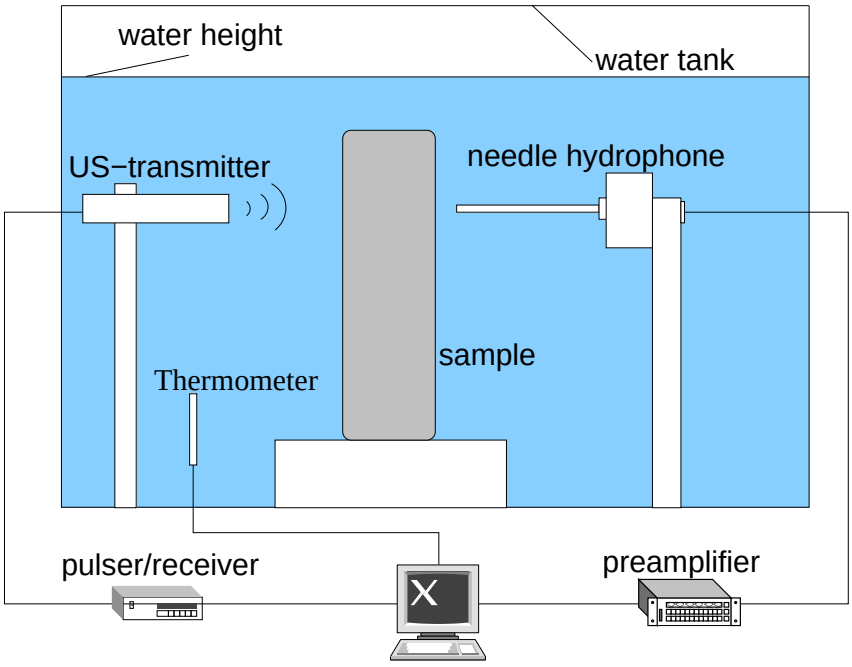

Figure 3.1: Experimental setup

experimental setups can be found in e.g. [40], [18]. The pressure wave velocity of the sample c_p is a function of the water wave velocity c_p^w, the thickness of the sample Δd and

the measured time difference Δt from measurements with and without a sample (cf. [42]).

$$c_p = \frac{c_p^w \Delta d}{\Delta d - c_p^w \Delta t} \tag{3.1}$$

Δt is obtained by the peak-method, which is explained in chapter 5. The time difference between the first peak of the reference signal and the first peak of the signal with the sample placed in between the transducers, is the time difference. Attenuation in dB/cm of the sample $\alpha(\omega)$ is calculated according to equation 3.2, where $A_s(\omega)$ is the absolute Fourier-amplitude signal received while the sample is placed in between the ultrasound transducers and $A_w(\omega)$ is the absolute value of the Fourier-amplitude signal received without a sample between the transducers (cf. [24], [39], [42]). The Fourier amplitudes are obtained using Matlab's fft-function.

$$\alpha(\omega) = \frac{1}{\Delta d} 20 \log\left(\frac{A_w(\omega)}{A_s(\omega)}\right) \tag{3.2}$$

If the thickness of the sample is neglected in this equation, the unit is dB. The reason why the thickness is usually not neglected can be found in the definition of the attenuation coefficient. The attenuation coefficient shows the loss of the signal due to scattering and absorption. Scattering and absorption are both effects that increase with space. Therefore, comparing samples of the same material, but of different thickness, leads to different attenuation values in dB/MHz. To exclude the dependence on the thickness, the attenuation value is divided by the thickness. Nevertheless, there are damping effects that are not influenced by the sample thickness. These can for example be interface reflection and refraction. Here, only reflection is considered. Of course, in the experimental attenuation value refraction is included, but its calculation is not explained in more detail, because in the used simulation method it is not present due to its restriction to the one dimensional case. However, the calculation is based on Snell's law [20]. Regarding reflection, if an ultrasonic wave travels from one medium into another and then again into a medium of first kind, it passes two times the same interface combination. Therefore the two inter-

faces have to be considered for through-transmission experiments with one solid sample held in a water tank.

With the described experimental setup and the mentioned equations, the wave velocity and the attenuation values are calculated. To pre-estimate the error in the wave velocity calculation due to errors of its input parameters (cf. eq. 3.1), the error propagation is calculated to show how sensitive the calculation procedure to these variables is. Then, the standard deviation σ_{c_p} can be obtained by summation of the products of the error propagation with the standard deviation of each possible error (cf. eq. 3.3).

$$\sigma_{c_p} \approx \sqrt{\left(\frac{\partial c_p}{\partial(\Delta t)}\right)^2 \sigma^2(\Delta t) + \left(\frac{\partial c_p}{\partial(\Delta d)}\right)^2 \sigma^2(\Delta d) + \left(\frac{\partial c_p}{c_p^w}\right)^2 \sigma^2(c_p)} \tag{3.3}$$

If a range of error for each variable is assumed from $0-5$ %, the standard deviation is a linear function of the error. Figure 3.2 shows the dependency of the standard deviation on the assumed individual and total errors. Here, the standard deviation of the wave velocity

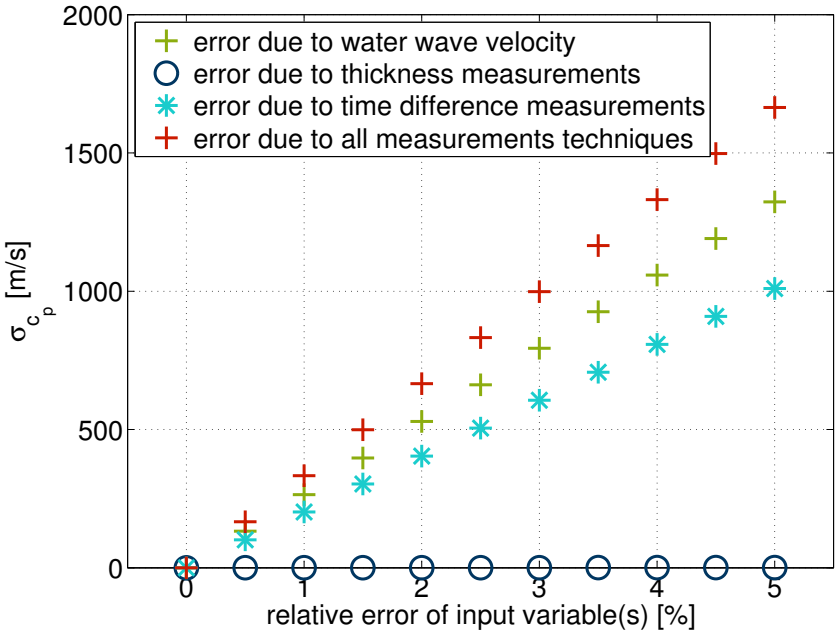

Figure 3.2: Error propagation of the wave velocity for the experimental wave calculation

is plotted over the relative error of the input variables. The relative error is assumed to be between 0 % and 5 %. Using this discrete range, the related standard deviations are calculated. From these standard deviations the error propagation is calculated (cf. eq.

3.3). The resulting standard deviation of the wave velocity is highest for the common error assumption. The biggest influence, in case of an individual error, is the influence of the water wave velocity. On the contrary, the influence of the thickness measurements is very low. It is only 7 m/s assuming an error of 5%.

3.2 Experiment with an aluminium sample

To validate the setup, an aluminium sample is placed between the ultrasound transducers. This aluminium sample is a homogeneous sample without any microstructure. Thus, this is one of the easiest case and can therefore be used to validate the setup and calibrate simulation. The wave velocity in the samples and the attenuation coefficient are calculated and compared to exisiting literature values. For the calculation of the wave velocity and the attenuation coefficient, the aluminium sample thickness is measured by an electronic gauge. The thickness is measured to be 6.08 mm. The water wave velocity for the measured temperature of 20 °C is looked up in literature, which gives a value of 1481 m/s.

3.2.1 Wave velocity

The received time-voltage signal for the reference and the sample measurement are shown in figure 3.3. The reference measurement is the measurement without a placed sample. It is plotted as the blue curve and the sample measurement as the green curve. The signal of the sample measurement arrives earlier, because the wave velocity in the aluminium sample is higher than in water. It is also weaker due to the higher reflection and the attenuation of the sample. The shapes of both signals clearly are created by a square pulse technique and are similar. Comparisons can be found in e.g. [31]. With formula 3.1 the wave velocity of aluminium can be calculated. First, the arrival times of both signals are measured, as shown in figure 3.3. Here, the red dots mark the arrival time of

the waves. The peaks are used to calculate the time difference Δt. The obtained wave velocity of 6259 m/s is in the range of literature values [9], [2], e.g. between 6230 m/s and 6420 m/s. An exact comparison value cannot be denoted, because the composition of the used aluminium sheet is unknown. Therefore, the purity of aluminium is also unknown, however, the calculated value is assumed to be accurate.

3.2.2 Frequency spectrum

For the frequency spectra of the reference and the sample signal, MATLAB's fft-function is applied to the signals in time domain. Instead of using the full time signal, the window of interest is cut using a rectangular window. In figure 3.4 the Fourier-amplitude in dB is plotted over the frequency. The Fourier spectrum related to the reference measurement is shown by the blue curve and the Fourier spectrum of the sample measurement is displayed by the green curve. Around 5 MHz to 6 MHz, both curves reach a peak, which is created by the signal wave form influenced by the transducer frequency and the pulser driving

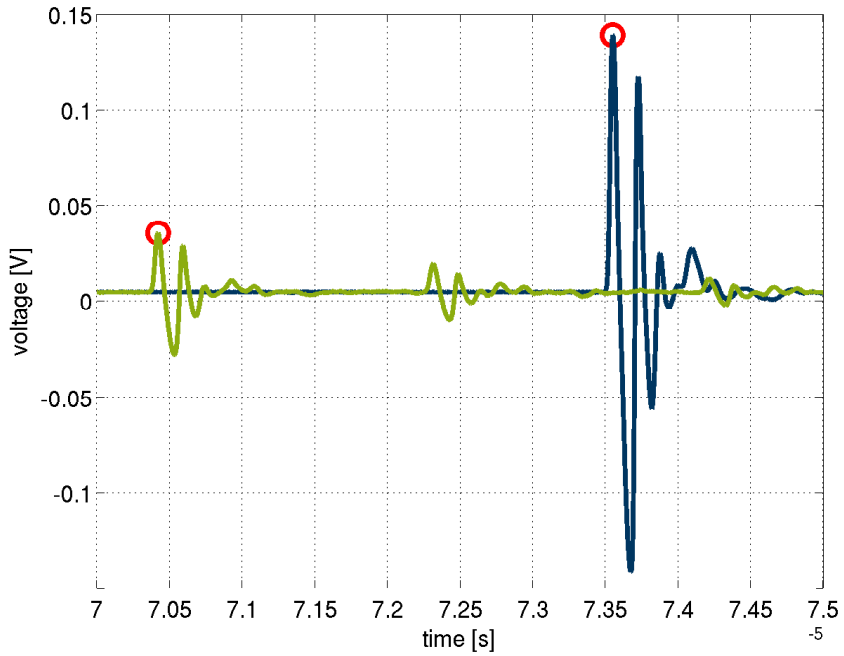

Figure 3.3: Experimental received time signals, blue curve: reference signal, green curve: examined aluminium sample, thickness: 6.08 mm

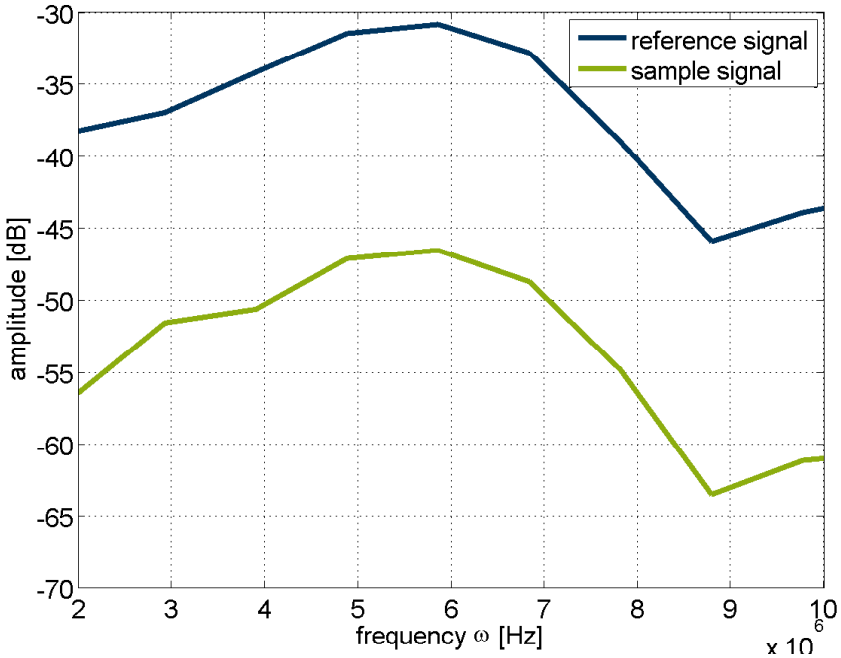

Figure 3.4: Frequency spectra, blue curve: reference signal, green curve: examined aluminium sample, thickness: 6.08 mm

frequency. After reaching the peaks, the amplitudes are decreasing, because the gap to the main frequency increases. The overall shapes of both curves are similar, so that one can recognize, that the interfaces or the sample itself do not change the shape of the frequency spectrum. The most remarkable effect of the inserted sample is the smaller amplitude, which is mainly due to attenuation, refraction and reflection.

3.2.3 Attenuation

Using both frequency spectra, attenuation can be calculated using formula 3.2. A positive attenuation value is obtained when the reference signal is higher than the sample signal. Vice versa, a negative attenuation value means the sample signal is higher than the reference signal. The calculated attenuation is plotted in figure 3.2. The attenuation values are plotted over the frequency. Attenuation (green curve) is high for small frequencies and then following a positive rising trend. Some frequencies are higher attenuated, which may be occurring due to the wave excitation form. The high offset of 19.27 db/cm is cre-

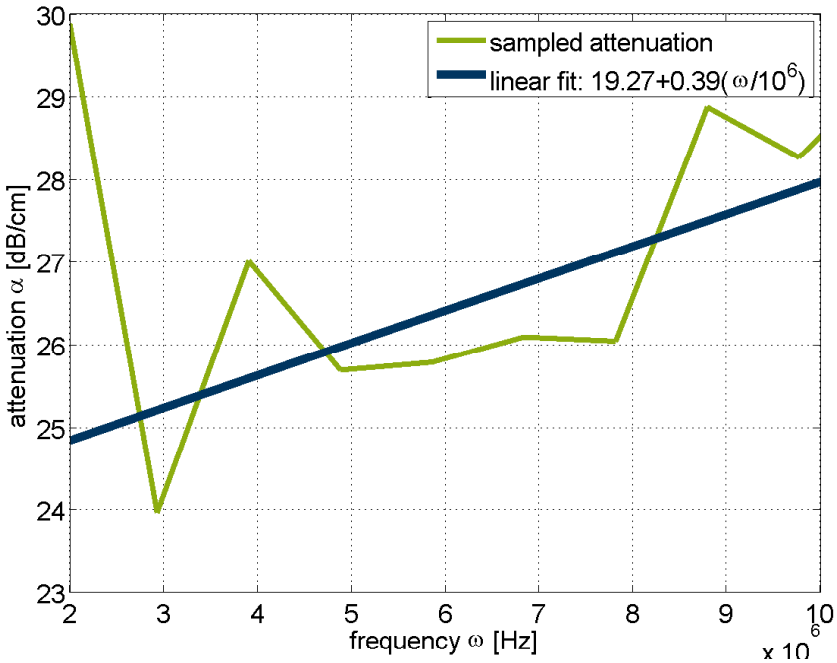

Figure 3.5: Attenuation, green curve: calculated attenuation values, blue curve: linear fit, examined aluminium sample, thickness: 6.08 mm

ated by the reflections at the sample-water interfaces. Another reason is refraction, which occurs due to imprecise alignment of the specimen. Then in addition to the reflection, the wave looses energy due to its change of direction. Considering only the interface effects, a transmission value of 10.58 dB (absolute value) is found. This means, that the difference between the theoretical and the experimental offset value is explicable with the remaining effects diffraction and refraction. Ignoring the offset, the steepness of the curve indicates the attenuation coefficient in dB/cm/MHz. Even if the correlation between attenuation and a linear fit (blue curve) is not high (the correlation coefficient is about 0.39), a linear fit can be used. The correlation coefficient describes the accuracy of the fit to the discrete values and becomes 1 if the fit is perfect and 0 if it is worst. Evaluating the linear fit, attenuation comes up to a value of 0.39 dB/cm/MHz. This value is close to values that can be found in literature, e.g. [43], 0.54 dB/cm/MHz. Again, a perfect match is not expected, because the type of investigated aluminium material is not known.

3.3 Experiment with a PMMA sample

The second experiment is conducted with a Poly(methyl methacrylate) (PMMA) sample. The material has a density of about 1180 kg/m^3. The thickness of the sample is 3.95 mm. The experiments are conducted under the same conditions as the validation experiment using an aluminium sample. The PMMA sample is a homogeneous sample without microstructure, too.

3.3.1 Wave velocity

For the calculation of the wave velocity first the time signals are considered. They are displayed in figure 3.6. The reference signal (blue curve) arrives later than the sample

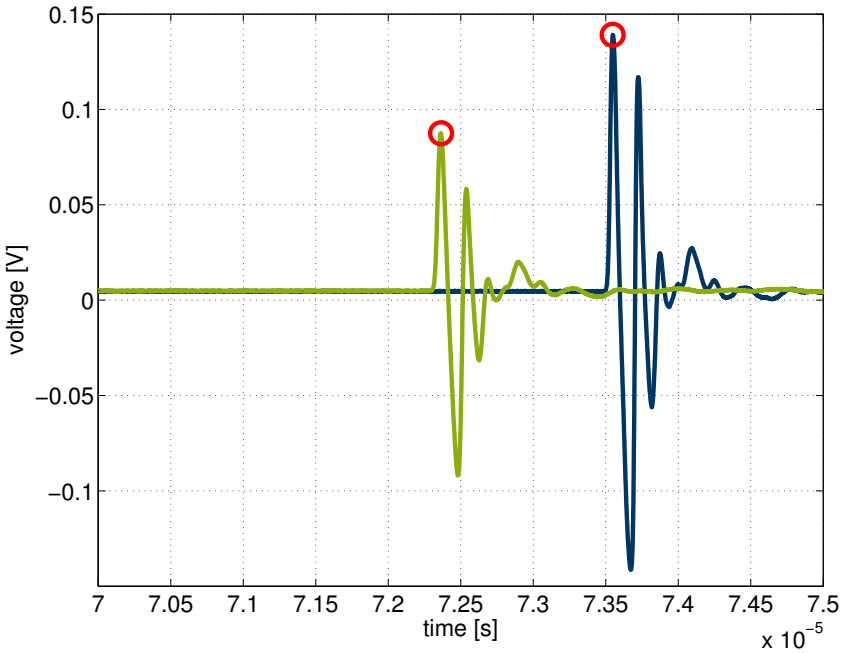

Figure 3.6: Experimental received time signals, blue curve: reference signal, green curve: examined PMMA sample, thickness: 3.95 mm

signal (green curve), because the wave velocity in PMMA is higher. This is expected, since the density and elasticity values are higher for the specimen. This expectation is confirmed by literature values (cf. [2]). The peaks of both signals are marked with red

circles, which are chosen to denote the arrival of the waves. The magnitude of the pure water signal is also higher, because the magnitude of the PMMA signal is attenuated. Additionally the wave is reflected and maybe refracted at the interfaces water-PMMA and PMMA-water. The wave velocity is obtained again using equation 3.1. The wave velocity calculates to 2670.5 m/s, which is close to literature values (cf. [2]), 2670.5 m/s.

3.3.2 Frequency spectrum

For the frequency spectrum the signal is cut by a rectangular window. The frequency spectrum is shown in figure 3.7. The frequency is plotted over the amplitude in dB.

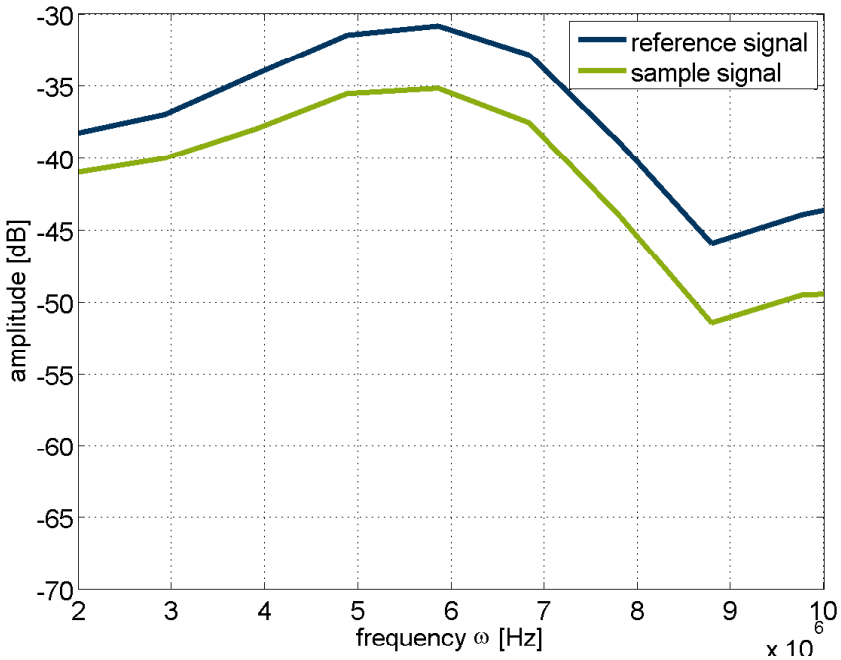

Figure 3.7: Frequency spectra, blue curve: reference signal, green curve: examined PMMA sample, thickness: 3.95 mm

The shape of the curve obtained with the PMMA sample placed between the ultrasound transducers is very similar to the curve related to the reference signal. Comparing the frequency spectrum of PMMA with the spectrum of aluminium, we can find that the amplitudes of the PMMA spectrum is much higher. Therefore, at least one signal-loss reason has to be significantly higher for the aluminium sample.

3.3.3 Attenuation

Looking at the attenuation values, shown in figure 3.8, it can be seen that the offset is much lower than for the aluminium sample. The offset is mainly caused by reflection and refraction at the interfaces. To evaluate the reflection loss, again equations 2.11 and 2.10 are evaluated. The transmission loss value is evaluated to be 1.21 dB (absolute value). This is about eight times lower than for the aluminium sample. Applying a linear fit to

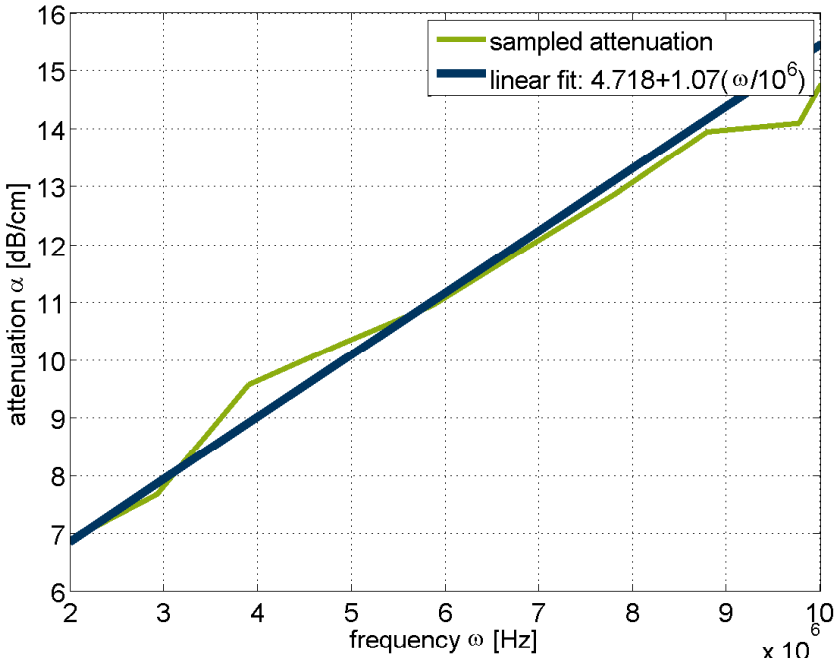

Figure 3.8: Attenuation, green curve: calculated attenuation values, blue curve: linear fit, examined PMMA sample, thickness: 3.95 mm

the discrete frequency-attenuation curve, a value of 1.07 dB/cm/MHz is found from the slope. Comparing with literature values, the determined value lies in the range of stated values (cf. [2], [?]), 1.13 dB/cm/MHz. After the experimental setup is introduced and the experiment is found to be precise due to matching literature data, in the next chapter the simulation method is introduced. This method is adjusted and the experiment with the aluminium sample is modeled to find the range of discretization that can be used.

Chapter 4

Simulation of a one-dimensional particle chain

In this chapter the technique to model the experimental setups (cf. chapter 3) is presented. To simulate wave propagation, a one-dimensional (1D) particle chain is used. Thus, continua are replaced by particles with a particle size, the discretization of space. The particles are connected by linear elastic springs that permit particle interaction (cf. [21], [26]). The mathematical description of this problem can be solved analytically, which accounts for a reliable start for the simulation of a propagating wave.

First, in this chapter the advantages and disadvantages of the one-dimensional particle chain with an analytic solution are discussed. Then, the mathematical procedure is described for the sine, the pulse and a square pulse excitation. In the end, the determination and the meaning of the input parameters are discussed.

4.1 Simplification to a one-dimensional particle chain

The simplification of the complex three dimensional problem of wave propagation to the more simply one dimensional wave propagation model is described in this section with its advantages and disadvantages.

One can consider wave propagation in bone from different angles. One possible start would be to use a complex theory applied to the macroscale, for example the Biot's theory (cf. [36], [13]). For this many information about the examined material is needed, e.g. Young's modulus, Poisson ratio, permeability, porosity and more. Knowing the input, it is then possible to determine for example the pressure wave velocities of slow and fast waves. But if we want to apply this theory to bone, all these parameters have to be known, which is not very handy in this case. Many studies exist, but parameters from literature can not be used, because many authors pointed out, that each bone has its own specific properties and therefore specific wave velocities and attenuation coefficients (cf. [44], [41]). Additionally, more detailed examinations regarding the wave velocity and attenuation coefficients are needed.

To reduce the input parameters the used model is restricted to elastic particle behavior, without consideration of viscosity, scattering and other effects. In this case only extinction due to reflection exists, so that it is possible to investigate the role of interfaces without influence of one of the other complex physical effects.

The investigated model is one dimensional. The advantage is that scattering due to interfaces is avoided and propagation of the wave in general in the two other spatial directions. This leads also to a reduction of the used particle number and a faster calculation time. Diffraction and refraction are also avoided for the one dimensional case, because they need at least two dimensions to exist. Concluding, if the model is calibrated in the right way, one would expect that the calculated weakening of the wave of the simulation matches the transmission coefficient τ in dB.

Due to the fact that attenuation in porous media like bone is not fully understood, it is

easier to study attenuation caused by the reflections at the water-sample interfaces only. Then the internal structure of the sample can be changed and the attenuation explored. For the analytical simulation the parameters can be classified in simulation parameters and physical properties, shown in table 4.1. Note, that only three physical parameters are

Physical Properties	Simulation Parameters
Particle mass m_p	Time step ΔT_{st}
Spring stiffness k_s	Simulation time T_{sim}
Sample porosity Φ	Particle radius r_p

Table 4.1: Physical and simulation input parameters for the analytical chain

necessary to run a simulation. Additionally, if a solid sample is considered, the porosity Φ is simply zero. In section 4.3 it is shown, how the particle mass and the spring stiffness can be calculated using a fixed particle size (discretization length)as simulation parameter and the bulk density and the wave velocity are obtained by the experiments as physical properties. The input parameters can be found in the equation of motion (cf. [22], [21]), which is introduced in the next section.

4.2 Mathematical procedure

The one dimensional chain is illustrated in figure 4.1. The particles of masses m_i are

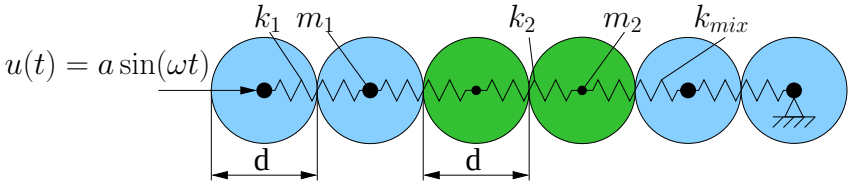

Figure 4.1: Scheme of the one dimensional particle chain

connected by springs of stiffness's k_i. Each particle has a specific particle size. In this illustration, the particle size is kept constant, but that is not a necessity. The spring stiffness is equal in a material chain. At the transition from one material to the next, a mixed spring stiffness k_{mix} has to be applied. The boundary conditions are as follows:

The first particle can be displaced continuously sinusoidal over the time (as shown in the scheme) or the displacement can be set for the first time step. The last particle is fixed, so that the chain cannot move away and the system of equations is solve-able. For the initial conditions the velocity and the displacement are set to zero.
The analyitcal solution is described in the following to a point, at which the solution differs for different excitation. Then, the specified mathematical solutions for different excitation are presented. The analytical solution is taken from [21] and implemented in Matlab. Equation 4.1 describes the motion of each particle of the one-dimensional particle chain caused by an external force. It is present in the linearized state, but in general it is not linear. The linearization procedure can be looked up in [21].

$$\mathbf{M\ddot{u}} = \mathbf{Ku} + \mathbf{f} \quad , \tag{4.1}$$

where, $\mathbf{M}$ is the diagonal mass matrix, $\mathbf{K}$ is a tri-band diagonal stiffness matrix, $\mathbf{u}$ is the displacement vector, $\ddot{\mathbf{u}}$ is the acceleration vector and $\mathbf{f}$ the external force vector.

4.2.1 Eigenvector-space transformation

The equation of motion 4.1 can be solved in time domain or in frequency domain. In the eigenvector basis, the equations of 4.1 are decoupled and therefore easier to solve. The solution of the one dimensional chain is based on the following eigenvalue problem 4.2.

$$\mathbf{Au} = \omega^2\mathbf{u} \tag{4.2}$$

It is obtained by setting $\mathbf{A} = -\mathbf{M}^{-1}\mathbf{K}$ and comparing with the right hand term. From there, the eigenvalues and eigenvectors are calculated. This can be done using the matlab-function eig(). The eigenvectors and eigenvalues are sorted by increasing order and nor-

malized to arrive at the orthonormality conditions.

$$\mathbf{s}_i^T \mathbf{M} \mathbf{s}_j = \delta_{ij} \tag{4.3}$$

The indices range from 1 to the number of particles in the chain. $\mathbf{s}$ are the eigenmodes of the chain. Equation 4.1 in eigenspace can be rewritten as following. For details, please look at [21].

$$\frac{d^2\mathbf{z}}{d\hat{\tau}^2} = -\mathbf{D}\mathbf{z} + \mathbf{h} \quad , \tag{4.4}$$

where $\mathbf{z}$ is the transformed displacement matrix, $\mathbf{D}$ is a diagonal matrix, containing the eigenvalues on the diagonal, $\hat{\tau}$ denotes the scaled time and $\mathbf{h}$ is the transformed force vector (cf. [21]). At this point it is important to distinguish between the sinusoidal and the pulse excitation, because here the displacements are calculated in time-space.

4.2.2 Sinusoidal excitation

For the sinusoidal excitation the first particle is displaced with a harmonic sine-function over all time steps. Therefore a transformation to eigenspace is needed. The history of each particle can be obtained by the transformation of the solution of eq. 4.4. For this, the homogeneous and heterogeneous parts of the differential equation have to be solved. The displacement for a particle is calculated as in equation 4.5.

$$u^p(\hat{\tau}) = \epsilon \sum_{j=1}^{N} \frac{S_{pj} S_{1j}}{(\omega_j^2 - \omega_0^2)} \left(\sin \omega_0 \hat{\tau} - \frac{\omega_0}{\omega_j} \sin \omega_j \hat{\tau} \right) \tag{4.5}$$

For this solution, initial conditions can be looked up in [21]. In equation 4.5 ϵ is the amplitude of the sine excitation and ω_0 its frequency.

4.2.3 Pulse excitation

For the pulse excitation the first particle is displaced in the first time step. In all following time step it is free to move in both directions. Using again the results of subsection 4.2.2, the displacements of each particle at each time step can be calculated. Starting again at the eigenvalue problem (eq. 4.2), the particle displacement for a particle can be calculated using following formula.

$$\mathbf{u} = \mathbf{SCS}^{-1}\mathbf{u}_0 \tag{4.6}$$

Here, $\mathbf{S}$ is the matrix of eigenvectors and $\mathbf{C}$ contains contains the values of $\cos\omega\hat{\tau}$ on the diagonal. The way to this equation can be read again in [21]. The particle displacements can now be calculated for two types of excitation. Additionally, a general excitation for a pulse is studied. It is based on transforming a signal into a Fourier-series.

4.2.4 Square pulse excitation

The calculation of the history with a square pulse was not included in [21]. To calculate the displacement history of the linear chain, with a square pulse as a boundary, in equation 4.4 the vector $\mathbf{h}$ has to be replaced. Therefore the Fourier series for a square-pulse has to be introduced.

$$f(t) = \sum_{k=1}^{N} b_k \sin\left(\frac{2\pi k}{L}t\right) \tag{4.7}$$

The factor b_k describes the waveform and $2\pi/L$ is the frequency of the wave. Then $\mathbf{h}$ becomes

$$\mathbf{h} = \sum_{k=1}^{N} b_k \sin\left(\frac{2\pi k}{L}t\right)\mathbf{y} \quad . \tag{4.8}$$

To solve the differential equation, the homogeneous and the heterogeneous solutions have to be found. The homogeneous solution is

$$\mathbf{z}_h = \mathbf{C}^1\mathbf{a}^1 + \mathbf{C}^2\mathbf{a}^2 \quad , \tag{4.9}$$

where $\mathbf{C}^1$ and $\mathbf{C}^2$ are diagonal matrices with the entries $\sin\omega\tau$ and $\cos\omega\tau$. $\mathbf{a}^1$ and $\mathbf{a}^2$ are the coefficients, obtained later by the initial conditions. The particular solution is derived by inserting

$$\mathbf{z}_p = \sum_{k=1}^{k_{max}} \grave{K} \sin(\Phi_k t) \tag{4.10}$$

and

$$\ddot{\mathbf{z}}_p = \sum_{k=1}^{k_{max}} \Phi_k^2 \grave{K} \sin(\Phi_k t) \tag{4.11}$$

into equation 4.4. In equations 4.10 and 4.11 the cos termes are neglected, because they cancel out in the next step. By comparison of the coefficients, $\grave{K}$ can be determined to

$$\grave{K} = \frac{b_k}{\omega^2 - \Phi^2} \quad . \tag{4.12}$$

Applying the initial conditions $\mathbf{u}(0) = \mathbf{u}_0$ and $\mathbf{v}(0) = \mathbf{v}_0$, the coefficients $\mathbf{a}^1$ and $\mathbf{a}^2$ are calculated:

$$\mathbf{a}^1 = \frac{\mathbf{S}\mathbf{v}_0 - \sum_{k=1}^{k_{max}} \Phi_k \sin(\Phi_k t)\mathbf{S}}{\grave{K}} \tag{4.13}$$

$$\mathbf{a}^2 = \mathbf{S}^{-1}\mathbf{u}_0 \tag{4.14}$$

The general solution of eq. 4.4 is written in equation 4.15.

$$\mathbf{z} = \mathbf{z}_h + \mathbf{z}_p \tag{4.15}$$

Implementing this code in Matlab leads to a huge calculation effort. Another loop over the Fourier coefficients is required, where the maximum of iterations are dependent on the chosen maximum number of Fourier terms. For a precise representation of the pulse due to the Fourier series, a high number of terms is needed. Summarized, the simulation of wave excitation using a Fourier series, is only feasible with a very small chain, that is not considered here.

4.3 Adjusting the particles

To mimic specific material, the particle mass and the spring stiffness have to be adjusted. Then, the displacement calculation procedure can be applied. The way how to adjust the particle mass and the spring stiffness is presented here.

The experimentally obtained wave velocity is used as the experimental input parameter for the adjusting procedure. Additionally, the bulk density of the material has to be known, e.g. by literature. In the first step we fix the particle radius and refer to it as the discretization length. The effect of the particle radius has to be investigated after that. The mass of one particle can then be achieved by the knowledge of the particle density.

$$m_p = \rho_p V_p = \frac{4}{3}\pi\rho_p r_p^3 \tag{4.16}$$

V_p is the particle volume and ρ_p is the particle density. For a one dimensional particle system the particle density can be replaced by the one dimensional-chain bulk density, where A is the cross-section and $\rho_c = \rho_p/A$ is the mass per length.

$$m_p = \frac{4}{3}\pi\frac{\rho_c}{A}r_p^3 \tag{4.17}$$

In the bar equation the experimental obtained wave velocity c_p is related to the bulk density of the same material (cf. chapter 3).

$$c_p = \sqrt{\frac{C_{11}}{\rho_b}} \tag{4.18}$$

C_{11} is the entry of the elasticity Tensor. These equations together with the one dimensional constitutive equation

$$\varsigma = C_{11}\varepsilon \quad , \tag{4.19}$$

where ς is the one dimensional stress and ε the one dimensional strain, the equation for the spring stiffness,

$$f = k_s \delta \tag{4.20}$$

where f is the force, and the definition of the strain as determination per particle size,

$$\varepsilon = \frac{\delta}{2r_p} \tag{4.21}$$

the spring stiffness of the analytical chain can be defined. δ is the subtraction of the equilibrium length of the spring and the absolute displacement.

$$k_{spring} = \frac{c_p^2 \rho_b A}{2r_p} \tag{4.22}$$

Further on, the maximum frequency can be calculated. The maximum frequency is a function of the spring stiffness and the mass.

$$\omega_{max} = \frac{2}{\sqrt{\frac{m_p}{k_{spring}}}} \tag{4.23}$$

If frequencies in the frequency bandwidth exist above the maximum frequency, they are damped highly. That means, that the maximum frequency, or cut off frequency, is the maximum value supported by the system, without high damping. Frequencies below the maximum frequency can propagate nearly without being damped.

In figure 4.2 the relation between the particle radius and the maximum frequency is plotted. The applied values of water for the wave velocity and bulk density are used. The higher the particle radius the smaller the maximum frequency. That is, if a chain consisting of big particles is excited sinusoidal with a high frequency, the main frequency cannot propagate because, it is cut off by the limiting maximum frequency. A physical explanation is that wavelengths are related with the frequencies. The propagating wavelength is limited by the particle diameter due to the discretization length. If the wavelength is smaller than the particle diameter; the wave is 'trapped' inside the particle and cannot

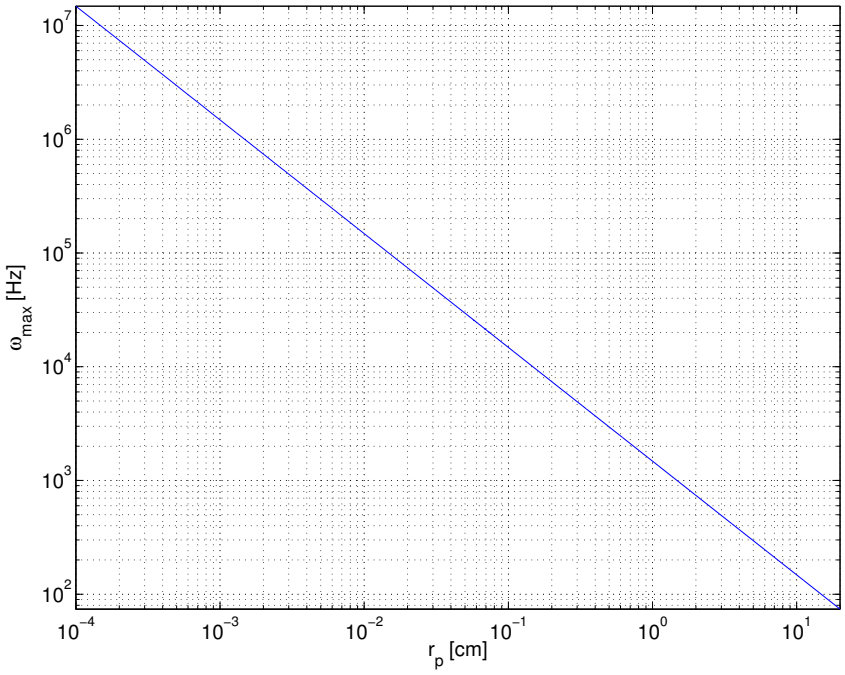

Figure 4.2: 1D-chain: theoretical solution of the maximum frequency in dependency of the particle radius, water, both axes are scaled logarithmic

propagate.

4.4 Summary and conclusion

The one dimensional chain is introduced and it is shown that the particles of masses m_p are connected with springs of stiffnesse's k_s. This means, that the model includes elasticity only. Effects like viscosity are neglected here. Equation 4.1 was solved for the sine, the pulse excitation and a general sine excitation using a Fourier series. The general sine excitation was found as computationally too expensive, because an extra loop for the Fourier series has to be implemented in the code to solve the equation 4.1.

To adjust the particles to mimic materials, the particle radius is fixed. From there, the mass and the stiffness is determined. This determination uses the bulk density of the material and the experimentally obtained wave velocity.

Chapter 5

Analysis methods for simulations

The methods how to analyze the simulation results are investigated here to identify the most accurate methods for the simulations in chapter 6 and 7. As mentioned before, wave propagation can be examined by looking at the wave velocity, the frequency spectrum and the attenuation. In this chapter the methods to obtain the wave velocity and the frequency spectrum are presented only. Attenuation is not regarded, because the calculation depends on the frequency spectra only. The according formula 3.2 has already been introduced in chapter 3.

The analysis methods are examined using a perfect uniformly water chain ($c_p^{input} = 1481$ m/s) to avoid influences due to structure, disorder and different materials. This chain is called reference chain. For this chain a particle radius of 0.01 mm, length of the chain of 108 mm, a simulation time of $80 * 10^{-6}$ s and the number of time steps of 2^{13} are used. The spring stiffness and particle properties mass and radius are tuned to match water properties. The cut off frequency (cf. 4.23) is 148.1 MHz. For both types of wave excitation the reference chain is examined. The first particle is sinusoidal excited with a frequency of 5 MHz and an amplitude of 0.05 m, which is called sine excitation. It is in a parameter study found out, that the amplitude does not play an important role for the propagation of the wave. This study is not included in this thesis. The pulse excitation

uses the same amplitude.

5.1 Wave velocity

The wave characteristic wave velocity is here investigated for the reference chain using the following methods: the peak method, the threshold method, two edge finding algorithms, and the cross-correlation. The accuracy of these methods are compared with respect to the relative error between the input and the back calculated wave velocity. For the threshold and the peak method the wave velocity can be calculated between two particles using the related time and spatial differences. The two used particles can be arbitrarily chosen. To introduce a structure to the way how the two particles are chosen, here a forward and a mixed switching method is used. For the forward switching method the last particle of the chain is fixed, while the first particle is switched from the first particle to the second last particle. Using a pseudo code, a for loop can be used to describe the forward switching method.

```
for   i = 1 : N − 1
```

$$c_p = \frac{x_N - x_i}{t_N - t_i} \tag{5.1}$$

```
end
```

x_N and t_N are the position and the time of the displacement peak of particle N. x_i and t_i are the position and the time of the displacement peak of particle i. When both used particles are switched from the boundaries to the inside, the method is called mixed

switching method. The related pseudo-code is shown in 5.2

$$\begin{aligned} &\texttt{for} \quad i = 1 : N/2 - 2 \\ &\qquad c_p = \frac{x_{N-i} - x_i}{t_{N-i} - t_i} \\ &\texttt{end} \end{aligned} \tag{5.2}$$

The two switching methods are used to investigate if the calculation method is dependent on the chosen particles. Especially, a boundary effect due to the excitation and the fixed end of the chain is expected. Knowing how the boundaries influence the wave velocity, the chain may be extended, if needed.

One way to visualize the wave velocity is using a carpet-diagram, in which the time is plotted over the space. In figure 5.1 the carpet diagram is shown for the reference chain. For each particle at each time step the displacement is shown in this figure. Green indicates

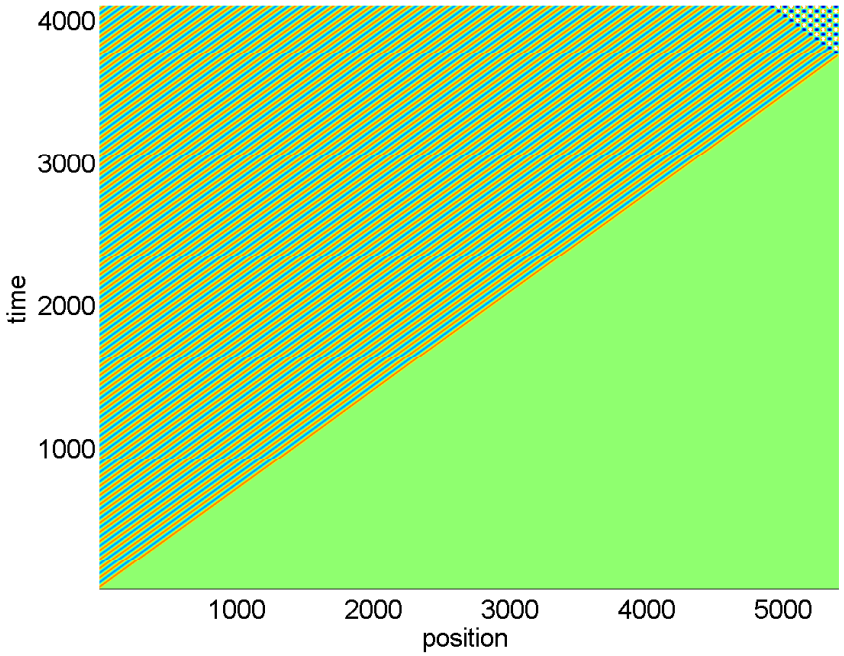

Figure 5.1: Carpet diagram space-time, reference chain, sine excitation, the time is scaled by $1/(2t_{step})$

no displacement, yellow means a positive displacement and blue a negative displacement. On the right bottom half we can see that the particles are not displaced, because at time

step one only the first particle is displaced. This is the excitation particle. Looking from the right bottom corner to the left top corner, the first yellow line marks the propagating wave. A linear slope can be found, which is related to the uniform chain and describes the wave velocity. The wave velocity in this plot can be calculated using the position-time fraction. Going from bottom right to top left, the yellow line is followed by a blue, a green, and again a yellow line and further on. This is related to the sine function used to excite the first particle. The sine function continues to rise to its maximum and then it is going back towards zero (yellow). Around the zero value the color code changes to green. Then the sine becomes negative (blue), reaches a minimum and tends to zero again (green). This sine-period repeats and the related color code can therefore be found multiple times. After the propagating wave reaches the end of the chain, it is reflected and going back to the beginning.

The carpet diagram for the chain using the pulse excitation is shown in figure 5.2. For this,

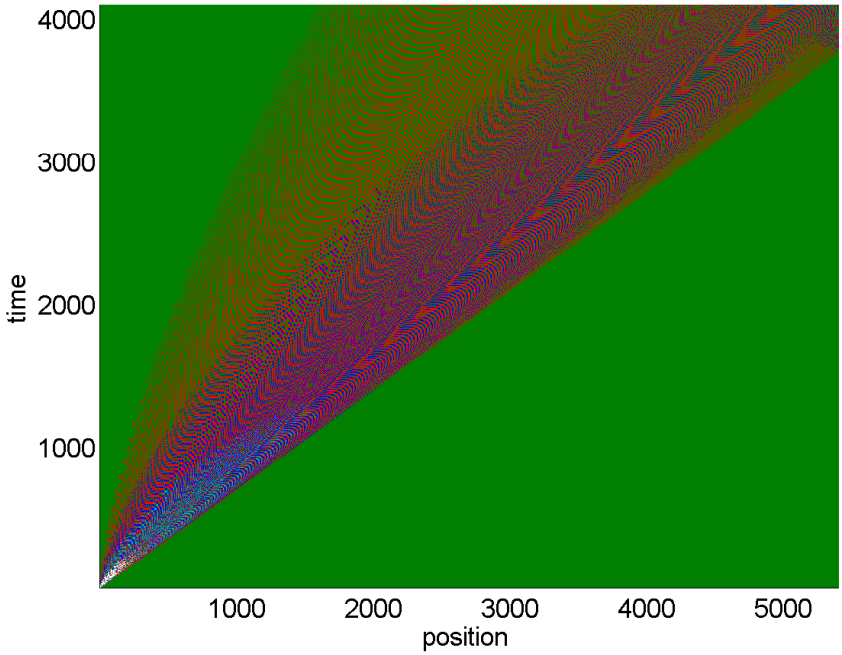

Figure 5.2: Carpet diagram space-time, reference chain, pulse excitation, the time is scaled by $1/(2t_{step})$

a different color code is used, because the amplitudes of the displacements are different, speaking about order of 10^6. Additionally the sine excitation leads to a more uniform (periodical) wave propagation than the pulse excitation. Purple means no displacement

and yellow a positive displacement. Again we can see the propagating wave, displayed by the linear yellow line. Here, no periodic structure can be found, but combinations of forward and backward propagation. At the end, again the wave is reflected.
After one method to visualize the wave propagation was introduced, the different wave calculation methods are described.

5.1.1 Peak method

To calculate the wave velocity, the peaks of two signals can be chosen. The related difference in space and time can be extracted or calculated from there. The peak method has the advantage, that the arrival of the wave is clearly defined by the first peak of the signal.
The general formula for the wave velocity calculations for the forward and the mixed switching methods were introduced before (cf. eq. 5.1, 5.2). For the peak method the related equation (5.3) is similar, only here the time difference is measured specifically using the first peaks of both signals. The peaks are measured in the displacement domain of the particles. That means, at the first peak of the displacement signal the correlated time is defined as the arrival time of the wave. The pseudo-code reads:

$$c_p = \frac{x_1 - x_0}{t_1^P - t_0^P} \quad . \tag{5.3}$$

An advantage of the method is that it ignores noise, which may occur before the wave signal arrives. That would be the case for experimental wave velocity measurements. Another advantage is that the measurement point is well defined. Even, if the peak height can vary, the arrival point of the wave is not an arbitrary value. However, the peak method may fails when the difference between the signal forms are too different. Then, the arrival time could be possibly not exactly determined.

Due to the fact that the waves are measured using the displacement signals, it has to be distinguished between the initial and the current configuration. If the spatial difference is measured at the same peaks as used for the time difference measurement, the calculation is related to the current configuration. If the spatial difference is the initial spatial difference, the calculation is related to the reference configuration. Figure 5.3 illustrates the time peaks, which are used to calculate the wave velocity. Between the way how the particles

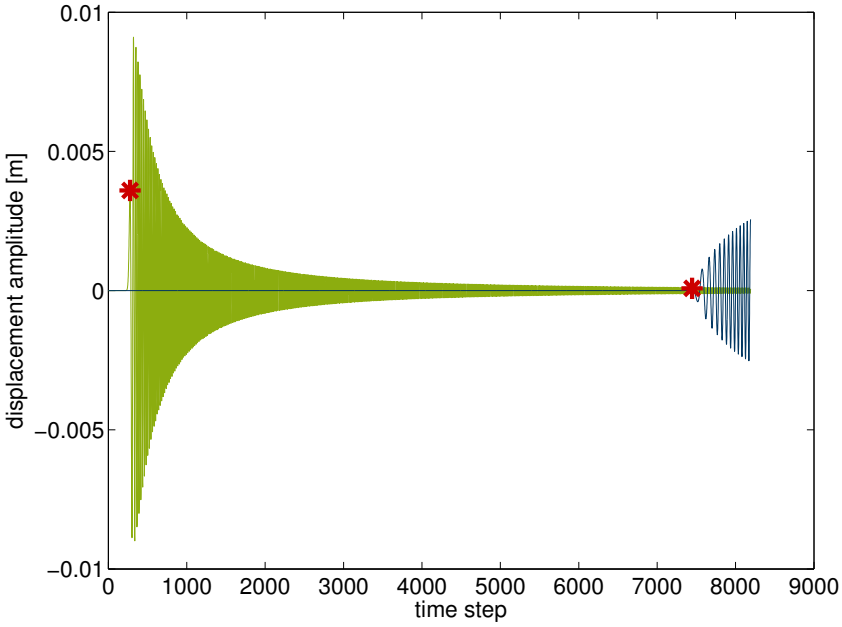

Figure 5.3: Displacement signals of two particles, one near the excitation (green) and one near the end of the chain (blue), excitation method: pulse, reference chain

are chosen is now distinguished. For the forward switching method in figure 5.4 the results for the reference chains are shown. The calculations were done using the initial configuration.

Shortly after the beginning of the slopes in both figures the velocities match the input velocity of 1481 m/s. Then the values increase and reach the 1% error-limit at the offset number 1011 for the sine-excitation and for the pulse-excitation at the offset number 1052. The error is defined as the relative error between the input wave velocity and the back-calculated velocity from the simulations.

Both figures show that in the beginning and at the end there are boundary effects, which probably will disappear when the calculation of the wave velocity is done for particles

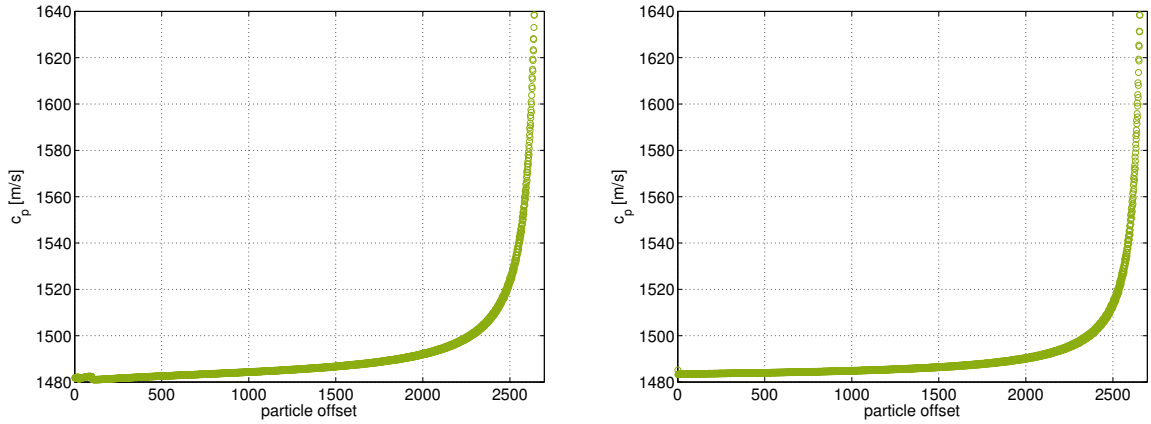

Figure 5.4: Wave velocities obtained by the forward switching peak-method for two different excitations: left: pulse, right: sine

that have a certain distance to both boundaries. Therefore in the second way the mixed switching method is used. The results are shown in figure 5.5 for the pulse and the sine

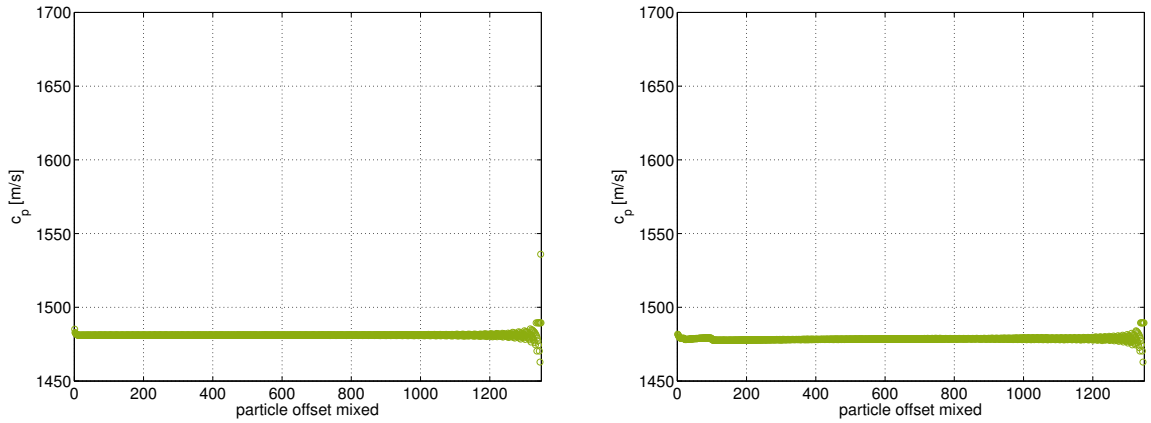

Figure 5.5: Wave velocities obtained by the mixed-offset peak-method using the initial configuration for two different excitations: left: pulse, right: sine, reference chain

excitation. The wave velocity is shown over both offsets from the first particle of the first and the last boundary. Comparing this results to figure 5.4, the wave velocities are much more stable. Only in the beginning the first offsets have a higher relative error, but still the error is smaller than 1%. At the end only the last two offsets have an relative error higher than 1%. Both plots were created using the initial configuration. Considering the current configuration, a big difference between the two excitation methods could be found (cf. 5.6). For the pulse excitation the current configuration is found to be useless, because the deviation of the back-calculated wave velocity from the input wave velocity

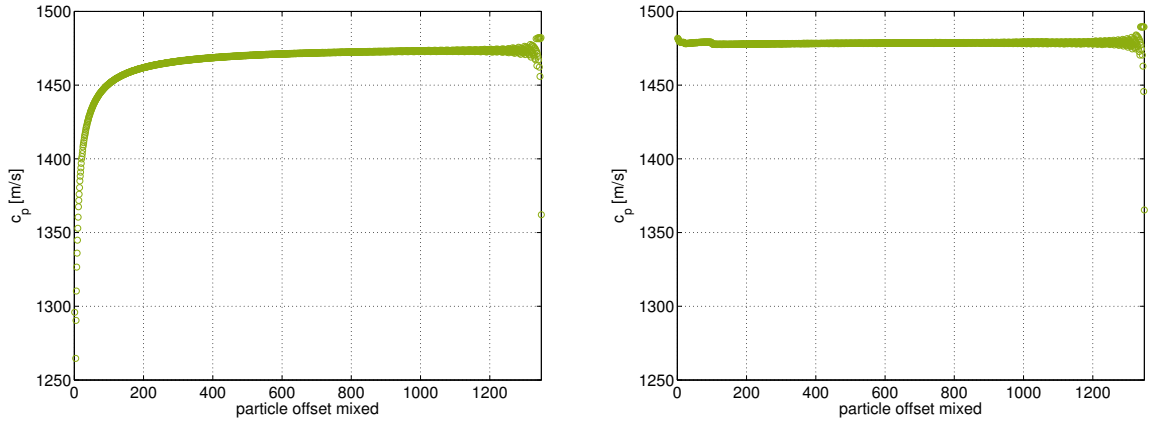

Figure 5.6: Wave velocities obtained by the mixed-offset peak-method using the current configuration for two different excitations: left: Pulse, right: Sine

is very high. On the right side it is recognizable that for the sine excitation it is not important if one considers the current or the initial configuration. The right curve of figure 5.6 looks very similar to the right curve of figure 5.5. Thus, it is important to distinguish if the wave velocity is calculated for a simulation using either a sine or a pulse excitation. The peak-method showed accurate results for both excitation methods, if the initial configuration is considered. In the next subsection the accuracy of the threshold method is investigated.

5.1.2 Threshold method

The arrival of each wave is detected by using a threshold with a fixed value as a marker of the arrival of the wave. If the displacement signal is greater than the threshold, the arrival time at this point is defined. In opposite to the peak method, here a very early arrival can be found. Following, the used threshold should be as small as possible to get rid of the dependence of the signal shape. However, a threshold can be only used if there are not big fluctuations in the signal that could be misinterpreted as the arrival time of the wave. For example, in experiments only the electrical noise of the electrical current and devices would make it difficult to use a threshold. Due to the analytic solution, it is even possible to to set the threshold very small, because no fluctuations and no noise are

present. The disadvantage is that the threshold can only be chosen arbitrary. Of course, some criteria like the half or the quarter of a the first peak can be chosen, but still this is an arbitrary choice without a clear physical meaning. For the achievement of figure 5.7 the same simulation results were used as for the pulse technique. The displacements of a particle close to the excitation and of a particle near to the end of the chain are illustrated. The arrival times of the waves are marked with a red star. The peak of the arrival time of

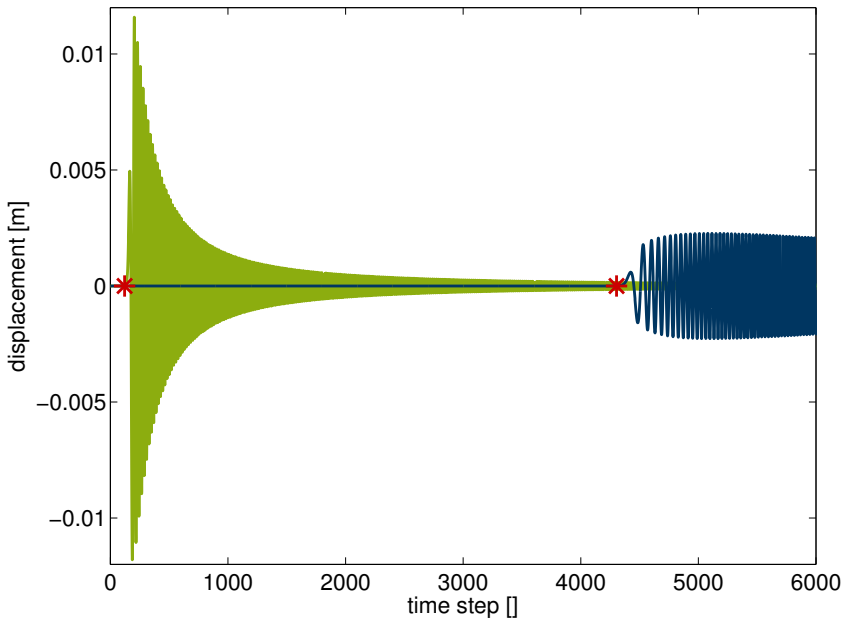

Figure 5.7: Displacement signals of two particles, one near the excitation (green) and one near the end of the chain (blue), excitation method: pulse, used threshold: 10^{-6}m, reference chain

the signal close to the excitation is very small in compare to the first maximum. Following, the arrival time is independent of the shape of the curve and the arrival time is smaller than using the first maximum. The displacements of the particle close to the boundary are in general lower, but the amount of displacement at which the arrival time is defined, is in compare to the first peak very small, too. Considering the reference chain and using the forward shifting method, the wave velocities for the pulse and the sine excitation are showed in figure (5.8). For the pulse excitation the back-calculated wave velocities match in the beginning more precise the input wave velocity in compare to the sine excitation. However, the general behavior is similar. In the beginning the curve changes it slope fast. In the middle part the slope is flat and at the end the it becomes very steep. The

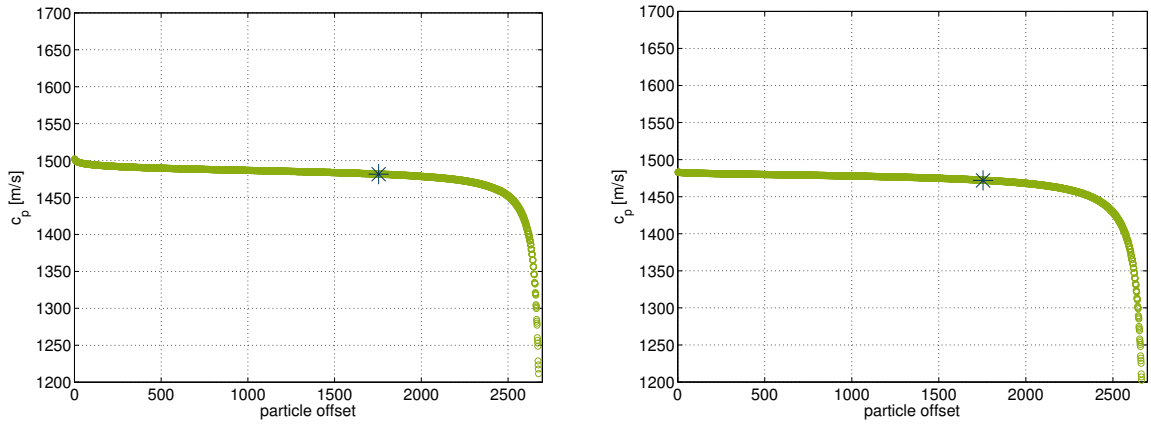

Figure 5.8: Wave velocities obtained by the forward shifting threshold-method for two different excitation: left: pulse, right: sine, threshold pulse: 10^{-6} m, threshold sine: 10^{-8} m, reference chain

changes in slope clearly show boundary effects, that lead to an inaccurate wave velocity calculation. To avoid both boundaries, in the following figure 5.9 the already explained mixed shifting method is used. The wave velocity is plotted over the mixed shifting offset.

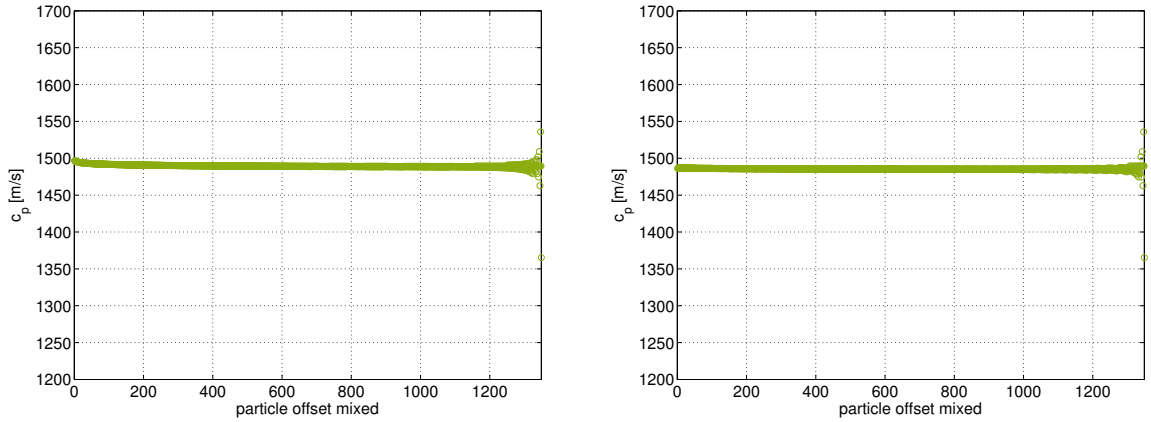

Figure 5.9: Wave velocities obtained by the mixed shifting threshold-method for two different excitations: left: pulse, right: sine, threshold pulse: 10^{-6} m, threshold sine: 10^{-8} m, reference chain

The boundary effects disappear clearly with distance to both boundaries. In the middle a plain is recognizable, with a relative error of the back calculated wave velocity from the input wave velocity smaller than 1 %. This plain is much more stable than the one found in the plotted wave velocities for the forward shifting method. At the end the slope is steep and the wave velocity has a huge error.

The two next described methods "Edge-finding using test functions" and AIC method try

to localize the very first arrival of the wave. These are more mathematical based methods to find the first arrival than using an arbitrary threshold.

5.1.3 Edge-finding algorithm

To find the edge of the arrival wave, two test functions are defined (cf. [19]. For each test function, an area in time space is defined. Both areas start at the same point and have an equal length. The difference is the movement direction, on to smaller time values, the other to higher time values. Then the sum of the amplitudes in the right area are divided by the sum of the points in the left area to get a maximum at exactly that starting point, at which the wave arrives. The length of the areas are constant and the starting point is looped over the time. The procedure is displayed in equation 5.4, a pseudo code.

$$D_k = \left(\sum_{i=k}^{k+n} abs(X_i) \right) / \left(\sum_{i=k-n}^{k} abs(X_i) \right) \tag{5.4}$$

The range is represented by n and the starting point is represented by k. X_i is the (displacement) amplitude at each point. Applying the test function to the reference chain, and picking up the peaks, the resulting wave velocities for the mixed offset method are shown in figure 5.10. The wave velocity is plotted over the mixed particle offset. The calculated wave velocity is strongly distributed, which is not correlated to the input value. This figure suggests, that there can be slopes of the curve found, that are not visible in the normal zoom. If we zoom in the signal, we can find slopes that cause the peaks of high intensity. Slopes that do not correspond to the arrival of the wave, for example shown in figure 5.11, are identified by the method as arrival times, because the code detects only points at which any significant change in the curve happens and it does not care about the amount of values. In figure 5.11 the displacements over the time is shown. The time is sclaed by the time step. The range n was chosen to be 10. The curve in the

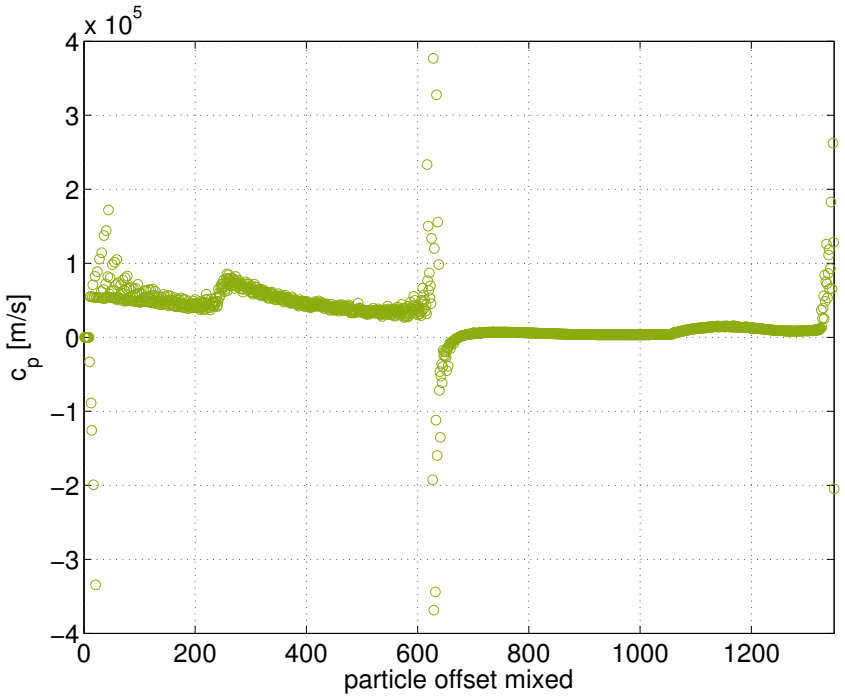

Figure 5.10: Wave velocities obtained by the mixed offset edge-finding algorithm for the pulse excitation, reference chain

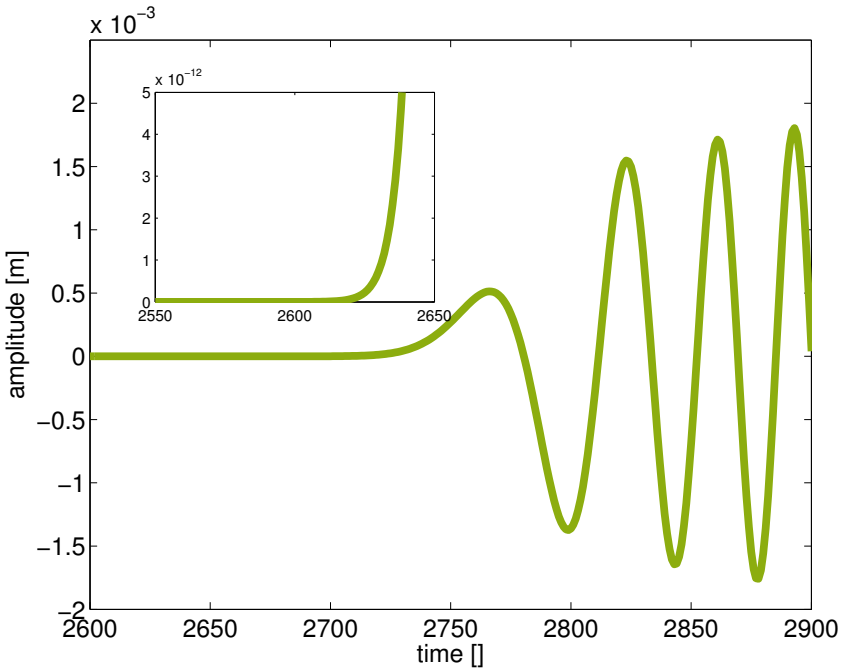

Figure 5.11: Displacements obtained by a simulation of the reference chain using a pulse excitation

inside-figure is a window-shot taken from the curve in the main figure. The curve in the main figure shows clearly the arrival of the wave, identified by the change of the slope. In

the beginning, the curve is flat and remains flat if we would go to the left. However, in the in-plot figure one can detect a slope, with completely different amount-values. This slope lies obviously out of the range of the arrival time of the wave velocity and could be misinterpreted as the arrival time. Changing the range does not lead to a better result. Smaller values are not useful, because then the difference between the two summations is too small. If the range is enhanced, the discarded first and last time steps must be also enhanced. Anyway, the change of a bigger range was investigated and only a slight improvement was found.

5.1.4 Akaike Information Criterion-based (AIC) method

The AIC method is a "measure of goodness-of-fit between a signal and a model" [19]. In contrary to the previous edge-finding method, here a minimum is reached, when the wave arrives.

$$D_k = \left(\sum_{i=k}^{k+n} abs(X_i) \right) / \left(\sum_{i=k-n}^{k} abs(X_i) \right) \tag{5.5}$$

It is noted that the AIC method should in general handle better signals with noise, disturbing the real signal. Therefore the method is expected to handle also better with the "false arrival times" found in the subsection before. Again, the reference chain is used to analyze the AIC method. In figure 5.12 the wave velocity is plotted over the mixed particle offset. The arrival times are determined by picking the first minimum and the initial configuration for the distance is used. The AIC-method used to calculate the wave velocity shows in general more accuracy than the previous presented edge finding algorithm. In the beginning of the slope, the values are higher, then start to decrease till they reach a flat of about 1500 m/s to 1505 m/s. The start is characterized by the boundary effects. At the end, the deviation from the input wave velocity rises again,

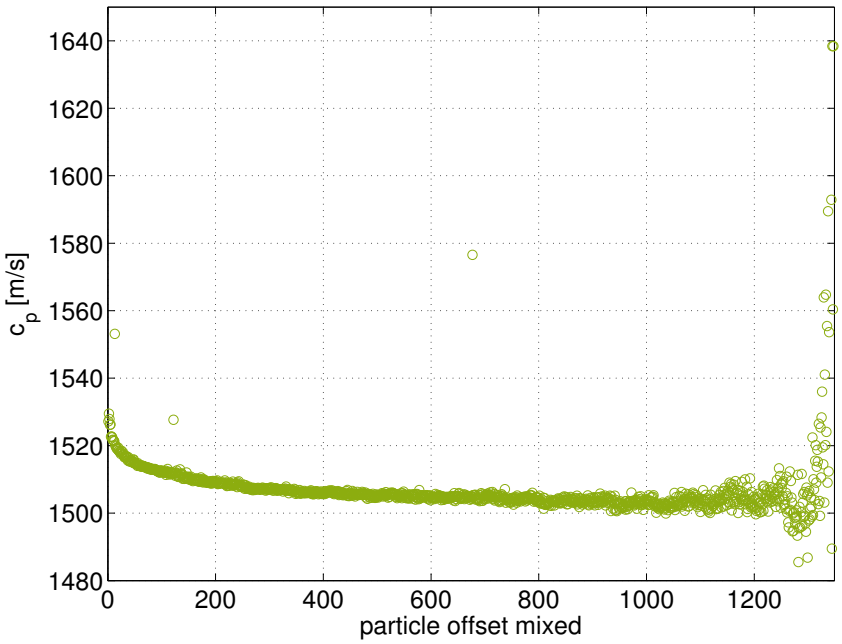

Figure 5.12: Wave velocities obtained by the mixed offset AIC method, pulse excitation, reference chain

because the distance between the particles is going towards zero. In general, the relative error between the calculated wave velocity and the input wave velocity is at no stable area smaller than 1%. In the flat part, the error is between 1.3% and 1.6%.

5.1.5 Cross-correlation

Cross correlation (cf. [6], [38]) is a method that does not consider the arrival time of a propagating wave to determine the wave velocity. It compares two signals on equality and observes their time shift. If for example two signals are only time shifted with three time steps, the output is a function, with the peak at the third time-step. If the curves have not the same shape, the differences between the peak and the surrounded values are getting smaller with rising inequality in shape. Therefore, if the wave forms are too different, the method would fail. On the other hand, this method has the advantage, that it does not need to consider the arrival times of the waves and may be for this reason more precise. The method is proceeded with MATLAB, using the `xcorr()` function. In figure 5.13 the wave velocity of the sine and pulse excited reference chains are plotted over the mixed

particle offset. The back calculated wave velocities are shown for the pulse excitation on

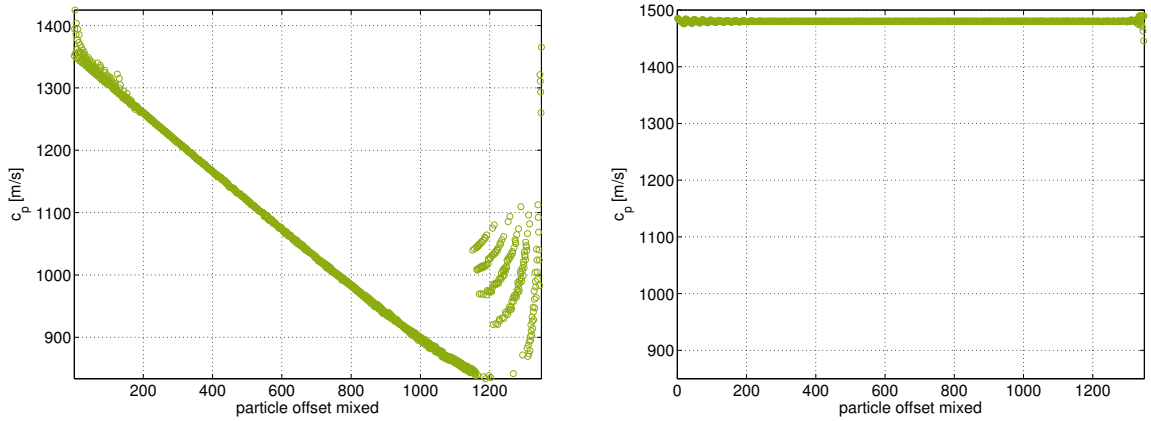

Figure 5.13: Wave velocities obtained by the Cross correlation-method for two different excitations: left: pulse, right: sine, reference chain

the left. A linear graph is found, that is decreasing with the particle offset. The relative error is never found to be smaller than 5%. For the sine excitation the relative error is much smaller. It is in the beginning, where both boundaries influence the wave velocity, about 0.35%. In the middle part the wave velocity reaches a flat curve, where the wave velocity fluctuates of about ± 1 m/s around the input wave velocity of 1481 m/s. At the end, both figures reflect the smaller distance between the particle numbers and the error rises.

For the sine excitation the cross correlation is found to be useful, because a flat exist, where the relative error is between 0.04% and 0.1%. Using cross correlation for a pulse excited wave is useless, since the wave velocity never reaches a flat and the relative error is never smaller than 5%. Looking for the big relative error of the cross correlation applied to a pulse excited chain, the reason is found in the change of shape of the time signals while the wave propagates through the chain. In figure 5.14 the time amplitude signals are plotted for two particles. The first and the last particle time signals are scaled by their maximum value and plotted. The time is also scaled dimensionless by the time step. The signal for the first particle is in the beginning high, that is related to the excitation displacement, and then the oscillations disappear over the time. For the last particle the behavior of the signal is contrary. First it is small, and then the oscillations are getting bigger. This process-order is related to the development of the wave. The contrary

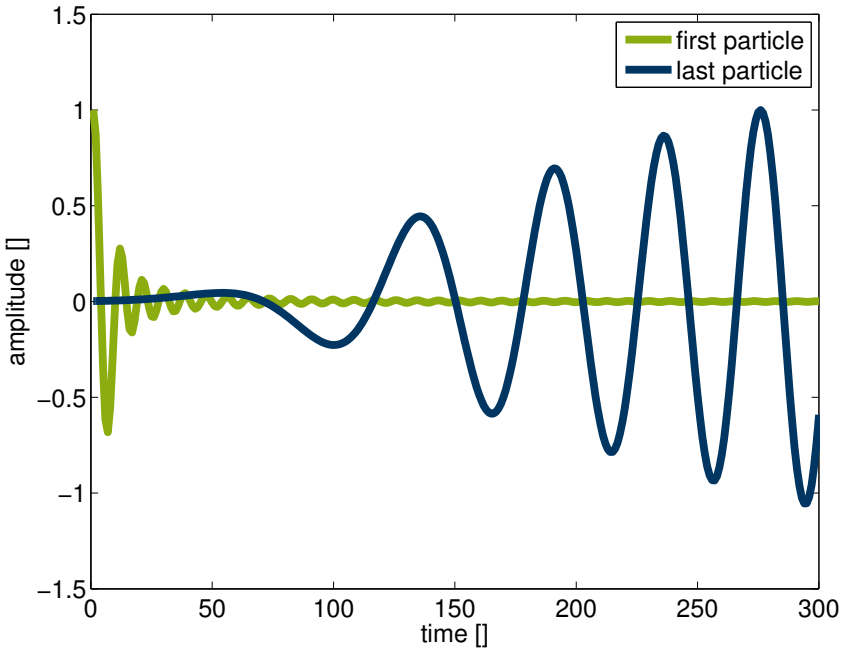

Figure 5.14: Two time signals plotted of the pulse excited reference chain, cut signals, the time is scaled by the time step, the amplitude is scaled by its positive maximum

behavior of the signals is responsible for the big relative errors of the cross correlation method. It is not possible for the algorithm to find a good time shift for that the curves are well correlated.

5.1.6 Summary and conclusion

The introduced methods to obtain the wave velocity were introduced and compared. The peak method leads to the most accurate and stable results of the wave velocity. Additionally, the relative errors in % are shown in table 5.1. For the peak and the threshold the errors are calculated between the first and the last particle, so that these values are comparable with those obtained by the cross correlation. Additionally in this way always the full chains are considered, which is important if an experimental setup as shown in chapter 3 is modeled. For the edge finding algorithm and the AIC method the wave velocity is calculated between the tenth and the (N-10)th particle. The peak method leads to the smallest errors for both excitation methods, while with the cross

	Sine excitation	Pulse excitation
Peak method	0.089	0.317
Threshold method	0.348	1.050
Edge finding	-	>30
AIC method	-	3.518
Cross correlation	0.3309	3.852

Table 5.1: Relative errors in % of the wave velocities for the different presented methods dependent on the excitation methods

correlation the second smallest error is obtained for the sine excitation. The threshold method is the second most accurate for the pulse excitation. Because the peak method is the most accurate one and rather insensitive to the driving shape, it is used for the calculation of the wave velocity for all following simulations. To minimize the calculation effort, here the boundary effects are accepted, because for the peak method the relative error between the first and the last particle of the reference chain was smaller than 0.4%.

5.2 Frequency spectrum

The wave propagation can be also studied in the frequency domain. For this, the transformation of the time signal to the frequency domain is investigated for the reference chain. The methods to obtain the frequency spectrum are divided into a pure fast-Fourier transformation method (FFT) over all time steps, a FFT method applied to a cut signal using a rectangular and a Hanning window. The frequency spectrum is dependent on the time step, because the frequency is related with time by $f = 1/t$. If a signal is discrete, which is here the case, the width of the time step must be so small, that the discretization reshapes the signal fully. If the time step is too big and the signal cannot be recovered by looking at the discretization, then this error is called aliasing. To avoid aliasing, the

Nyquist-Shannon sampling theorem (cf. [12]) can be used.

$$f_{sampling} \geq 2 f_{max} \tag{5.6}$$

It states that the sampling frequency should be greater or equal to two times the highest frequency of the signal component. This condition is applied to all following simulations. To show the effect of aliasing, three different time steps were investigated. In figure 5.15 the Fourier amplitude is plotted over the frequency for different sampling frequencies. The

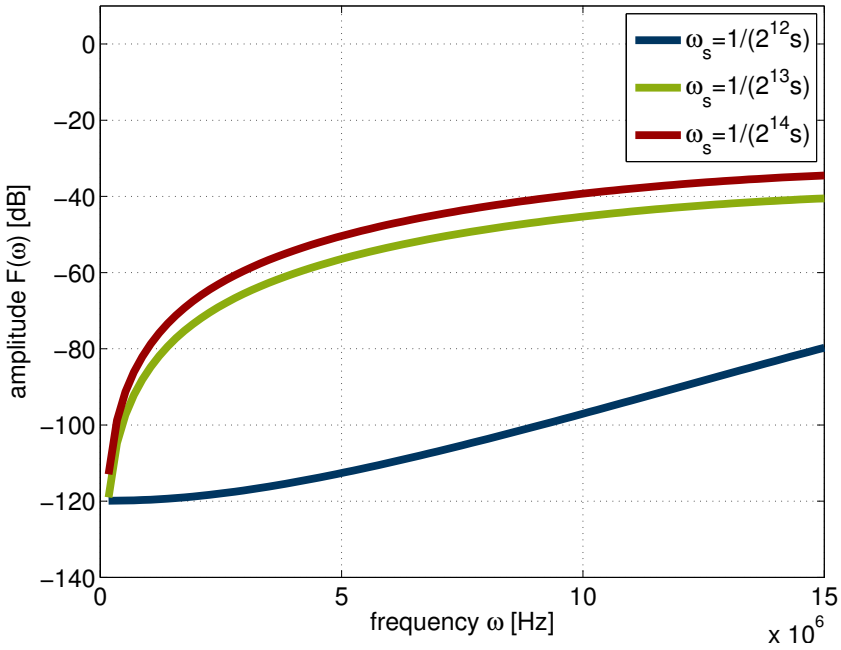

Figure 5.15: Fourier Spectra obtained from simulations of reference chains with different time steps, pulse excitation

displacement-time signal was taken from the last particle of the chain. The two highest sampling rates (green and red curves) lead to the same qualitative shape of the Fourier spectrum. Only the magnitude is a little bit lower for the second highest frequency. Looking at the smallest sampling frequency (blue curve), a totally different shape of the curve is found, caused by the aliasing effect.

Knowing that the results of the FFT depends on the input and knowing that the sine and

pulse excitation lead to different wave forms (5.16), both cases have to be investigated considering the frequency spectra. The displacement time signals are plotted for the pulse

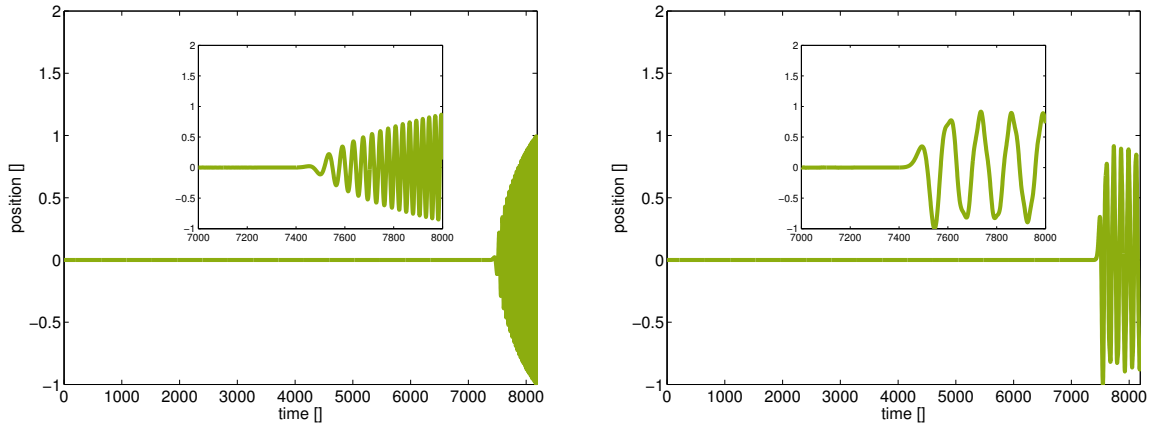

Figure 5.16: Displacement-time signals of the last particles for the pulse excitation (left) and the sine excitation (right), reference chain. the inset shows a zoom into the arrival area of the wave

(left) and sine excitation (right). The displacement is scaled by its maximum value and the time is scaled by the length of one time step. The inner figure is a zoom of the cut of the time signal. The signals shown here are obtained by looking at the last particle of a chain. Therefore, in the beginning no displacement is visible. For the case of the pulse excitation, the wave reaches the signal and is getting stronger with time. The peaks build up a smooth envelope. The time signal for the sine excitation is not as ordered and shows no increase. Without consideration of more details, it is obvious that the signals should lead to different frequency spectra, if a FFT is applied.

5.2.1 FFT-method over time

The FFT-method treats the particle signals for all time steps, without any change in the signal. The Fourier transform was applied to the last particle signal of the reference chain for both excitation methods. The result is displayed in figure 5.17. Left, the Fourier spectrum for the pulse and right for the sine excitation are shown. As expected, the spectra are different in shape and amplitude. The left spectra is more flat and the amplitudes

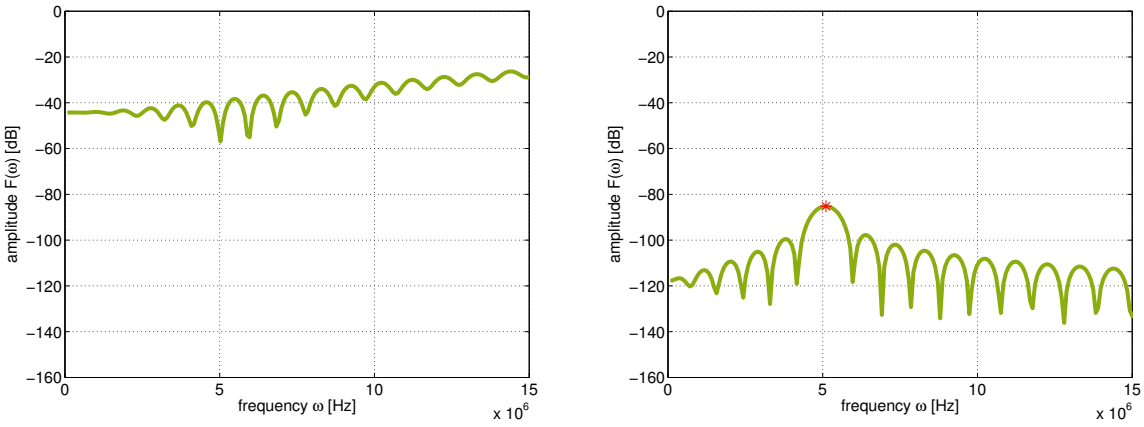

Figure 5.17: Fourier spectra for the pulse excitation (left) and the sine excitation (right), reference chain

are higher, while the right spectra has a clear peak around 5 MHz. The peak is marked with a red star. In both cases, oscillations are visible, which correspond to the boundary reflections. To remember, the cut off frequency of this chain is 148.1 MHz. Recalling by looking at the position-time carpet, e.g. for the pulse excitation 5.2, that shows the displacements at each position for each time step, one can see at the wave is reflected at the fixed end of the chain. The use of a time window can avoid the influence of the reflections on the Fourier spectrum. Another possibility would be to use a particle signal, that is not influenced by the reflections: However, when different material layers are used, the frequency develops over space. Therefore the problem has to be handled different. The third possibility is to use a simulation time that ends at the arrival of the wave, but this has the disadvantage that the wave velocity cannot determined by the peak method anymore, which was found as most precise (comparing the here investigated methods). The fourth possibility is based on a longer chain, which circumvents the problem just letting the signal develop to particles that are not part of the investigation chain. The disadvantage is that this method leads to a higher computational effort due to more particles. In the next two subsections, it is investigated how to cut the signal of the last particle, so that no reflections are visible. This can be used then to determine the frequency spectrum without higher effort or loss of information. Two windows, a rectangular and a Hanning window are investigated in 5.2.2 and 5.2.3, respectively.

Before the windows are discussed, the frequency propagation is introduced. This visualizes

which frequency component is carried by the wave more strongly, which are weak and which are erased along the chain. The frequency propagation for the pulse and the sine excitation is shown in figure 5.18. The frequency is plotted against the position. White

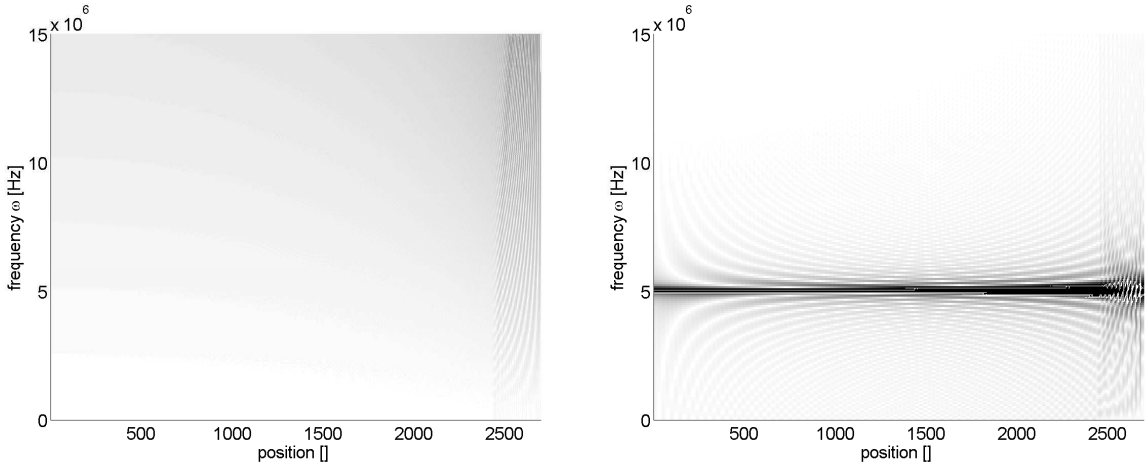

Figure 5.18: Frequency propagation: left: pulse, right: sine, reference chain

means no frequency component of the wave is available and the darker the signal, the more the Fourier-component is available. In the left, the frequency propagation for the pulse excitation is shown. A wide range of gray values are visible, which indicates that the pulse excitation leads to a frequency propagation of many frequencies. Higher frequencies propagate better than the low frequencies. In the right, a clear branch of 5 MHz is visible. This branch is created by the excitation frequency. At the end of both plots a reflection is visible marked by the vertical stitching. For both excitation methods the frequency propagation is undisturbed, which leads to a smooth and constant frequency propagation. The waves carry the frequencies quite differently. The sine carries mainly the excitation frequency and the pulse leads to a wide bandwidth of frequencies.

To emphasize the necessity of a time window, in figure 5.19 the frequency spectra over all time steps for different particles are shown. The frequency amplitude in dB is plotted over the frequency. It is found, that all frequency spectra have oscillations, independent on the particle position in the chain. Therefore, a windows has to be applied to the time signal before the FFT is used.

The frequency spectra of the reference (pure water) chain were obtained by the FFT. It was applied to the last particle for the full time, because it is assumed that the frequency

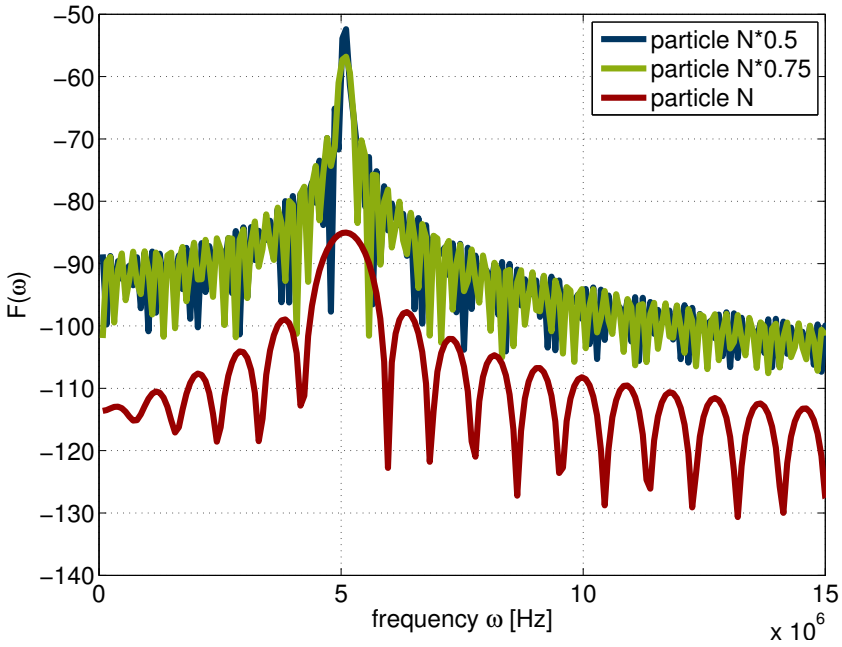

Figure 5.19: Fourier Spectra obtained from simulations of reference chains over the complete time for different particles, N is the total number of particles, sine excitation

propagation changes, if a sample is placed in-between two water layers. It is found, that oscillations spoil the frequency spectrum. In the next two section the time signal (on which the FFT is applied) is cut by two types of windows, to reduce the oscillations.

5.2.2 FFT-method over time using a rectangular window

The rectangular window cuts off the signals outside the window range. It is of the form

$$R_n^k(x) = \begin{cases} 1, & \text{if } n \leq x \leq k \\ 0, & \text{otherwise} \end{cases} . \tag{5.7}$$

All values that are out of the range are cut off. The values inside the range are kept originally. This can lead to a high jump from one to the next value, depending on the signal. The chosen time range is from $0.45 * T_{\text{sim}}$ to $0.98 * T_{\text{sim}}$. The frequency spectrum

of the last particle of the reference chain is shown in figure 5.20, left. The Fourier spectra

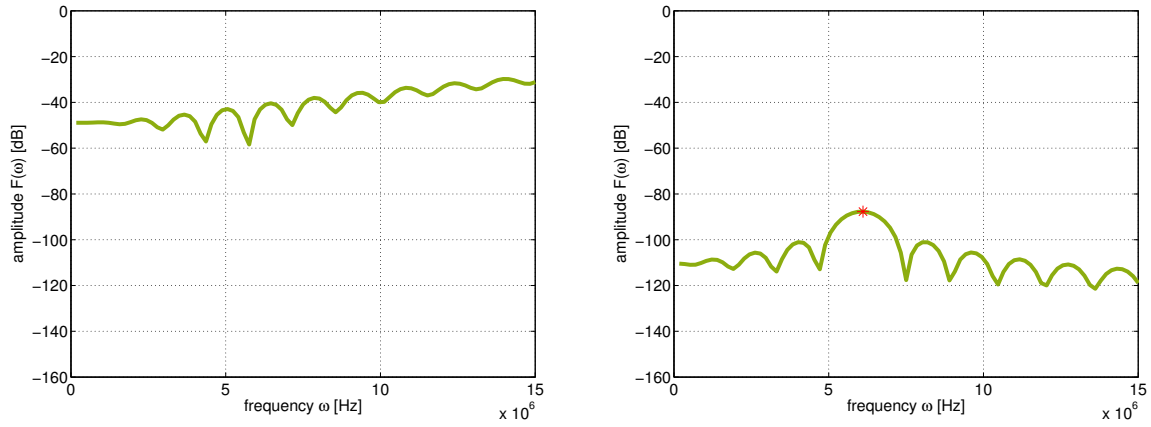

Figure 5.20: Frequency propagation calculated using a cut time signals: left: pulse excitation; right: sine excitation

look similar to them obtained by using the full time signal. The main difference is that oscillations in the signals are weaker and less existent. This is due to the cut off of the reflections and the cut off of the beginning of the signal, which contains no information about the wave. The left oscillations are existent, since not all reflections can be cut. It is not exactly clear, where the reflection occurs and at which time the signal has to be cut off. Additionally, the boundaries of the rectangular window create oscillations. The boundary effects can be avoided if a window is used, that has smooth edges. Therefore in the next subsection 5.2.3 the Hanning window is used.

5.2.3 FFT-method over time using a Hanning window

The Hanning window is applied to the same time range as used for the rectangular window. Instead of cutting the ends, a smooth approximation at both ends is made. This smooth progression is defined by the related function, which pseudo code is presented in equation 5.8.

$$H(x) = 0.5\left[1 - \cos\left(2\pi\frac{x}{n}\right)\right], \quad 0 \leq x \leq n \tag{5.8}$$

The Hanning window, computed with the MATLAB function `hann()`, is visualized in 5.21. The amplitude values of the value are plotted over an arbitrary length. At both

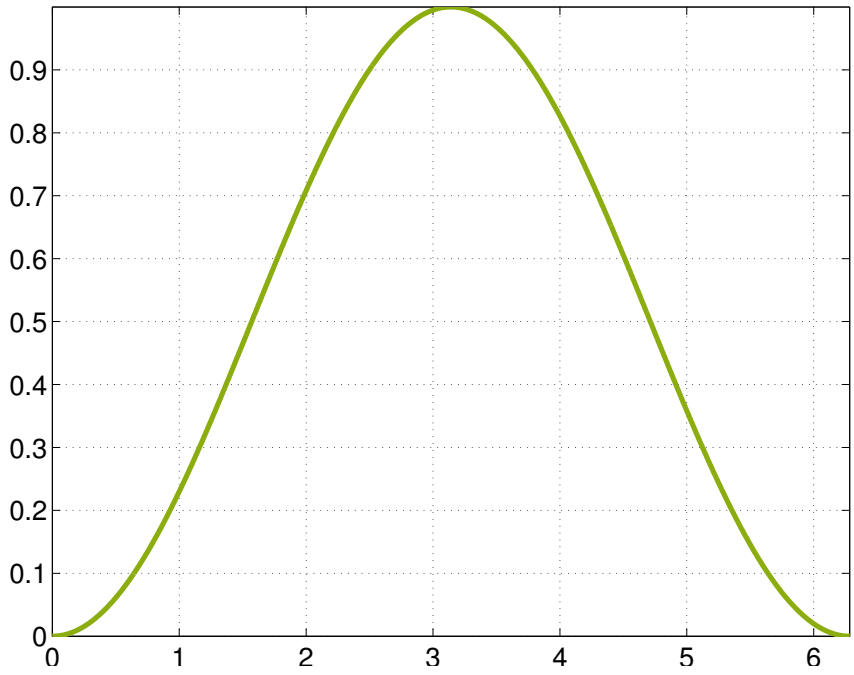

Figure 5.21: Hanning window

sides, the window is getting smaller and nestles to zero. The sharp effect from the zero value to the original signal value, what is created by the rectangular window, is avoided. Therefore, less periodic oscillations are expected. In the middle of the window the value is one, so that there the signal is kept originally. One disadvantage of the window, or a window in general is, that it is a data manipulation. It changes the values by scaling with the related amplitude values of the window. Data manipulation can lead to for the worst case to wrong values. The chosen time range is from $0.45 * T_{textsim}$ to $0.98 * T_{textsim}$. The window is applied to the signal by multiplying each value of the window with each value of the signal. In figure 5.22 the frequency spectra for the reference chain with a cut signal using a Hanning window for the pulse and the sine excitation are shown. In the right, the Fourier spectrum obtained from the sine excited chain is shown. A clear main peak of around 5 MHz is visible. Aside this peak, the amplitudes fall. No more oscillations are visible in the signal, which was the case for the rectangular window. The amplitudes in general are smaller than the amplitudes obtained without any window (cf. fig. 5.17).

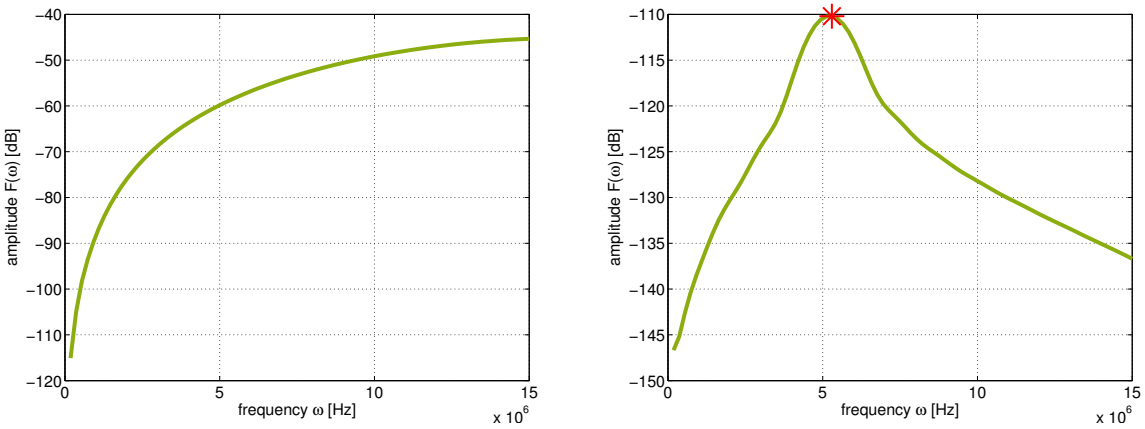

Figure 5.22: Frequency spectra calculated using cut time signal (Hanning window): left: pulse excitation; right: sine excitation, the chosen time range is from $0.45*T_{\text{sim}}$ to $0.98*T_{\text{sim}}$

This is caused by the cut and additionally by the reduction of the remained values caused by the multiplication of the signal with the window. In the left, the Fourier spectrum obtained from the pulse excited chain is shown. Here, comparing the signal with the one obtained by the overall FFT, a change of the shape is found. The smaller frequencies are less visualized than the higher amplitudes, so that the former linear branch is not more visible. The amplitudes are lower, comparing again with the spectrum obtained using the full time signal or the rectangular window. The positive remark is, that the oscillations vanished. Another advantage is that the main frequency peak can be detected accurately. The disadvantage of that window is that the width of the signals is getting larger, which is for example visible by looking at the main peak around 5 MHz of the sine excitation. This may be also the reason why the shape of the spectrum changed in compare to the two other spectra. However, beside the change of the shape for small frequencies of the spectrum for the pulse excited chain, the method using the Hanning window lead to the smoothed Fourier spectrum. The smoothed spectra are now investigated with respect to the chosen time window. In figure 5.23 the time signal (purple) obtained by a Sine excitation, different Hanning windows (blue, green and red) are compared to the related frequency spectra. The qualitative frequency spectra are found as independent on the chosen time windows. The wider the Hanning window is chosen, the higher the resolution found in the frequency spectra. Thus, the blue window is chosen as the best, because in

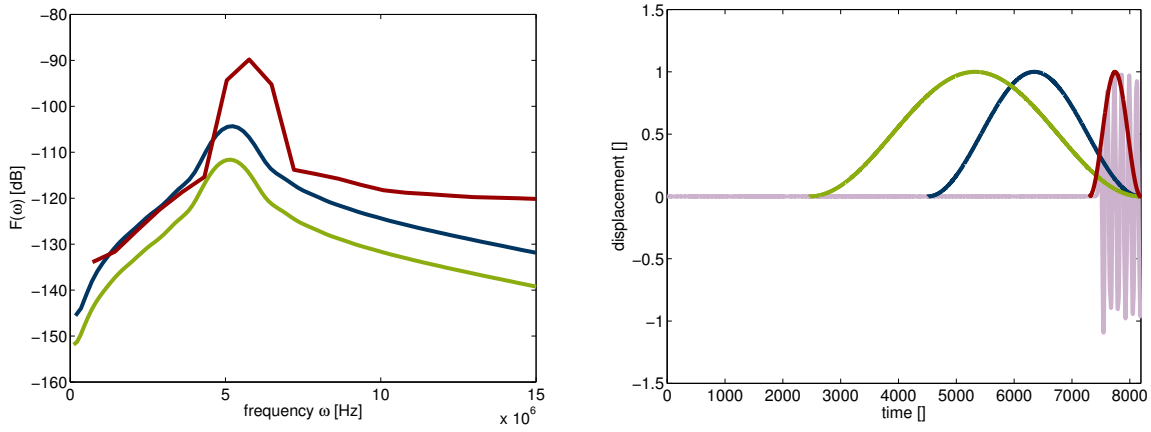

Figure 5.23: Frequency spectra compared calculated using different Hanning windows (blue, green and red), reference chain, sine excitation, on the right the time signal is shown purple

the related frequency spectrum (blue) no discretization is visible. The range is given as $0.45 * T_{\text{sim}}$ to $0.98 * T_{\text{sim}}$. Since the Fourier-amplitudes are only important for attenuation, it is here not considered. Anyway, the amplitudes of attenuation are obtained by the ratio of two frequency spectra.

5.2.4 Summary and conclusion

Different ways how to obtain the frequency spectrum were described. They all have advantages and disadvantages. The fourier spectrum using the whole time window has the advantage, that all frequencies of the propagating waves are completely included. The disadvantage is, that the reflections are also considered. To avoid the reflection contents, two time windows were introduced, the rectangular and the Hanning window. The oscillations and therefore the reflections were reduced, but not completely. The Hanning window smoothed the curve, but the shape for the pulse excitation was changed. Keeping that in mind while looking at the calculation of the attenuation (ratio of two frequency spectra), it is assumed that the change of shape does not influence the attenuation values. The Hanning window is used before applying the FFT on the time signals in the above given range for all following simulations.

Chapter 6

Simulation of the experimental setup

To show that the one-dimensional particle chain (cf. 4) predicts experimental results well, a model wit the real experimental setup (cf. 3) is investigated. For the determination of the spring stiffness, the experimentally obtained wave velocity is used (cf. 4.22). The simulation results wave velocity, frequency spectrum and attenuation are then analyzed and compared with the experimental results to validate the simulation model. For a solid sample, no influence of micro-structure is present. The model is investigated first with respect to the particle size, the discretization. For that, the simulation results wave velocity, frequency spectrum and attenuation are examined for independency on the discretization. The particle chain is divided into three layers, water-aluminium-water, as shown in figure 6.1. The aluminium layer is as long as the real aluminium specimen, namely 6.08 mm and it is placed symmetrically in the middle of both water layers. For each layer, the input to adjust the particles are different. The particles in the water layers are adjusted with the wave velocity of water, 1481 m/s and the density of 1000 kg/m^3. Theses values are obtained by literature, e.g. [2]. The particles in the aluminium chain are adjusted by the experimental obtained wave velocity of 6294 m/s and the density of aluminium of 2700 kg/m^3, looked up in the literature. Because this model needs aside of physical input parameters also discretization parameters (cf. table 4.1), different particle radii and time

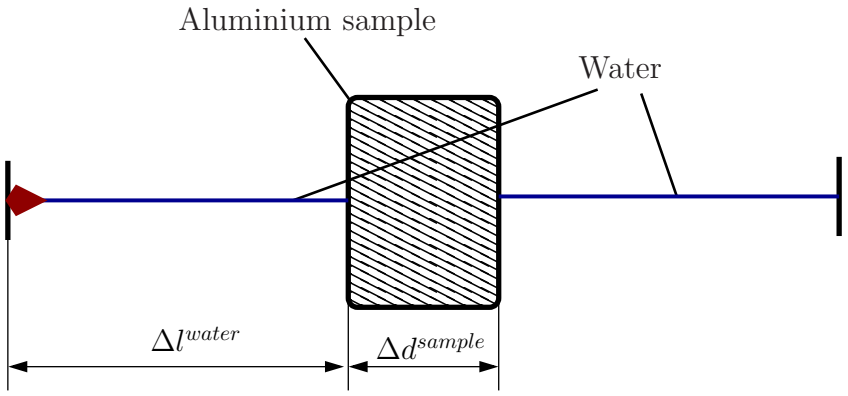

Figure 6.1: Scheme of the experimental setup with the aluminium sample

steps are investigated. The length of the chains are build as most similar to the experimental setup as possible. That means, if the particle radius is changed, the length of the chain is kept constant with respect to the distance between the ultrasound transmitter and receiver of the experiments. The excitation frequency for the sine excitation is 5 MHz and the amplitudes for the pulse and the sine excitation are 0.05 m. The number of time steps are 2^{13} and the simulation time is $80 * 10^{-6} s$; for all simulations. The wave velocity obtained by the the simulations should match the wave velocity of the experiments, because the velocities of water and aluminium are used to adjust the particles. It is not expected, that the frequency and attenuation spectra are matched, because another wave excitation is used.

In table 6.1, the properties of three exemplary different investigated chains are shown to explain the dependency of the chain on the particle size. These chains use one uniform particle diameter and three layers representing the phases water-aluminium-water. By

r_p [mm]	N_p^s	N_p^w	ΔT_{st} [s]	N_I^{total}	N_I^s
0.008	380	3185	$9.76562 * 10^{-9}$	2	0
0.04	76	637	$9.76562 * 10^{-9}$	2	0
0.4	7	64	$9.76562 * 10^{-9}$	2	0

Table 6.1: Chain parameters

decreasing the particle radius, the number of particles have to be increased in order to keep a constant chain length. Due to the fact that a simulation for a chain of many particles needs more memory and more time than a simulation with less particles, the

discretization parameter particle radius should be chosen as small as necessary and as big as possible. The time step is not responsible for the accuracy of the analytical solution, but it is responsible for the discretization in time. It should be as small as necessary (with respect to the Shannon-Nyquist Theorem) and as big as possible. In the following section, the spatial discretization is investigated by the choose of different particle radii.

6.1 Chains of constant particle radii

To simulate the experimental setup, the one dimensional chain is build up as close as possible to the experimental setup. In this section, the same particle radius for all particles are used, independent of the layer. The effect of the particle radius is then investigated with respect to the output. The dependency of the wave velocity, the frequency spectra and attenuation on the spatial discretization, the particle size, is investigated.

6.1.1 Wave velocity

The wave velocity is back-calculated from the simulation results, using the peak method, which is introduced in chapter 5. The overall and the sample wave velocities are calculated. The overall wave velocity is the mean wave velocity between the ultrasound transducers or regarding simulations the mean wave velocity between the the first particle and the last particle. Additionally, the experimental way of wave velocity calculation (cf. 3.1) is used to determine the sample wave velocity. For the comparison of the back-calculated wave velocities, first the experimental value has to be determined. The sample wave velocity was already calculated and is 6259 m/s. For the calculation of the overall velocity, the arrival time of the reference wave and the wave velocity of water is used to calculate the distance between the transducers. Further on, the arrival of the wave of the examined setup with the sample is used together with the distance between the transducers to

calculate the wave velocity. This leads to the equation 6.1.

$$c_p^{overall} = \frac{\Delta d_{Transducers}}{\Delta t_{sample}} \tag{6.1}$$

The overall wave velocity value is calculated to be 1535.4 m/s.

6.1.1.1 Wave velocity of the sample material

The wave velocities of the aluminium specimen are examined with respect to the discretization. The discretization should be as small, so that the wave velocity is not influenced by the particle radius. For this, additional to the chain of the three layers water-aluminium-water, full water chains of the same particle radius are simulated. Using the full water chain and the chain with the sample, the wave velocity of the aluminium sample can be calculated using equation 3.1. The results of the wave velocity using the experimental way can be found in figure 6.2 for sine and pulse excited waves. The cal-

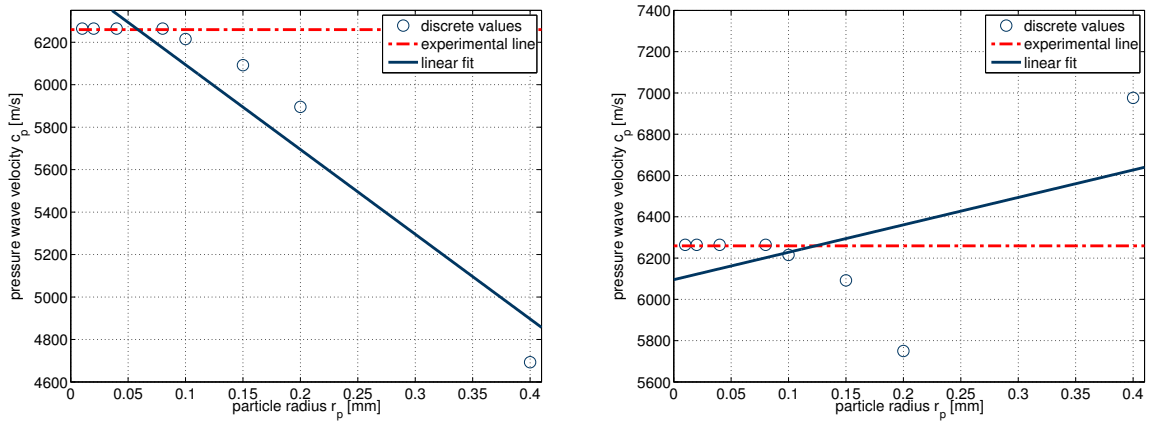

Figure 6.2: Sample wave velocities obtained by the experimental wave calculation, the time difference Δt is obtained by the first peaks of the signals, left: pulse excitation, right: sine excitation; experiments simulating particle chains (water-aluminium-water)

culated wave velocity is plotted (blue circles, discrete values) over the particle radius. The experimental line shows the input wave velocity and the linear branch (blue solid line) is the fit of the discrete wave velocities. It is found out, that for the fourth smallest examined particle radii, the wave velocity can matched with an error smaller than 1% for

both excitation methods. In fact, the values are constant with an value of 6264.40 m/s for both methods. Considering the relative error of 0.077%, it is very small. For the chains using higher particle radii than 0.08 mm, the wave velocity calculation fails and leads to a high error. In summary, for the calculation of the wave velocity of the sample using the experimental way, a plateau was found, where the wave velocities are constant. That means, in that range the wave velocity is independent of the discretization particle radius. Stepping out of the range, which means using higher particle radii, the method fails.
The wave velocities from the simulations using particle radii smaller than 0.08 mm, compared with the experimental wave velocity, show a very good match. The method leads to an acceptable error, so that the wave calculation method for this case is confirmed and it is shown that a range of discretization exists that is small enough to not influence the sample wave velocity.

6.1.1.2 Overall wave velocity

Here, the overall wave velocity of pulse and sine excited waves are observed to find the influence of the discretization (the particle radius) on the overall wave velocity. In figure 6.3 the wave velocities back calculated from the simulations (discrete values) are displayed for some specific particle radii. These wave velocities are the wave velocities of the full chain, representing the experimental model. In the left the wave velocities are plotted over the particle radius and for the excitation the pulse method was used. The experimental line shows the input wave velocity. The back calculated velocities (discrete values) are obtained from the simulations. In opposite to the right figure, the wave velocity obtained by the particle chain of 0.5 mm is strongly deviated to the input wave velocity and out of sight. All other wave velocities are located slightly over the input velocity, except the value for 0.01 mm, which matches the input wave velocity very precise. Regarding the wave velocities that lie commonly about the input wave velocity, the error could be either a general error by the back calculating method of the wave velocity, or the error is

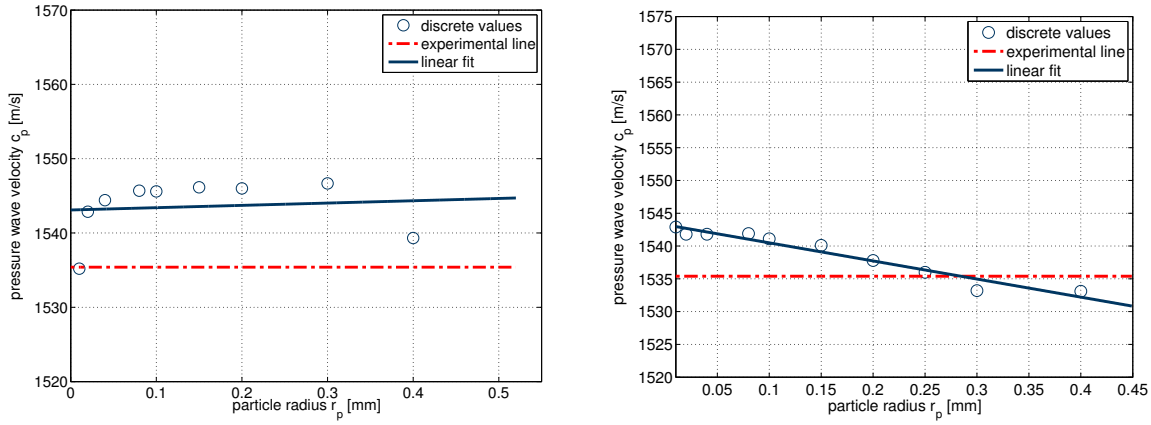

Figure 6.3: Overall wave velocities obtained by the mixed offset peak method, using the first and the last particle: left: pulse excitation, right: sine excitations; experiments simulating particle chains (water-aluminium-water)

created by the interfaces. This last assumption is based on a parameter study regarding the number of interfaces in A.1. Contrary to the here found higher wave velocities, it is shown that with increasing interfaces the wave velocity is decreasing. Therefore these errors are handled as general errors due to the calculation method. Creating a linear fit without considering the last particle, the constant trend is confirmed. The linear curve approximately does not change with the particle radius. All relative errors between the back calculated wave velocities and the input wave velocity are smaller than 1%, except for the discordant value regarding the particle radius of 0.5 mm. On the right of figure 6.3 we can see the results using the sine excitation. All related relative errors to the input wave velocity are smaller than 1%. The input wave velocity is represented by the experimental line, which shows the wave velocity obtained by the experiments. It can be recognized, that the wave velocity for smaller particle radii is higher than the input wave velocity. It is decreasing for higher particle radius. Using a linear fit, the back calculated wave velocity would exactly match the input wave velocity only at a particle radius around 0.28 mm. Passing that matching point, the wave velocities are smaller than the input wave velocity.

Here, the experimental chain was simulated with chains of constant particle radii and the wave velocities were calculated for the sample and for the full chain. For the back calculation of the overall wave velocity, the time and the spatial difference between the

first and the last particle of the chain was used. For the pulse excitation a plateau that lies slightly over the input values was found. There, the discretization does not influence the wave velocity highly. For the sine excitation a decreasing behavior was found. For both excitation methods, the errors are smaller than 1%, the biggest error is 0.734 % for $r_p = 0.3$ mm of the pulse excitation. The only exception is the particle radius $r_p = 0.5$ mm, that was found as not usable due to its high relative error of more than 4%, so that larger particle radii are not studied. Additionally, with a particle radius of 0.05 mm, the sample can not be modeled with respect to the exact length.

6.1.1.3 Visualization of the structure

To visualize the structure in the whole chain, the carpet diagram position-time can be used. The wave propagation can then be understood more easily and reflections in the model are visible. For the pulse and the sine excitation the carpet diagrams are shown in figure 6.4. The displacement intensity is plotted over the time. In both diagrams, left

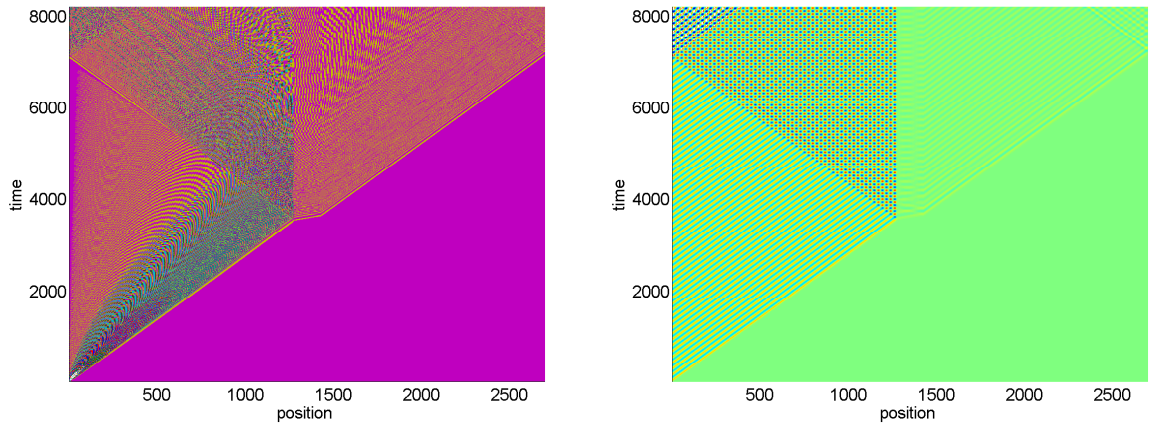

Figure 6.4: Carpet diagram position-time, the time is scaled by the time step and the position by the particle diameter, particle radius for both chains $r_p = 0.02$ mm, left: pulse excitation, right: sine excitation, experimental chain setup

for the pulse excitation and right for the sine excitation, the wave propagation is clear visible. The slope is constant, until the wave reaches the aluminium specimen. Then the slope is becoming flatter. This means, that the wave passes a longer distance in the same time. This is well known to a higher wave velocity. After passing the specimen, the slope

is turning back to the slope found in the beginning. At both interfaces, water-specimen and specimen-water, reflections are visible. The reflections are the lines which begin at the interfaces and point back in position. The amount of transmission is determined for each frequency component separately in 6.1.2. Another way to visualize the structure is the forward switching method. For this, the resulting wave velocities depending on the chosen particle offsets are plotted (cf. 5.1). For the experimental chain consisting of 0.02 mm the forward switching peak method is plotted in figure 6.5 Both figures, left

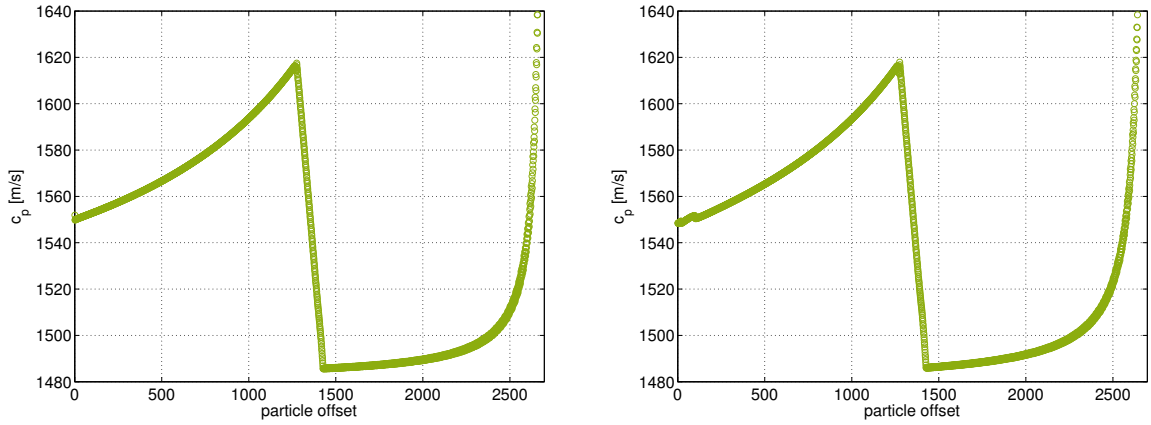

Figure 6.5: Visualization of the evolution of the wave velocity, using the forward switching method, experimental chain setup, reference chain, left: pulse excitation; right: sine excitation

for the pulse excitation and right for the sine excitation, show the same shape formed by the discrete wave velocity values. In the beginning, the left boundary effect is visible by the points lying out of the smooth shape. Away from the boundary, the wave velocity is rising due to a decreasing number of water particles included in the wave calculation. After reaching the interface water-sample the wave velocity is decreasing fast, because the number of aluminium particles are reduced. At the end of the sample-layer the pure water wave velocity can be found. Then the wave velocities are rising caused by the right boundary effect. Regarding the visualization of the structure we can see that the wave velocity is highly dependent on the adjusted particles and that the observed results for the overall and sample velocity is not random or an accident.

The forward switching peak method shows the wave velocity between the first and the last particle, when the particle offset is zero. That is the same velocity as the overall velocity.

Additionally, the structure is revealed by switching the first particle for the calculation.

6.1.2 Frequency spectrum

After the wave velocity was described and visualized for the experimental chains with a solid aluminium sample, here the frequency spectra are shown and the frequency propagation is explained. The frequency spectrum is calculated using the FFT. Before the time signal is transformed into the frequency domain, the Hanning window is applied to the time signal. The length of the Hanning window is the same for each application and the range is chosen as: $[N * 0.45\ N * 0.98]$. It is not expected that the frequency spectra match the experimental frequency spectrum, because the excitation form is different. In the experiments a negative square pulse is used and here the sine and pulse excitations are investigated.

6.1.2.1 Sine excitation

The frequency spectra are here investigated for chains using the sine excitation and compared with the experimentally obtained frequency spectra to validate the simulation model. In figure 6.6 the frequencies of the last particles of different pure water chains are shown. The amplitude is plotted over the frequency for simulations with different particle diameters and for the experiments. The length of the chains are kept constant, according to each particle size. Comparing the experimentally obtained frequency spectrum with the simulation frequency spectra, no qualitative and quantitative match can be found. The difference is caused mainly by the different excitation method.
The simulation curves are highly determined by the cut off frequency. The cut off frequency can be determined by looking at the steep decrease of the curves. It changes for each particle size, according to equation 4.23. It can be recognized, that only the three smallest particle sizes can carry the excitation frequency of the sine. For the other fre-

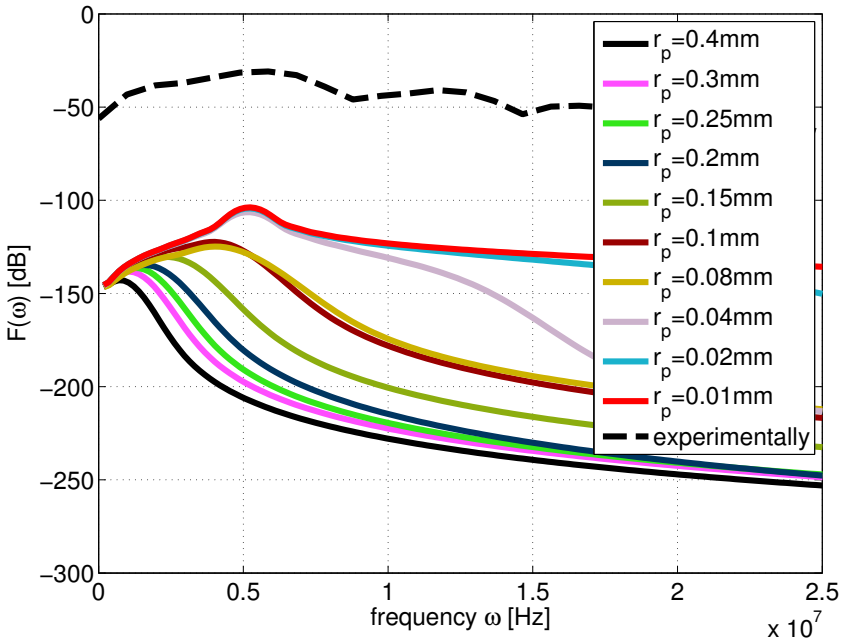

Figure 6.6: Frequency spectrum of the last particle for pure water chains, comparison of chains using different particle radius but same chain-length, sine excitation ($\omega = 5$ MHz)

quencies the cutoff frequency is too low to permit the propagation of the excitation. The curves related to the three smallest particle sizes converge in the beginning and around the peak of 5 MHz. After the peak, they start to separate, caused by the cut off frequency. To confirm that the steep decreases are related to the water cut off frequencies, the theoretical values are shown in table 6.2. The table shows the cut off frequencies for

radius [mm]	ω_{max}^{water} [MHz]	$\omega_{max}^{aluminium}$ [MHz]
0.4	3.70	15.65
0.3	4.94	20.86
0.25	5.92	25.04
0.2	7.41	31.30
0.15	9.87	41.73
0.1	14.81	62.59
0.08	18.51	78.24
0.04	37.02	156.50
0.02	74.05	313.00
0.01	148.10	625.90

Table 6.2: Comparison of maximum (cut off) frequencies depending on the particle radius and material

pure water and pure aluminium. It can be recognized, that the rising trend of the cut off frequencies match the trend found in the simulation. If a sine excitation of 5 MHz is used, the particles with a cut off frequency near to the excitation frequency can not be used. The excited wave would be influenced by the cut off frequency. In contrast, $r_p = 0.01$ mm has a cut off frequency far away from the excitation frequency of 5 MHz. Following, the excitation frequency is not influenced by the cut off frequency and this particle radius is useful for simulations.

In figure 6.7 and 6.8 the frequency spectra for chains of pure aluminium and for chains modeling the experimental setup are shown. The frequency spectra of the pure alu-

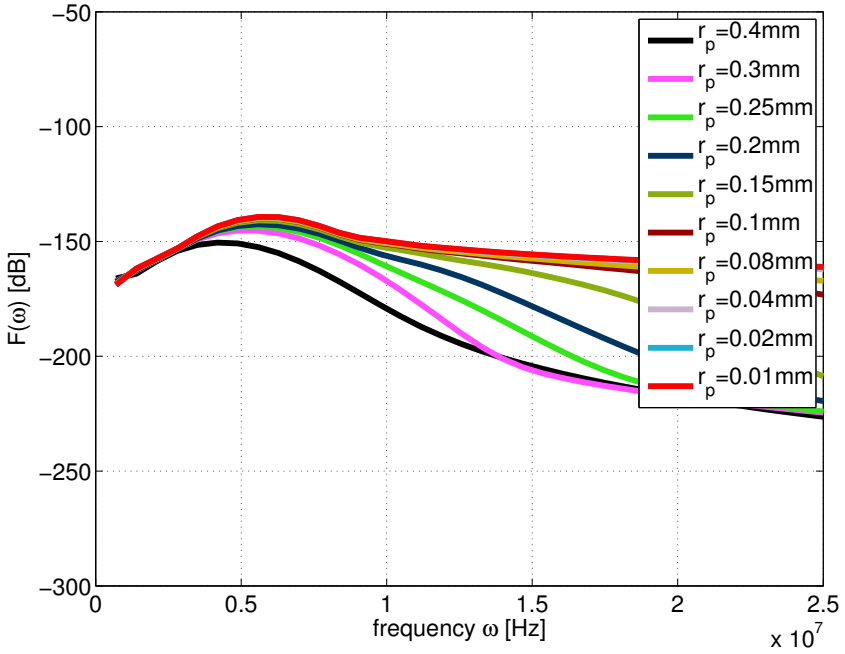

Figure 6.7: Frequency spectrum of the last particle for pure aluminium chains, comparison of chains using different particle radius but the same chain-length, sine excitation ($\omega =$ 5 MHz)

minium chains are smoother than the spectra of the pure water chains without having a steep peak around 5 MHz. Furthermore, the chains with the five smallest particle radii converge, instead of the two smallest particle radii of the water chain. This behavior can be explained with the higher cutoff-frequency of the aluminium chains. Looking at the frequency spectra of the experimental chain, additional peaks are visible. Comparing the magnitude of the peaks with the experimental results, the simulation values are much

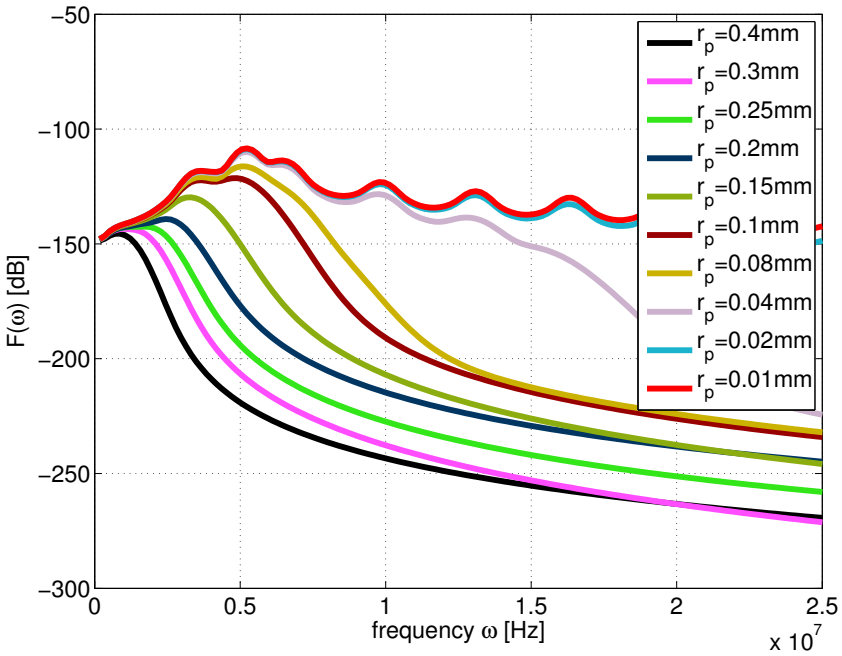

Figure 6.8: Frequency spectrum of the last particle for experimental chains (water-aluminium-water), comparison of chains using different particle radius but the same chain-length, sine excitation ($\omega = 5$ MHz)

smaller. Even for the highest value around 5 MHz, which is about −110 dB, the deviation to the experimental value of around 58 dB is very high. The peaks in the simulations are related to the structure created by the aluminium sample inside the water chain. For the bigger particle radii the extra peaks are not visible, because the frequency spectrum is cut off earlier. The frequency change related to the structure can be made visible by looking at the frequency propagation. In figure 6.9, the frequency propagation is shown for chains with the particle radius of 0.02 mm and 0.4 mm. The propagating frequency is plotted over the position for the chain representing the experimental setup. Here, the main cut off is caused by the water cut off frequency. In both plots three layers are visible. In the left figure, the first layer is characterized by a main branch at 5 MHz. The end of the first layer is clearly determined in the left figure by the creation of some frequencies aside the main frequency of 5 MHz. It is shown in the right figure that the excitation frequency of 5 MHz is only available for the first particles, because higher frequencies than the cut off frequency (cf. table 6.2) are damped strongly out. The maximum frequency for a particle radius of 0.4 mm of water is 3.70 MHz. In the right figure, the first interface can

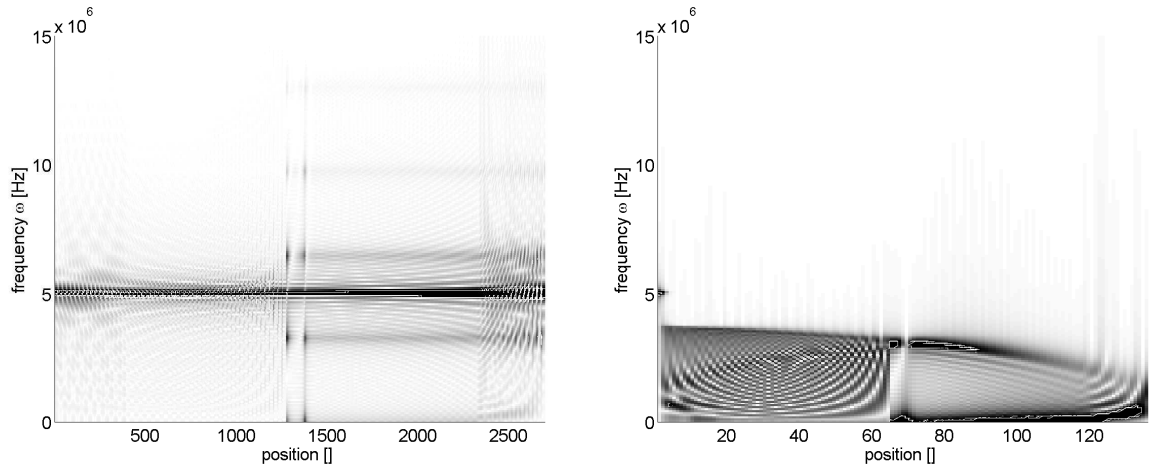

Figure 6.9: Frequency propagation for experimental chains (water-aluminium-water) consisting of particles with a particle radius of left: 0.02 mm, right: 0.4 mm, sine excitation ($\omega = 5$ MHz

be detected by the extinction of the frequencies below of 5 MHz. Additionally, the slope related to the main wave, changes further on due to the cutoff frequency. At the end of both figures reflections are visible that smear the frequencies, but the general character of the frequency spectrum is not changed.

Although for both chains a interface effect is visible, only in the left the study of the interface effect is useful, because in the right the frequency propagation is mainly influenced by the dispersion relation. The frequency is split into more branches that are related to the length of the specimen. This interface effect is not visible in the experimental results (cf. fig. 3.4). Since the dispersion relation and the cut off frequencies are of high importance for the frequency propagation, in figure 6.10 the dispersion relations are shown for the same simulations as used for figure 6.9. The frequency is plotted over the wavenumber. In both figures two branches are visible. The constant branch of a main frequency of 5 MHz is created by the sine excitation of 5 MHz. The excitation branch was also visible over the complete chain length in the related frequency propagation plot (cf. 6.9). For the dispersion relation on the right, the excitation branch was only visible in beginning of the chain (cf. 6.9). The slope of the dispersion relation is known as the wave velocity. For the higher particle radius, a non linear dispersion relation is found. That means, that the wave velocity is not the same dependent on the wavenumber. For particles that mimic

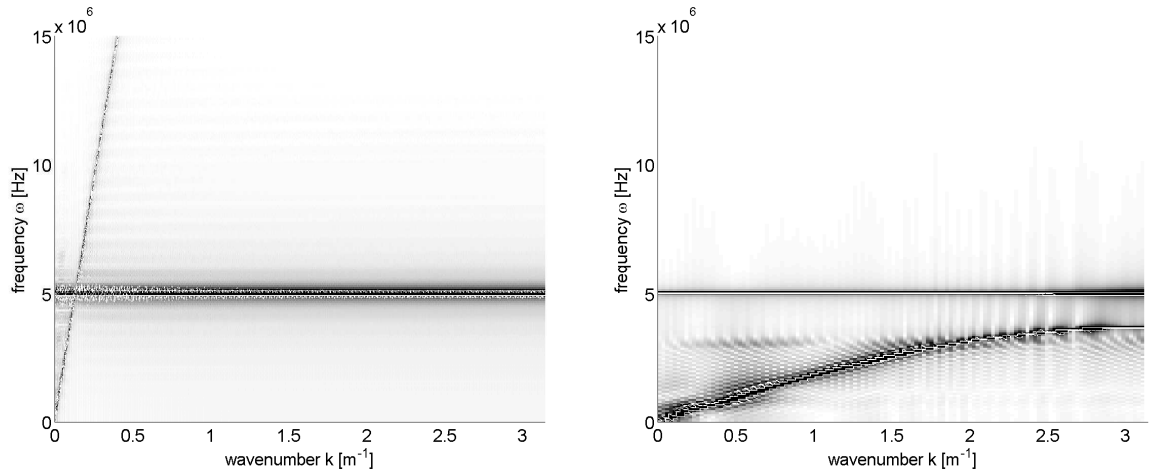

Figure 6.10: Dispersion relation for experimental chains (water-aluminium-water) consisting of particles with a particle radius of left: 0.02 mm, right: 0.4 mm, sine-excitation $\omega = 5$ MHz

one special material, this may be a disadvantage, because then the back calculated wave velocity can not match the input wave velocity. On the left, the branch is linear, which leads to a constant wave velocity. The related particle radius can then be used to model a media without the influence of dispersion. This would be the case if a water chain is modeled with respect to small frequencies.

6.1.2.2 Pulse excitation

After the frequency spectra for a sine excited wave were considered, the spectra for pulse excited chains are analyzed with respect to the dependency on the discretization. Additionally, the experimentally obtained frequency spectrum is compared with the simulation results. The investigated models are a pure water model and the experimental model (cf. 3). The frequency spectra are calculated as described in 5.2.3. First, the frequency spectra of pure water chains are considered. Plotting the amplitude values over the frequency (cf. fig. 6.11), the dependency of the cut off frequency can be detected. The smaller the particle radius, the less of the frequency spectrum is cut. Even if the frequency spectra do not converge quantitatively, the spectra for the two smallest particle radii converge qualitatively. The simulation frequency spectra compared with the experimentally ob-

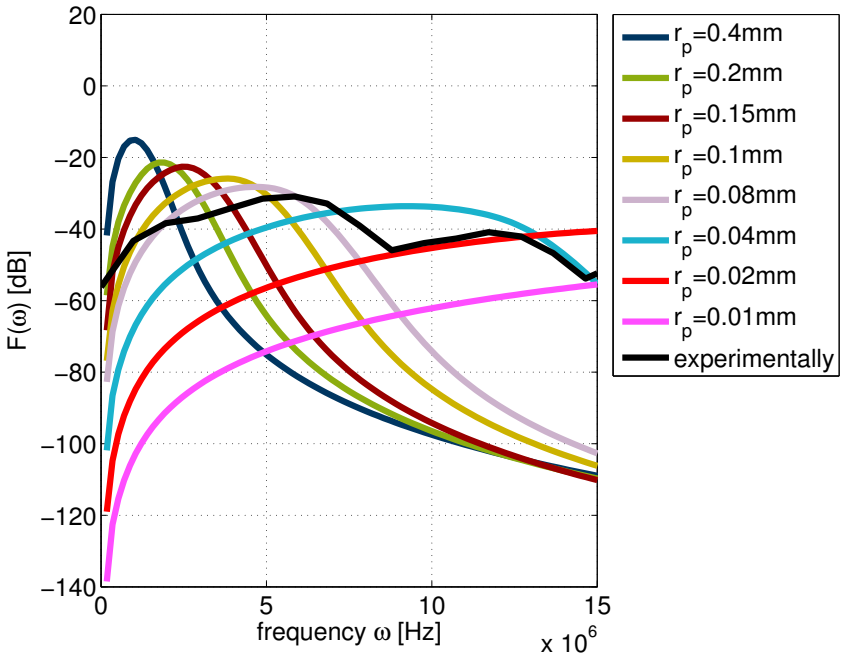

Figure 6.11: Frequency spectra of the last particles for pure water chains, comparison of chains using different particle radii but the same chain-length, pulse excitation

tained frequency spectrum lead to a better quantitatively and qualitatively match than seen for the sine excitation. The simulation excitation method is more close now (but not exact) to the experimental excitation method (different pulse excitation). The spectrum of 0.08 mm matches best.

In figure 6.12 frequency spectra of chains are shown, that represent the experiments. The wave was excited by a pulse. The same cut off is visible as for the chain using the sine excitation. The higher the particle radius, the smaller the cut-off frequency. An interesting difference can be found by looking at the curves related to the chains using the smallest particle radii. For the smallest three particle radii small peaks can be found in the frequency spectra at around 3.5 MHz, 7 MHz, 10 MHz and 13 MHz. The frequencies are related to the length of the specimen, because the peaks are placed at frequencies, that may be related to the length of the specimen. This means, that these frequencies are reflected in the sample back to the sample-water interface and then again reflected. This reinforce leads to the clear peaks. Reinforcement can also happen by interference of waves. Maybe the reflected waves interfere with the main wave.

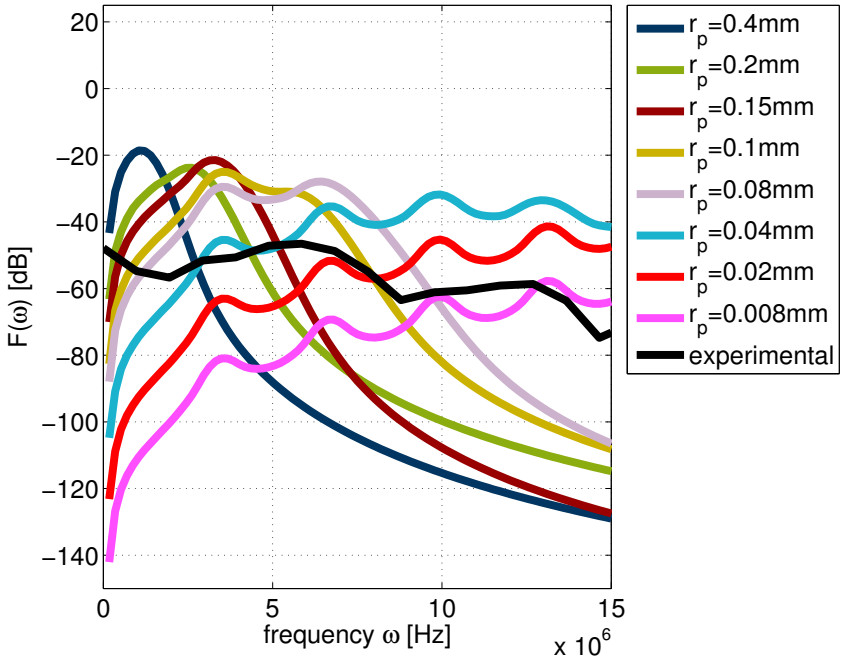

Figure 6.12: Frequency spectra of the last particles for experimental chains (water-aluminium-water), comparison of different particle radii but the same chain-length, pulse excitation

Investigation of the influence of the sample length on the frequency spectra

To substantiate these assumptions, two simulation with longer aluminium specimens were conducted. The frequency spectra are shown in figure 6.13 together with the spectrum of the simulation using the original sample length d. All curves show different oscillating peaks, but the oscillations have some same frequencies, which can be detected by the match of peaks of the biggest particle diameter. To evaluate the peak frequencies, the corresponding wavelengths in aluminium are calculated, using equation 2.1. With the input wave velocity of aluminium and the frequency of the first peak, the wavelengths are shown in table 6.3. The ratios in the last column are close to each other. The range is

Δd [mm]	peak position [MHz]	λ [mm]	rounded ratio $\lambda/\Delta d$
6.08	3.4	1.84	0.30
12.16	1.92	3.26	0.27
18.24	1.22	5.12	0.28

Table 6.3: Comparison of the ratio $\lambda/\Delta d$ for different sample thickness

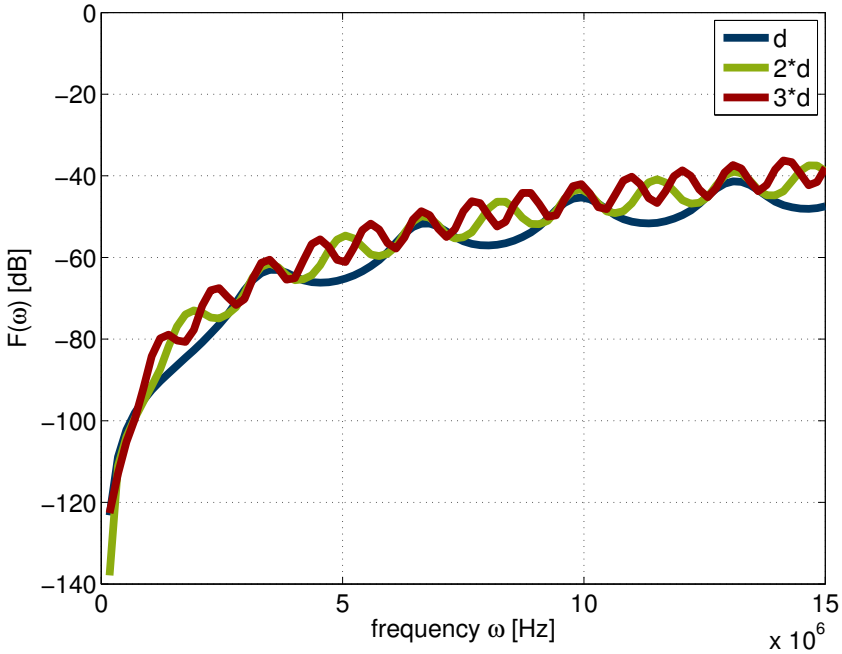

Figure 6.13: Frequency spectra obtained from simulations using different sample length, pulse excitation, uniform particle radius of 0.02 mm; sample thickness d

from 0.27 to 0.3. Considering that the peak measurement is not free of errors, it can be assumed that a specific wavelength is reinforced. The wavelength is dependent on the size of the sample, which is shown by the nearly constant ratios. Considering the obtained range for the relation wavelength/sample thickness in tabele 6.3, one can define it from 1/4 to 1/3 of the sample size. However, the calculated ratio values are closer to 1/3. It has to be further investigated, if these oscillations are created by interference of the main wave and the reflected waves, because the relation between the wavelength and the sample thickness is not conclusive.

6.1.3 Attenuation

The attenuation spectra for the sine and the pulse excitation of the experimental chain model are here evaluated. Even if a match to the experimental chain is not expected, the experimental attenuation spectrum is used as a comparison. In the analytical chain the energy of the wave is converged, but in the experiments the energy of the wave can be

dissipated. However, it can be investigated if the weakening of the wave signal is related to the acoustic interface, dependent on the particle radius.

6.1.3.1 Sine excitation

Calculating attenuation (cf. eq. 3.1) using the results of the experimental chain with the sine excitation, the attenuation in dB/cm over the frequency in Hz is plotted in figure 6.14. Results of the simulations are here compared with the experimental obtained attenuation spectrum. A match is not expected, because the excitation methods are different. Anyway, it is used as an reference. The attenuation is plotted for different particle radii

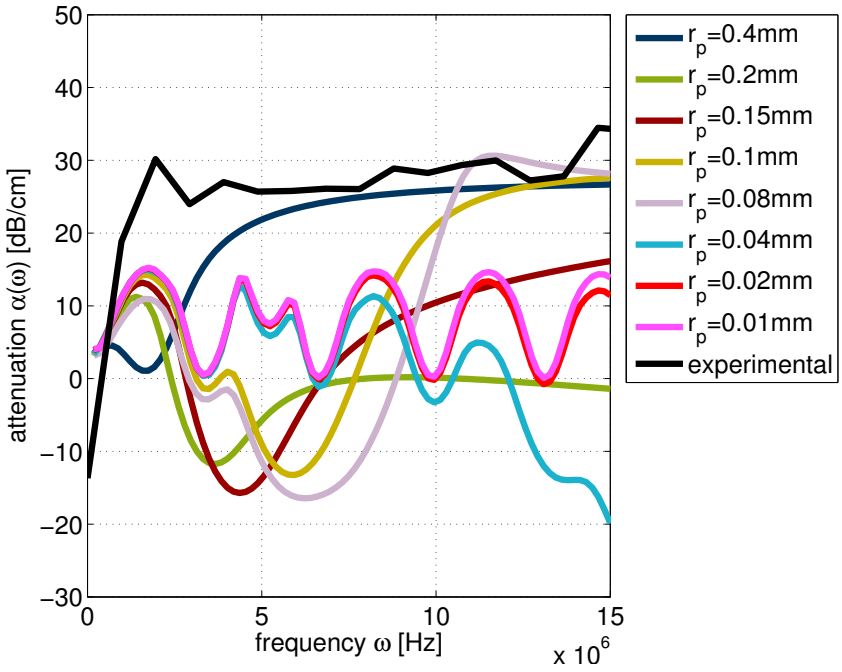

Figure 6.14: Frequency dependent attenuation (db/cm) for experimental chains (water-aluminium-water), comparison of chains using different particle radius but same chain-length, sine excitation

from 0.01 mm to 0.4 mm. Because attenuation is the fraction between two signals and here the numerator is the reference signal, attenuation is highly influenced by the cut off frequency. For the biggest particle radius the complete attenuation is positive, which means that the Fourier spectrum of the water signal is at any point greater than the Fourier sample of the signal with the sample. For that radius, the influence of the cut

off is equal on both chains. A minimum of the attenuation is reached at about 2 MHz, which is created by the cut off frequency of 3.7 MHz. Then the curve remains flat in the observed scope, after reaching almost the maximum. With higher particle radius the minimum shifts to higher frequencies, because the cut off frequency of water is also shifting to the right. Additionally, till a particle radius of 0.15 mm, the minimum is decreasing. After that point, the influence of the cut off frequency in the observed frequency area is dissolving, because it is higher than the observed scope. Then, for the last two highest particle radii, the attenuation curves almost converge.

Comparing the simulation results with the experimental result, the attenuation is not matched in shape and magnitude. In the beginning of the experimental curve the attenuation is much higher than for the converging simulation results. But the oscillations created by the interface effects avoid a linear trend in the simulations. Therefore, the 'hard' interfaces are one of the parameters that are responsible for the mismatch. Considering as comparison the acoustic interface loss, the attenuation values in dB are plotted over the frequency in figure 6.15. The acoustic interface transmission value was calculated by equation 2.11. The same attenuation values as in figure 6.14 are plotted only in another unit, dB. The theoretical attenuation value of 10.58 dB is nearly reached by the peaks of the curves related to the two smallest particle radii. The interface caused signal loss appeals on all frequencies. Thus, the theoretical value should be found as the offset value. However, it is not reached by the simulation offset value.

6.1.3.2 Pulse excitation

The attenuation values in dB/cm of the pulse excited waves are plotted over the frequency in figure (6.16). The particle dependent attenuation spectra follow the same trend as visible for the frequency spectra (cf. fig. 6.12. The cut off frequency determines the minimum, till the influence of the cut off is disappearing. Then the hard offsets create the oscillations found for the curves related with the smaller particle radii. Comparing

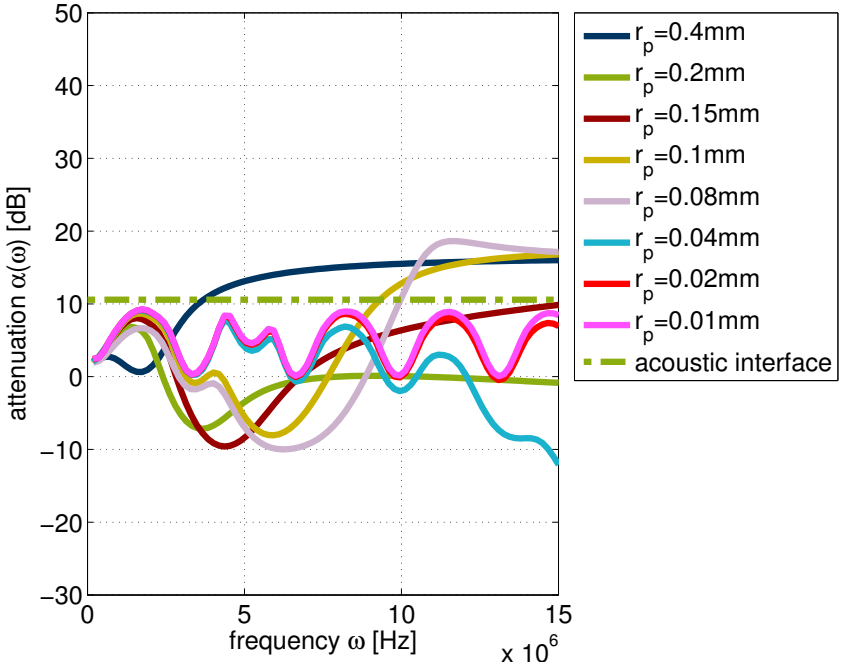

Figure 6.15: Frequency dependent attenuation (dB) for experimental chains (water-aluminium-water), comparison of chains using different particle radius but same chain-length, sine excitation

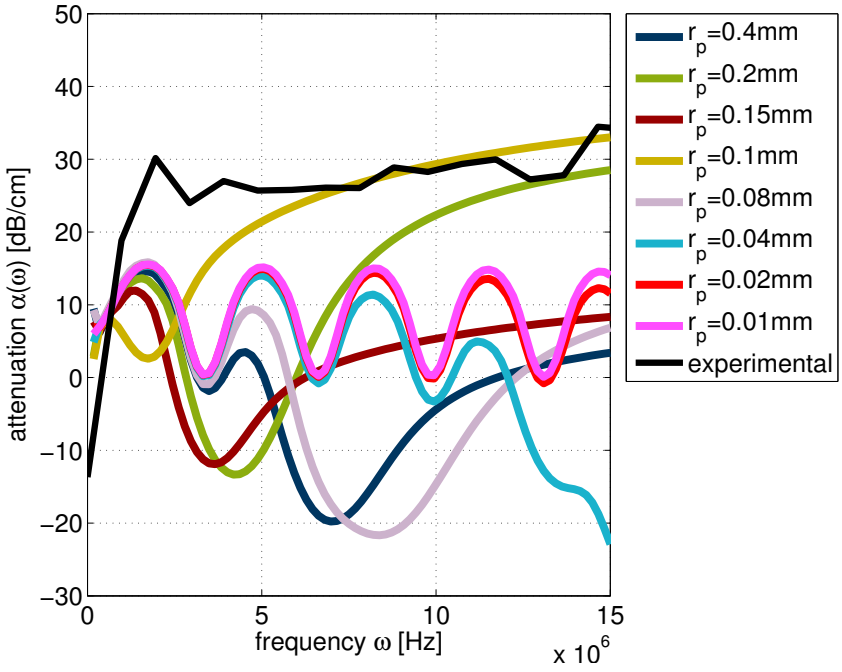

Figure 6.16: Frequency dependent attenuation for experimental setup chains, comparison of chains using different particle radius but same chain-length, pulse excitation

the simulation results with the experimental result, no similar shape is found. Again, the 'hard' interfaces and the difference pulse excitation are possibly the reasons why the

attenuation curves do not match. The oscillations are created by the reflections, or in other word the 'hard interfaces'. For the comparison of the simulation attenuation values in dB with the acoustic interface loss, they are plotted together in figure (6.15). The theoretical

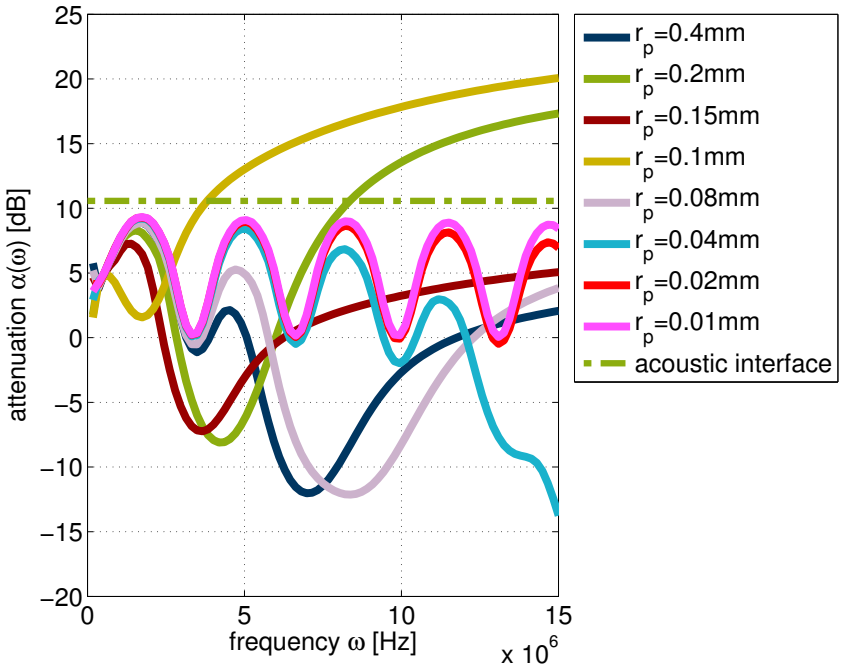

Figure 6.17: Frequency dependent attenuation for experimental setup chains, comparison of chains using different particle radius but same chain-length, pulse excitation

interface values are approximately matched by the peaks of the converging curves related to the two smallest particle radii. However, again the shape of the simulation results prevents a match of the acoustic interface loss.

6.2 Chains with different particle radii

After experimental chains of particles with the same radius were examined by observing the wave velocity, frequency spectrum and attenuation in section 6.1, experimental chains of particle with different radii are now studied. The idea is to change the interface to investigate the effect on the frequency spectra and attenuation values. As comparison for the obtained attenuation values, also the theoretical loss due to the interface is used. For each layer, the particle radius is kept constant. In this way, different means that the layers

of different materials are build up with different particle sizes. For the pulse excitation the water particle radii are constant 0.02 mm and the aluminium particle radius is varied. The value of 0.02 mm is chosen, because the maximum frequency for this value is so high, that a linear dispersion relation in the working range was found. In this way, only the specimen is changed, while the water layers are constant. The aluminium particle radii are restricted to be higher than the water particle size. Here, only the pulse excited waves are studied.

6.2.1 Wave velocity

It is investigated, if the difference of the particle radii in the layers influences the overall and the experimental wave velocity. The obtained velocities from experimental chains using a pulse excitation are plotted in figure 6.18 over the used particle radius for the aluminium sample. All relative errors to the experimental obtained velocities are smaller

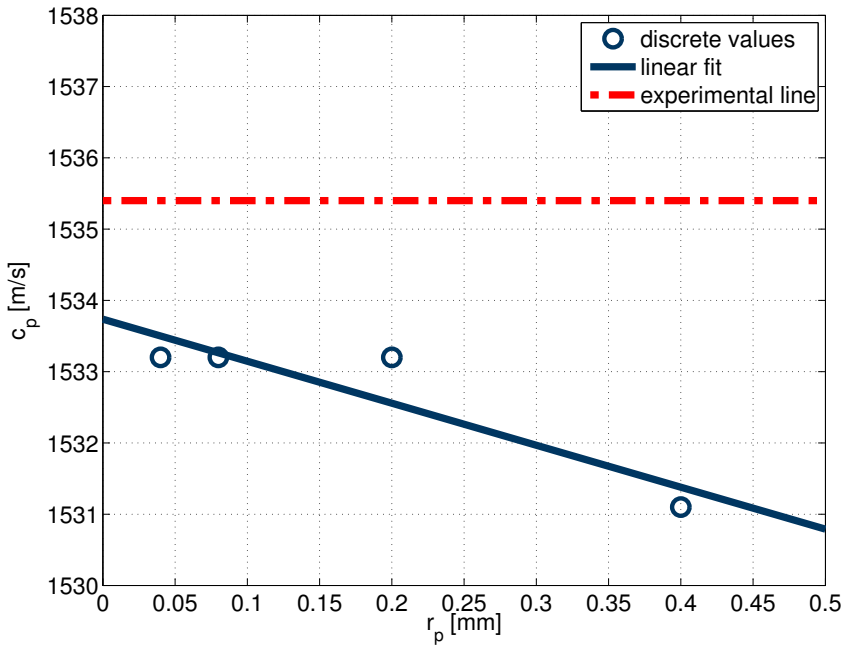

Figure 6.18: Wave velocities (overall) obtained by the peak method for experimental chains (water-aluminium-water) build up using different particle radii in the sample, $r_p^{\text{water}} = 0.02$ mm

than 1%. Thus, the change of the interface by applying different particle radii does not

influence the overall wave velocity crucial. The highest relative error of 0.29% is obtained by the comparison of the wave velocities of the chain with an aluminium particle radius of 0.4 mm with the experimental value.

The wave velocity in the sample is calculated using the experimental way. The results are shown in figure 6.19. The wave velocity is plotted over the particle radius of the

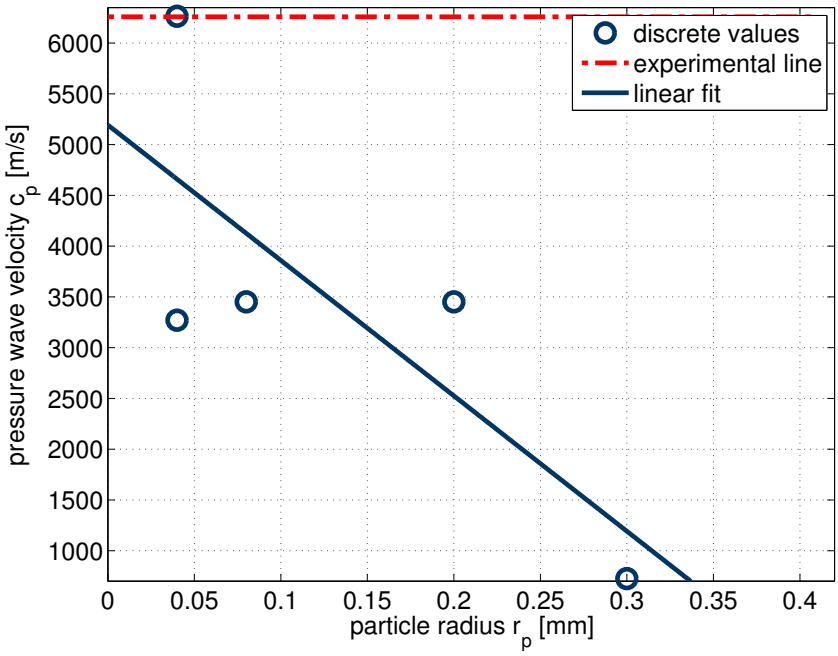

Figure 6.19: Wave velocities (aluminium) obtained by the experimental wave calculation for experimental chains (water-aluminim-water) build up using different particle radii in the sample, $r_p^{\text{water}} = 0.02$ mm

aluminium layer. The particle radius of the water particles are 0.02 mm. Additionally to the discrete values obtained by the back calculation, a line representing the experimental obtained wave velocity is plotted (red stitched line). It is found, that the wave velocity is only matched for the particle radius 0.04 mm. The relative errors for simulations using higher particle radii for the aluminium layer, are much higher than 1%.

6.2.2 Frequency spectrum

In this section, the influence of different particle radii in the sample on the frequency spectrum is investigated. The Fourier spectra are shown in figure 6.20. In the Fourier spectra

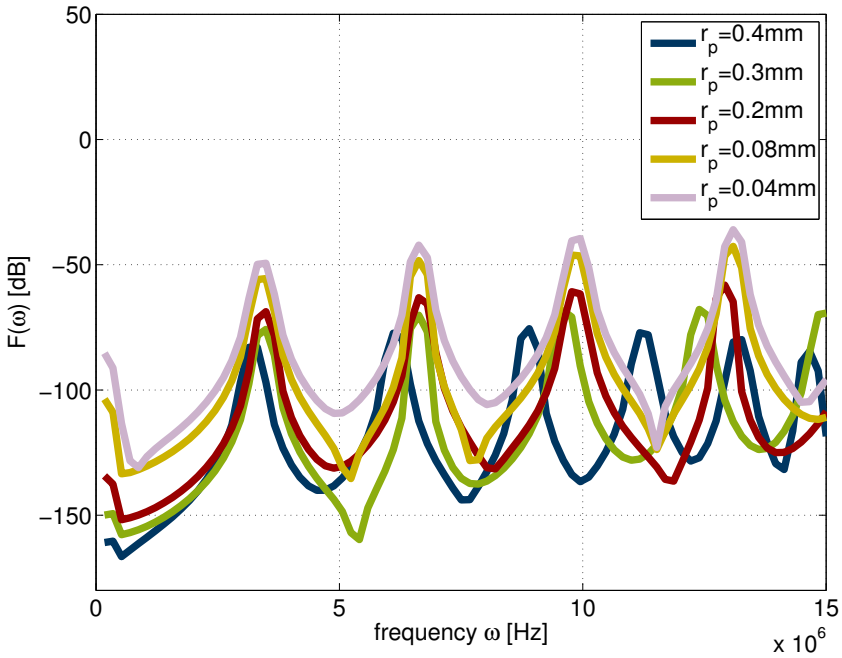

Figure 6.20: Fourier spectra obtained for experimental chains build up using different particle radii in the sample, $r_p^{\text{water}} = 0.02$ mm, pulse excitation

for all chains with different particle radii clear peaks can be found. The chains using the aluminium particle of 0.04 mm, 0.08 mm and 0.2 mm coincide nearly in frequency position. The chain using the aluminium particle radius of 0.3 mm is also placed at the same frequencies as the other. Then the frequency range between the peaks is getting smaller and the peaks are displaced in frequency. For the chain using a aluminium particle radius of 0.4 mm only the first peak location matches the location of the other peaks. Then the distance between the peaks is getting smaller, too. The same peaks were slightly visible before in the frequency spectra for the uniform particle chains of 0.01 mm, 0.02 mm and 0.04 mm. Thus, changing the interface by using a higher particle radius for the modeling of the specimen leads to a stronger frequency structure.

6.2.3 Attenuation

Here, the dependency of the attenuation spectra on the different particle radii in the sample is investigated. In figure 6.21 the attenuation in dB/cm is plotted over the frequency.

The same structure as found in the frequency spectrum is observed (cf. fig. 6.20). The

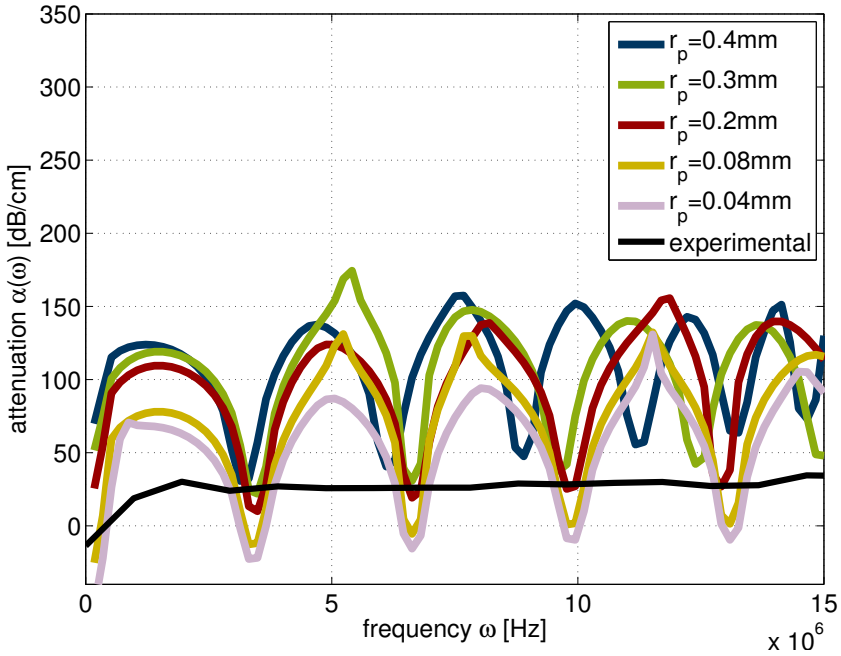

Figure 6.21: Attenuation obtained for experimental chains build up using different particle radii in the sample, $r_p^{\text{water}} = 0.02$ mm, pulse excitation

peaks due to the hard interfaces and the shift of the oscillations are present. The peak attenuation magnitude is found to be much higher as the experimental value. The values increase with a higher difference between the particle radii of the layers. Comparing the magnitudes with the chain of uniform particle radii, they are much higher. This is related to the higher difference in mass and stiffness's.

6.3 Summary and conclusion

The experimental model consisting of three layers (water-aluminium-water) was compared to the experiments under the aspects wave velocity, frequency spectrum and attenuation. For the constant particle chain using both excitation methods, pulse and sine excitation, the wave velocity was back for the complete chain and for the sample. For the wave velocity over the complete chain, the relative errors were smaller than 1%, which is in the author's opinion a good match. Considering the sample velocity, the relative errors are

smaller than 1% for the four smallest particle radii. In these obtained range the particle discretization does not effect the wave velocity. Regarding the chain with different particle radii, the relative errors of the back calculated wave velocities using the peak method are smaller than 1%. The calculation by the experimental way is only precise for the smallest aluminium particle radius 0.04 mm, but this match can be doubted due to the single occurrence of match. The other calculations lead to errors greater than 1%.

The frequency spectra were calculated using the Hanning window before the FFT. For both excitation methods the obtained frequency spectra from the one particle chains do not match the experimental frequency spectrum, what was not expected. One reason is the different excitation of the wave. In the experiments a negative square pulse is used, which leads to a time signal as shown in 3.3. The sine and the pulse excitations used for the simulations lead to different time signals, e.g. for the pulse excitation look at figure 5.3. The signal is also not damped, what is visible by the upkeep of the signal. This is different for the experiments, where the signal disappears with time. A reason apart from the time signal can be maybe found by looking at the interfaces. The interfaces are 'hard' and therefore create a wave decomposition, which allows only specific frequencies to propagate. This statement has to be validated, because a dependency on the chosen time window is also possible. This could include the reflections at the interfaces, which disturb the frequency spectrum of the propagating wave. However, it is not clear by looking at the signal, how the time range has to be chosen. Different time ranges were chose, but the frequency peaks still existed. This investigation is not included in the thesis. The calculation of the wavelength related to the frequency peaks (cf. table 6.3), showed that the peaks are related to the length of the specimen. The comparison reveals for the author not the cause for the peaks, but amplifies the possibility that the seen oscillations are caused by reflections and maybe the related interference.

The error of the frequency shape propagates to the attenuation calculation. Thus, the same peaks can be found in the attenuation over frequency diagrams. The statements about the frequency and the attenuation are valid for the constant and different particle chains. The difference can be found in the more 'hard' interfaces of the different particle

chains. Additionally, the attenuation values are much higher, because the acoustic interface leads to a higher loss, or reflection.

The model was shown as very precise regarding wave velocities, if one stays in the described range of particle radii. It needs to be more carefully build up with respect to the interfaces to match the acoustic interface loss/ transmission values. Additionally, the time range for the FFT has to be chosen more carefully. The excitation method should be also adapted to the experimental way to match the shape of the frequency spectrum of the experiments.

Chapter 7

Porous scaffolds: samples and structure

Since the goal is to simulate bone, the next step from a solid sample to bone is to investigate a regular structured sample. A regular structured model has a distinct microstructure, which is a more simpler case of a random bone structure. In chapter 6 the analytical chain simulation technique was applied and adjusted to the experiments with the solid aluminium sample. A range for the particle radius is found, in which the discretization does not influence the wave velocity, the qualitative frequency spectra and the attenuation values. Therefore, for the application of the one dimensional particle chain on another sample, the particle radius has to be in the described range. The particle radius of 0.01 mm is chosen for the simulation of a chain with a regular porous scaffold. A parameter study with respect the number of layers and the porosity is included to study their influence on the wave characteristics. The wave velocity, the frequency spectrum and attenuation is predicted for sine and pulse excited waves. These prediction can be then validated by experiments.

7.1 Sample material and structure

Two samples are present, a pure solid one and one regular structured. The samples were provided by the department of Tissue Regeneration, which is part of the institute for biomedical technology and technical medicine (MIRA) at the Universiteit Twente. The two investigated solid and a porous samples are shown in figure 7.1. On the left, the

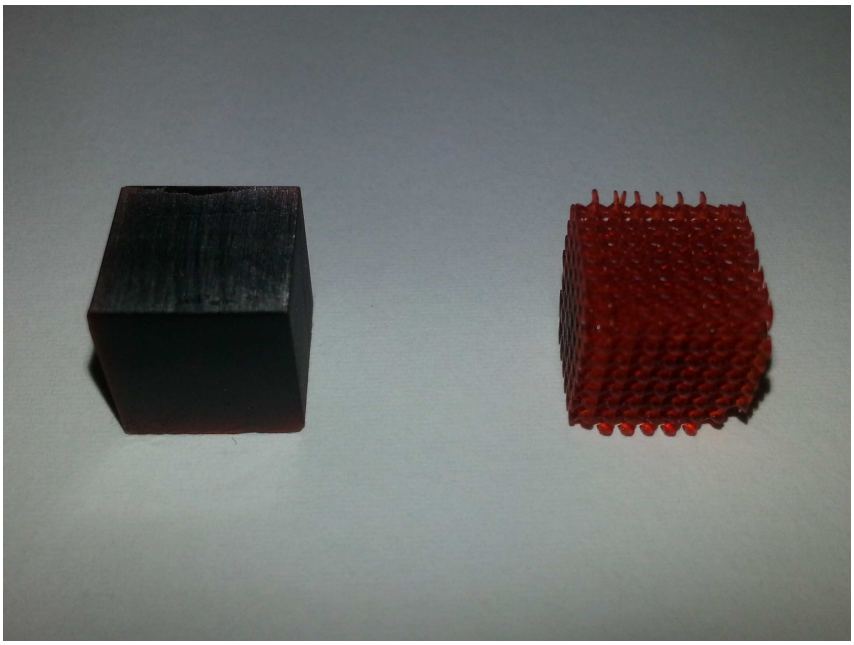

Figure 7.1: Pictures of the used samples, solid and porous

solid sample is visible. It is a cube with the side length of 10 mm. The porous sample is also shown, with the same side length as the solid cube. The material for both is Polycaprolactone (PCL) (cf. [33], [4], [11]), which can be used to mimic bone material (cf. [1]). Its properties are found to be in between trabecular bone and cortical bone. For example if a bone needs to regrow in medical practice, it can be also used as a matrix where the bone can rebuild. The property to resist all forces in the human body is especially a result of its high elasticity (hyperalsticity, stretching up to 700%). PCL is an organic polymer with the structural formula $(C_6H_{10}O_2)_n$. Its melting point is $60°C$ and the physical properties are dependent on the temperature. The existing data for the solid material PCL and the structured sample are presented in table 7.1. The values of the Young's modulus and the density are provided by the supplier. The Poisson ratio was

Density ρ $[\frac{kg}{m^3}]$	1145
Young's modulus E [MPa]	204
Poisson ratio ν []	0.47
Porosity Φ	0.7
Number of interfaces N_I	10

Table 7.1: Physical properties of the samples

looked up in the above mentioned literature. The porosity and the number of interfaces relate only to the porous sample. For the investigation of this sample no experimental data are available. Thus, the wave velocity for the solid bulk material that is needed as an input parameter to adjust the model, is calculated in equation 7.1.

$$c_p = \sqrt{\left(\frac{E(1-\rho)}{(\rho(1+\nu)(1-2\nu)}\right)} \tag{7.1}$$

The wave velocity is calculated to be 1034.7 m/s. It is interesting, that the wave velocity of PCL is found to be smaller as the wave velocity of water, which cannot be validated, because experimental results are missing. However, it may be explained by its small Young's modulus. Using the assumption for the solid PCL wave velocity of 1034.7 m/s, the 1D chain is modeled. A pure solid sample is investigated as a comparison with the structured sample. Then, the stratified model (cf. 2.4) is applied to model the structured sample and the results of wave velocity, frequency propagation and attenuation are revisited. In figure 7.2 a scheme of the structured model is shown. The width of the water and sample layers are determined with respect to the porosity. Finally, as one way to simulate a naturally grown material as bone, a randomness of the particle size is applied to the sample. In this way the well ordered stiffnesses and masses are abrogated and the step to a disordered media is proceeded.

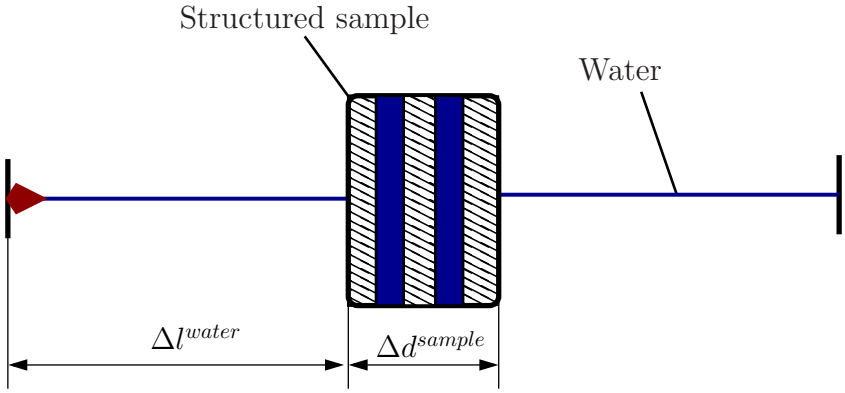

Figure 7.2: Scheme of the structured model

7.2 Results of the regular Scaffold model

Here, the specimen is modeled as a solid sample and an regular ordered scaffold. Then, the simulation results are analyzed regarding wave velocity, frequency spectrum and attenuation. Three layers are created in the chain, water-PCL-water. The chain length of 0.108 m is kept constant for all simulations in this section. For the water particles, the input wave velocity and the density is assumed to be 1481 m/s and 1000 kg/m^3. Both types of layers (water and PLC) are build up with particle sizes of 0.01 mm. This size has been found to be in the converging range for the frequency and attenuation for the investigations in chapter 6, where no radius dependency is visible. The wave velocity was also calculated very accurate for this particle radius and the wave calculation in this range is independent on the particle size. Additionally, the cut off frequencies for this particle size lie out of the investigated range, which is one of the conditions for using the right particle size for water. The cut off frequencies, the particle masses and the spring stiffness's of the PCL particles are shown for the used radii of 0.01 mm and compared to the water cut off frequencies in table 7.2. It is found that the cut off frequency for

material	r_p [mm]	ω_{max} [MHz]	m_p [kg]	k_s [N/m]
water	0.01	148.10	$8 * 10^{-12}$	$4.387 * 10^4$
PCL	0.01	103.5	$9.16 * 10^{-12}$	$2.452 * 10^4$

Table 7.2: Comparison of water and PCL simulation properties depending

PCL is lower than the cut off frequency of water. Considering the equation to calculate it (equation 4.23), it is related to the lower wave velocity value. The sample is first modeled as a regular solid. The parameters needed to model the solid can be found in table 7.1.

7.2.1 Pulse excitation

First, the analytic simulation results of chains using the pulse excitation are investigated.

7.2.1.1 Wave velocity

The dependency of the wave velocity on the porosity and the number of interfaces is investigated. The wave velocity is calculated for the complete chain and for the sample.

Porous samples First, the wave velocity obtained from the simulation of the solid sample is compared with wave velocities obtained from chains of different porosity. The relation between the wave velocity and the porosity is investigated. To create a certain porosity, the sample has to be divided into subsections. To minimize the influence of the interfaces, the smallest number of divisions is used. Therefore, the interface number from the solid to a porous sample is increased by two. In figure 7.3 the resulting wave velocities are shown. The sample wave velocity is plotted over the porosity. A porosity of 0 is related to the solid sample. The sample wave velocity is calculated by the experimental method. It is found as linear dependent on the porosity. The correlation coefficient higher than 0.99 marks a good interpolation. The back-calculated wave velocity for the solid sample should match the input wave velocity of 1034.7 m/s. By comparing the input and the back calculated sample wave velocities, an relative error is found as 0.126%, much smaller than 1%. Keeping the original porosity, the relation of the number of interfaces and the sample wave velocity is examined.

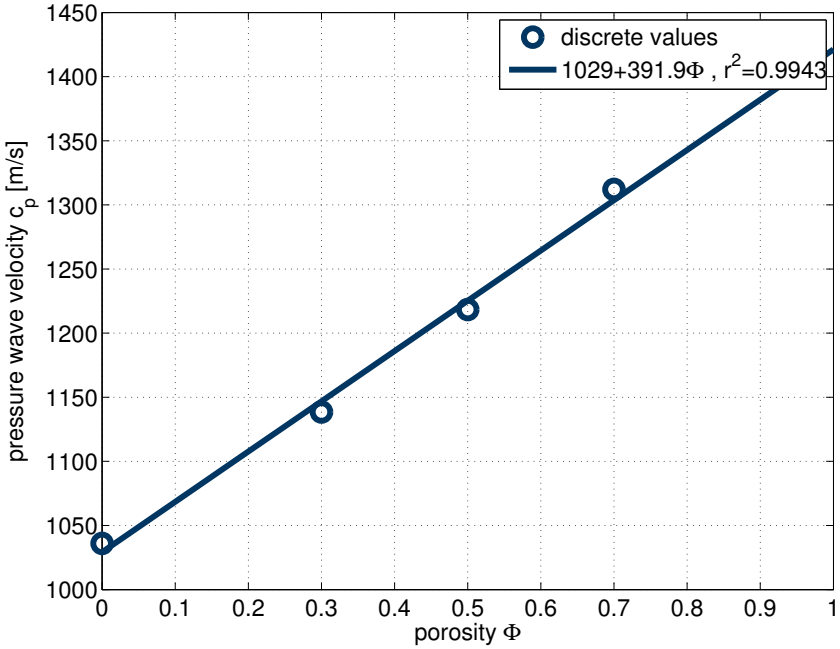

Figure 7.3: Sample wave velocity for the simulated scaffold dependent on the porosity, calculated the experimental way

Structured samples In figure 7.4 the sample wave velocity is shown for the original ($N_I = 10$) and variations of the number of interfaces. Using a linear fit, a very small slope

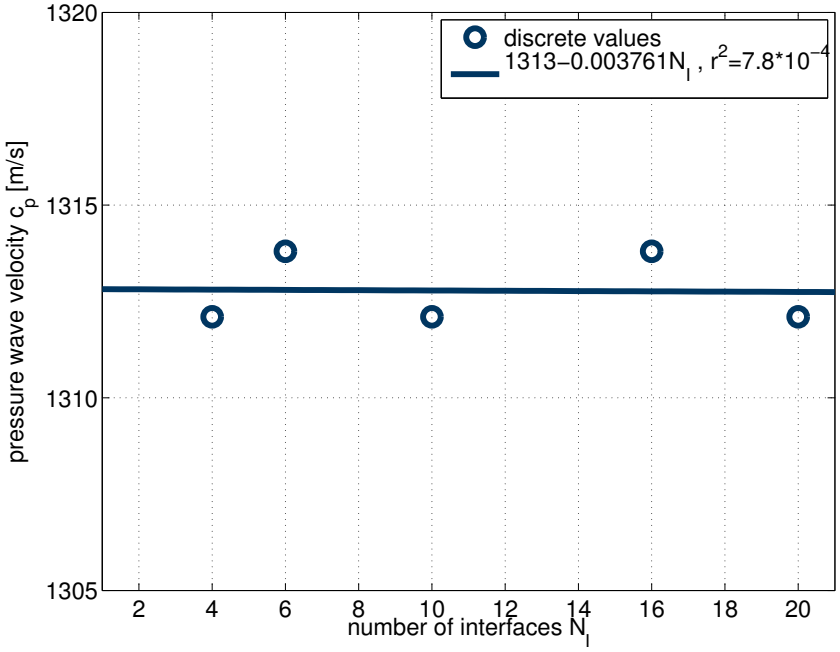

Figure 7.4: Sample wave velocity for the simulated scaffold dependent on the number of interfaces, calculated the experimental way

and a very small correlation coefficient was found. Approximately a constant relation

between the number of interfaces and the number of interfaces can be found. The wave velocity values are arranged around a mean value. Thus, it is assumed that here the wave velocity is not dependent on the number of interfaces. The investigation is shown in the appendix in figure A.1. This is contrary to the expectation and the prediction. The difference between these investigations is that the input wave velocities of both materials are much different, for the bone assumption it was 3200 m/s. Additionally, the density value is different. Thus, it may be possible, that the number of interfaces are not important for the calculation of the wave velocity for any kind of composition of materials. Anyway, no experimental comparison values are present to validate these assumptions. To visualize the wave propagation, the wave velocity is plotted over the forward particle offset for the original porosity and number of interfaces and for the sample with original porosity and the number of interfaces of 20 in figure 7.5. In the beginning of both plots, the same

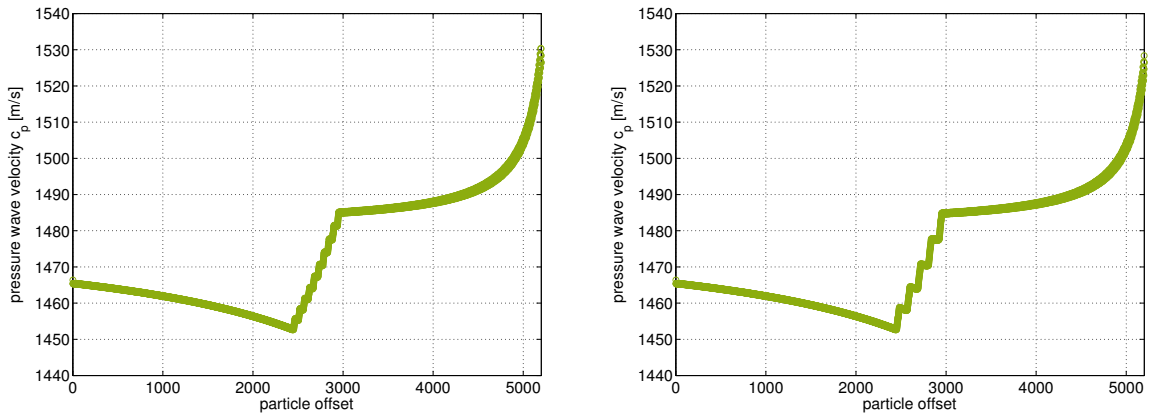

Figure 7.5: Carpet diagrams position time, left: porous sample ($\Phi = 0.7$, $N_I = 20$), right: porous sample ($\Phi = 0.7$, $N_I = 10$)

slope is found. A dependence on the sample structure is in the beginning not visible. For both diagrams the same sample length is visible, indicated by the first and the last slope changes. The main difference can be found in the different structure of the layers in the sample. In the right, clearly the different slopes of the different layers are visible. In the left, the slopes are not that clear, because the layers in the sample are smaller. However, the structure does not influence the trend of the curve of the sample wave velocity. This is recognized by nearly the same wave velocities at the beginning and the end of the sample. The wave velocities after the sample are then the wave velocities of water. In the end, the

wave velocity affected by the boundary condition increases to high meaningless values.

7.2.1.2 Frequency spectra

The dependence of the frequency spectrum on porosity and different structure is here investigated. The time signal of the last particle is cut using the Hanning window, as described in chapter 5. Then the FFT is applied and the Fourier spectrum can be observed.

Porous samples In figure 7.6 the Fourier spectra for the solid and porous samples are shown. The frequency spectra were calculated from the same simulations as the wave velocities shown in figure 7.3. In both figures the amplitude in dB is plotted over the

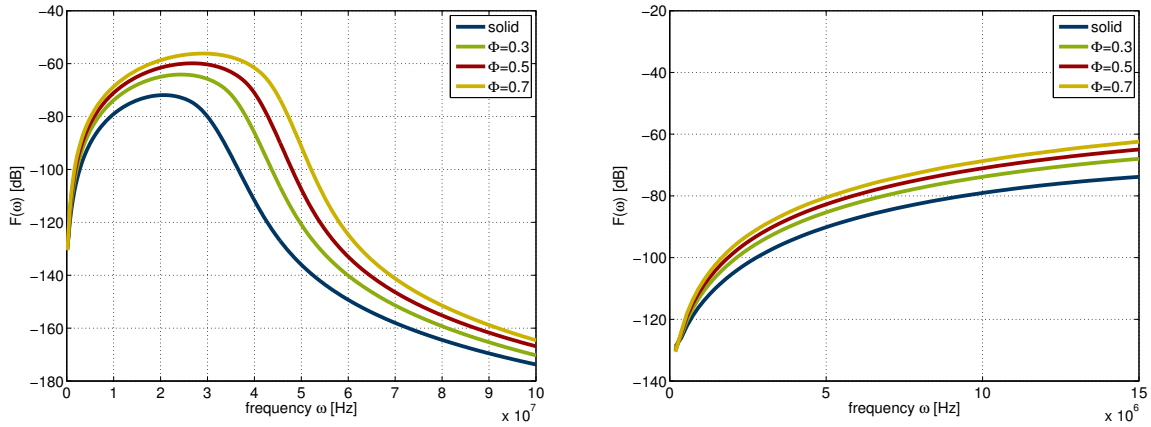

Figure 7.6: Frequency spectra for two different frequency scales, solid and porous samples

frequency in Hz. In the left figure a much wider frequency range is shown. There, the cut off frequency is visible, which is strongly related to the PCL layer in the middle of the chain. The influence of the cut off of the PCL simulating particles is less strong for the porous samples, because less PCL particles are present in the specimen. Thus, the cut off for the solid sample is most clearly and happens at earliest frequencies. To remind, the cut off frequency for PCL particles of the radius 0.01 mm is 103.5 MHz. This value can be find by looking at that point, where the frequency spectrum remains flat. The frequency spectrum is not scaled to that value, but the start of the flat is recognizable

anyway. The zoom in to the investigated frequency range in the right, shows again clearly that the amplitudes are higher for the more porous samples. The beginning of the slope is not interesting for resolving microstructure, because frequencies towards zero belong to long wavelength. The small frequencies are interesting for the stiffness calculation of the bulk material, since they are not influenced by the microstructure. The long wavelength cannot resolve the finer structure of the sample.

Structured samples In figure 7.7 the frequency spectra of samples of different number of interfaces are shown. The frequency spectra were calculated from the same simulations

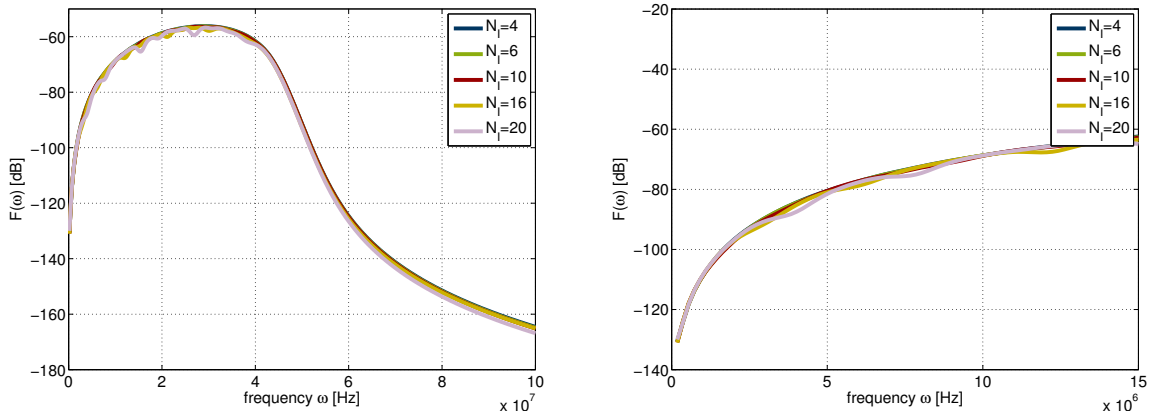

Figure 7.7: Frequency spectra for two different frequency scales, samples of different number of interfaces

as used to calculate the wave velocities in figure 7.4. In the left, the frequency spectra is shown for a larger frequency range than in the right. It is found that the shapes of the spectra are very close to each other. With a higher number of interfaces only small peaks are created, but they do not change the overall change at all. Looking at the right, only peaks for the two highest number of interfaces are visible. The peaks of the other frequency ranges are too small to recognize. The reason why the number of interfaces does not change the frequency spectrum crucially, can be found by looking at the transmission coefficient defined in equation 2.11. To do this, the acoustic impedance of PCL is needed: 1.1847 kgm/(sm^3). The transmission value in dB is then 0.1122 (absolute value), which is

very low for example compared with the value obtained for the water-aluminium interface of 10.58 dB (absolute value).

7.2.1.3 Attenuation

The dependence of the attenuation spectrum on the porosity and the structure of the sample (regular structured scaffold, cf. 7.1) is here investigated.

Porous samples The attenuation values dependent on the frequency is shown for the solid and the porous samples of same number of interfaces in figure 7.8. The attenuation

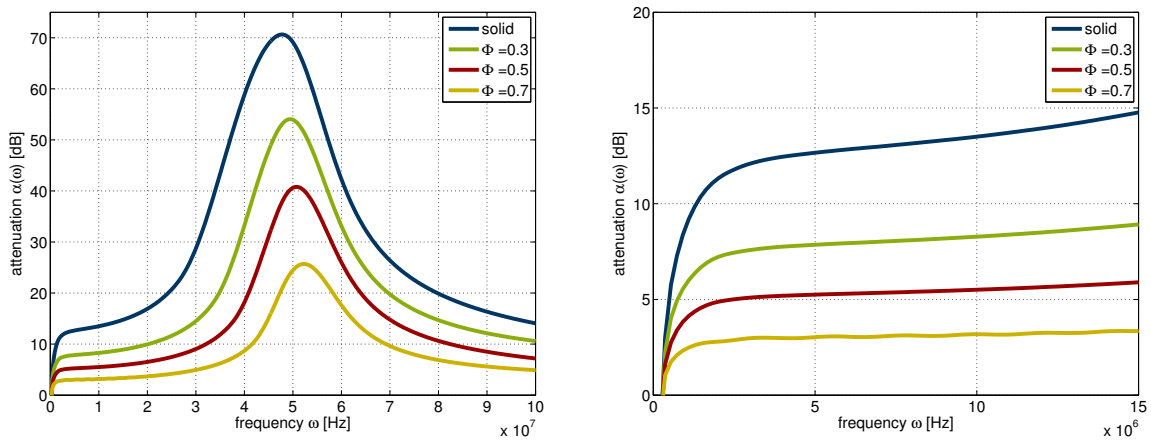

Figure 7.8: Attenuation for two different frequency scales, solid and porous samples

values are calculated as the ratio to the pure water chain (cf. eq. 3.2). In the left figure, the scale allows to study a wider frequency range than in the right. Ignoring the very small frequencies that are not in the range of interest, all curves show a behavior describable approximately by a Gaussian or something similar with an offset. The peaks are shifted from the left to the right, beginning with the solid and ending with the most porous sample. The amplitudes in general are decreasing from the solid to the most porous sample. This behavior is related to the calculation method, where the ratio of the two signals in frequency range is used. Comparing the signals, the sample signals are cut off earlier for higher porosity due to the smaller cut off frequency of the PCL simulating particles. The

earlier the frequencies are cut off, the weaker the signals are. A peak is created where the difference between the two signals is highest. After the peak, the signals start to decrease, because the highest frequencies are in both cases just cut off by the water and the PCL cut off frequencies. Therefore, the attenuation values for high frequencies are decreasing. In the right, zooming into the scale of interest, a nearly linear relation can be found for the attenuation values, when the values for the small frequencies are ignored. For the case of porosity equal to 0.7, nearly a flat curve is found. That means, that for this flat range attenuation is approximately determined mostly by the acoustic interfaces between the different materials. However, comparing this offset of about 3 dB with the the interface transmission value of 0.122 dB, the obtained value from the particle chain is much too high to be just caused by the interfaces. Maybe an error in the calculation of the frequency spectrum, e.g. the wrong time window, is responsible for the deviation.

Structured samples The dependency of the attenuation spectra on the number of interfaces is investigated. In figure 7.9, the attenuation spectra are shown obtained by the simulations of different number of interfaces. In the left a wider range of attenuation

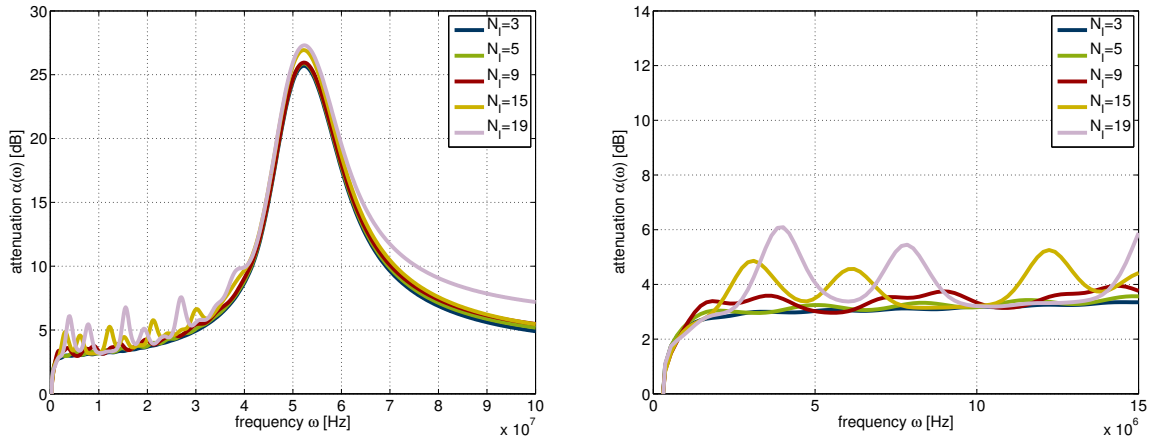

Figure 7.9: Frequency spectra for two different frequency scales, samples of different number of interface

values is shown as in the right, were the range of interest is displayed more clearly. The general behavior can be described as for the attenuation values using the porous samples.

The peak is present and the decay for the high frequencies. The curves are also very similar compared to each other. The main difference can be best seen in the right. Oscillations are visible, that may be linked to the number of interfaces. It seems, that for the simulations of the two highest number of interfaces the peaks are just shifted. The heights of the oscillations are following a more obvious trend: they increase with the number of interfaces, because at each interface reflection occurs.

7.2.2 Sine excitation

Here, less chains are investigated as in section 7.2.1, to model the regular scaffold. Particle radii of 0.01 mm are used. To solve the solution for a chain using a sine excitation needs a higher calculation effort. Therefore the number of simulations were reduced. The sine is used for the excitation, because it creates a different frequency spectrum of the wave. The effect of different porosity and number of interfaces is investigated with respect to the wave velocity, the frequency spectrum and the attenuation spectrum.

7.2.2.1 Wave velocity

First, the chains simulating the scaffold are investigated regarding the dependence of the sample wave velocity on the structure and the porosity. In table 7.3 wave velocities are shown calculated by the experimental way. The wave velocities are shown for the solid

	c_p [m/s] (sample)
Solid sample	1033.9
Porous sample	1310.4
Finer structured sample	1313.8

Table 7.3: Sample wave velocities obtained from the sine excited chains simulating the scaffold

sample, the porous sample with the original porosity and original number of interfaces

and for a finer structured sample ($N_I = 14$) with the original porosity. The wave velocities for the solid sample are for both calculation ways the smallest. This is consistent, because the sample particles let the wave propagate with a smaller velocity as the water particles. The wave velocity obtained for the solid sample, 1033.9 m/s matches with an error of 0.0773% the input wave velocity of 1034.7 m/s. The velocities for both porous sample are located in a similar range. The deviation for the sample velocity of the solid to the structured samples is too small to identify a significant deviation. The deviation could be just a consequence of the calculation method. Comparing with the results shown in subsection 7.2.1, the absolute deviation is about 2 m/s and smaller than 1%.

7.2.2.2 Frequency spectra

The dependency of the frequency spectrum on different porosity and structures of the regular scaffold are investigated. The time signal of the last particle is cut using the Hanning window, as described in chapter 5. Here, the wave is excited by a sine displacement. In figure 7.10 the frequency spectra are plotted for sine excited wave models. The frequency

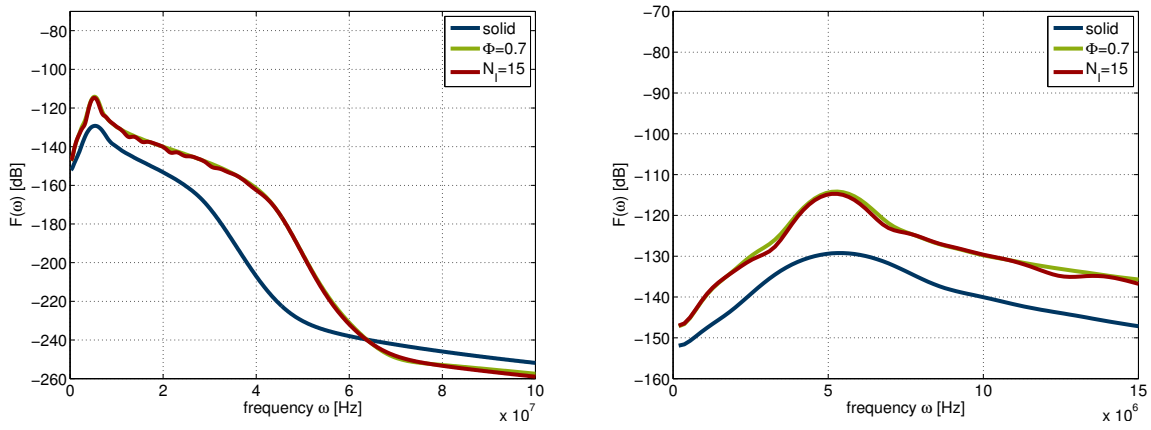

Figure 7.10: Frequency spectra for two different frequency scales, solid sample and samples of different structure

spectra are shown for the solid, the original sample ($\Phi = 0.7$ and $N_I = 10$) and the finer structured sample ($\Phi = 0.7$ and $N_I = 15$). In the left a wider frequency spectrum is shown as in the right. The frequencies of the solid are earlier cut off by the cut off frequency,

because in the solid sample the most possible number of solid particles exist. The smaller amplitudes in general for the solid can be also explained by the existence of the most possible number of PCL particles. The peaks of 5 MHz are created by the sine excitation with this excitation frequency. Comparing the two porous samples, the frequency shape is nearly the same. The difference can be better seen, when the frequency spectrum is scaled to the window of interest (right figure). Small deviations at frequencies at about 3 MHz, 7 MHz and 12 MHz are found. The structured sample transmits these frequencies worse.

7.2.2.3 Attenuation

In this subsection, dependency of the attenuation on the porosity and the structure is investigated. In figure 7.9 the attenuation values are plotted over the frequency. The

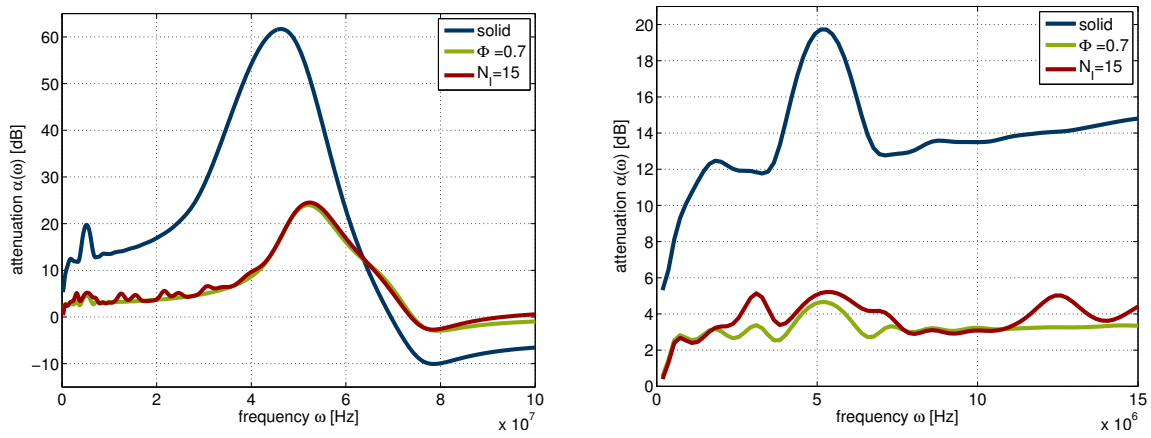

Figure 7.11: Attenuation dependent on the frequency for two different frequency scales, solid sample and samples of different structure

attenuation curves are calculated as the ratio between the Fourier spectra of the solid, of the original, of the finer structured samples and the Fourier spectra of the pure water sample. In the left, a wider frequency range of attenuation values is shown as in the right. The attenuation shape in the left follows the same rules as described for the pulse excitation in subsection 7.2.1. Looking at the scale of interest in the right, for all samples a peak around 5 MHz is visible. The highest peak is found for the solid sample. The peaks

of both other porous samples have smaller peaks, because less PCL particles are placed in the sample. Additional to the main peak of 5 MHz, peaks around 3 MHz, 7 MHz and 12 MHz are visible. These peaks are related to these found in the frequency spectrum in figure 7.10. The offset should be only created by the interface reflections, but it seems that the number of interfaces do not determine the transmission loss. Comparing the offsets of the solid and the porous, the one related to the solid sample is expected to be higher than the samples with structures and porosity. This expectation is validated.

7.3 Results of the random scaffold model

A realistic model of a natural grown bone is outlined by introducing a random disorder to the model of the scaffold with original properties (cf. 7.1). The particles sizes are randomized around a medium value. The values are generated from a standard distribution with a specified standard deviation r_{disorder}. For the generation of the random number the Matlab function `randn()` was used. Because the particle size is not given directly, but by the particle mass and the spring stiffness, these two have to be randomized. For the random numbers saved in the array R(n) of the length total number of particles the following formula 7.2 is used.

$$R(n) = 1 + \texttt{randn(1)} r_{\text{disorder}} \tag{7.2}$$

The '1' on the left after the equal sign is the mean value. The equation is then embedded in a for loop over from 1 to the total number of particles. The random numbers are then multiplied with the masses and the stiffness. Thus, the mass and the stiffness of the same particle is multiplied by the same random number. This ensures that the particles are not changed with respect to the material and input parameters. The smaller the disorder parameter, the smaller the standard distribution. The distributions of the particle radius for two pure water chains (5400 particles per chain) are shown in figure 7.12. The number

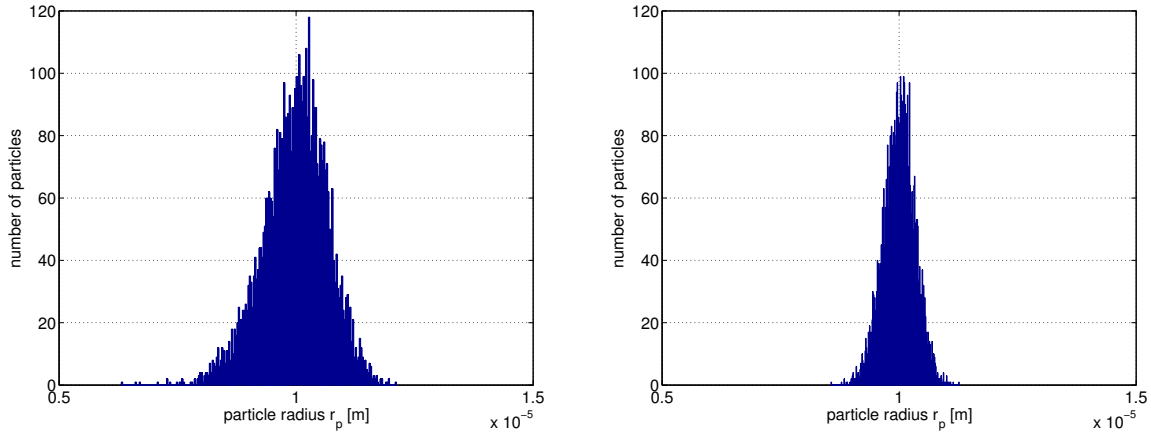

Figure 7.12: Normal distribution for water chain for two disorder parameters: left: 0.2, right: 0.1

of particles is plotted over the particle radius for a disorder parameter of 0.2 in the left and a disorder parameter of 0.1 in the right. The distribution for the higher disorder parameter is narrower, which is validated by comparing the standard deviations of the particle radii. The standard deviation for the chain with the disorder parameter 0.2 is $(6.84)10^{-7}$ m. For the disorder parameter of 0.1 it is $(3.36)10^{-7}$ m, which is nearly the half.

7.3.1 Pulse excitation

Here, the results for the pulse excited chains are shown. Two chains of disorders 0.2 and 0.1 are investigated regarding the wave velocity, the frequency propagation and attenuation.

7.3.1.1 Sample wave velocity

The dependency of the sample wave velocity of the random modeled scaffold on the disorder is here investigated. For the calculation it is assumed, that the length of the chain of 0.108 m does not change. This assumption is based on the mean value of the particle size. For example, the mean value of the particle radius for the chain using a disorder parameter of 0.2 is $9.99783(10)^{-6}$ m. This leads to a distance of 0.107766 m.

This simple calculation shows that the length of the chain should be back calculated from the particle sizes to get more confident velocity values. In figure 7.13 the wave velocity is shown in dependence of the particle size disorder. The sample wave velocity was

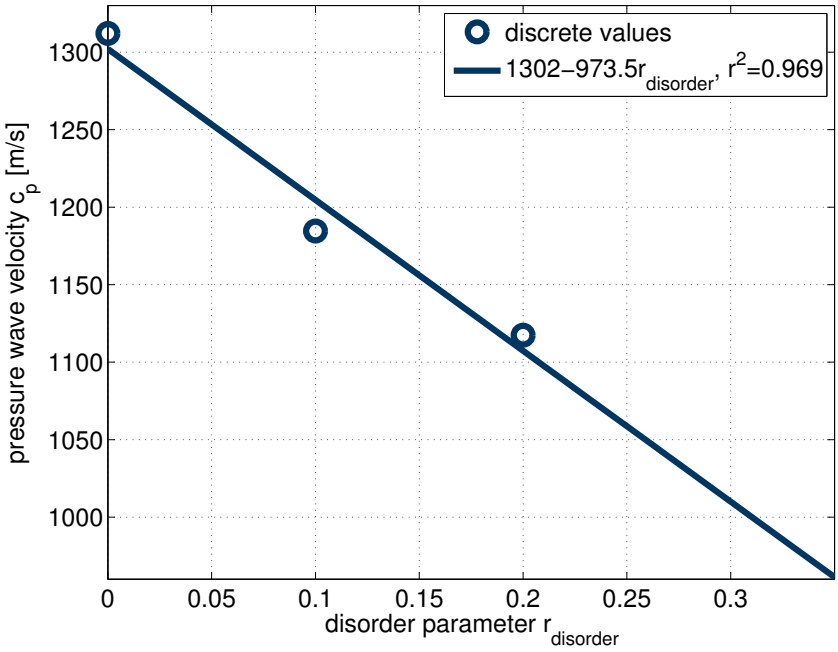

Figure 7.13: Sample wave velocities calculated the experimental way for scaffold chains comparing a non random model with two disordered models with disorder parameters 0.2 and 0.1

calculated the experimental way. A linear relation was found between the wave velocity and the disorder parameter. The higher the variance and the disorder parameter, the smaller the wave velocity. The correlation coefficient r^2 marks a good fit. A possible reason of the high influence of the disorder on the wave velocity could be the 'interfaces' between each particle caused by the disorder of the particle sizes. The high number of different particle radii could act like a 'brake' for the wave velocity.

7.3.1.2 Frequency spectrum

The influence of the disorder on the frequency spectrum is investigated. The time signal of the last particle is cut using the Hanning window, as described in chapter 5. In figure 7.14 the frequency spectra are plotted for the regular scaffold and the two random chains.

The frequency spectrum on the left is shown for a wider range of frequencies than on

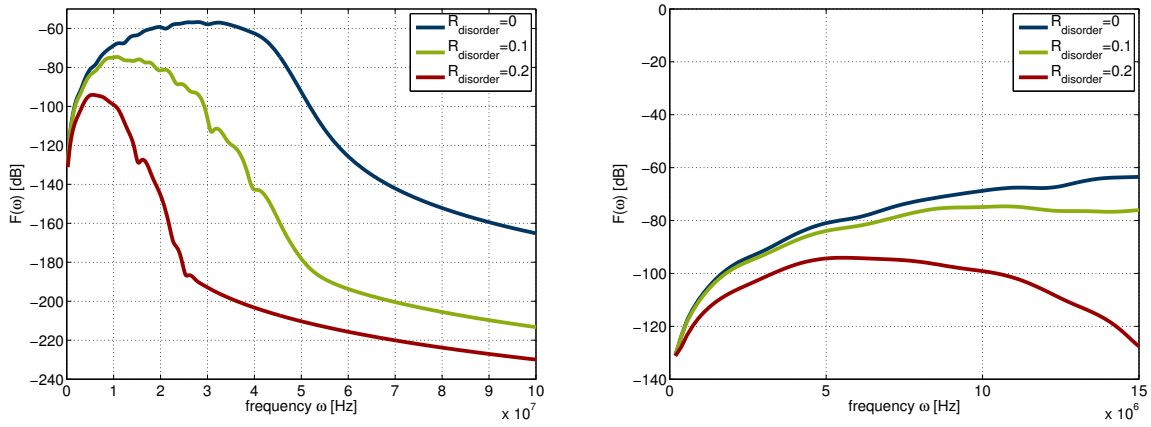

Figure 7.14: Frequency spectra for scaffold chains comparing a non random model with two disordered models with disorder parameters 0.2 and 0.1

the right. Recalling, the place of decay for a frequency spectrum of a regular chain is only determined by the cut off frequencies of the different layers. On the left, it can be seen that the spectra of the disordered chains are cut off earlier. The cut off is as earlier as higher the disorder parameter. Following, the amplitudes are smaller as higher the disorder parameter. The effect of frequency filtering of high frequencies for a one dimensional chain was investigated in [21] before. In the right, the frequency range of interest is shown. There, at the end the spectra of the regular and the disordered chain with the smaller disorder parameter come to a monotonic curve, while the spectrum of the highest disorder parameter is falling off. With the randomization of the particles the filtering of the high frequencies can be controlled independent of the cut off frequency of the particle size. Of course, the maximum possible frequency is still limited only by the cut off frequency. By defining a Fourier-amplitude threshold, maybe a relation between the decay of the spectra and the disorder parameter could be found. However, the filtering of high frequencies was found depending on the disorder.

7.3.1.3 Attenuation

The dependence of the attenuation on the disorder is here investigated. The reference signal for the calculation of the attenuation is obtained by a regular water chain of uniform particle radii. The attenuation values are shown in figure 7.15, depending on the frequency. In the left the frequency range is wider than in the left. For both diagrams the same

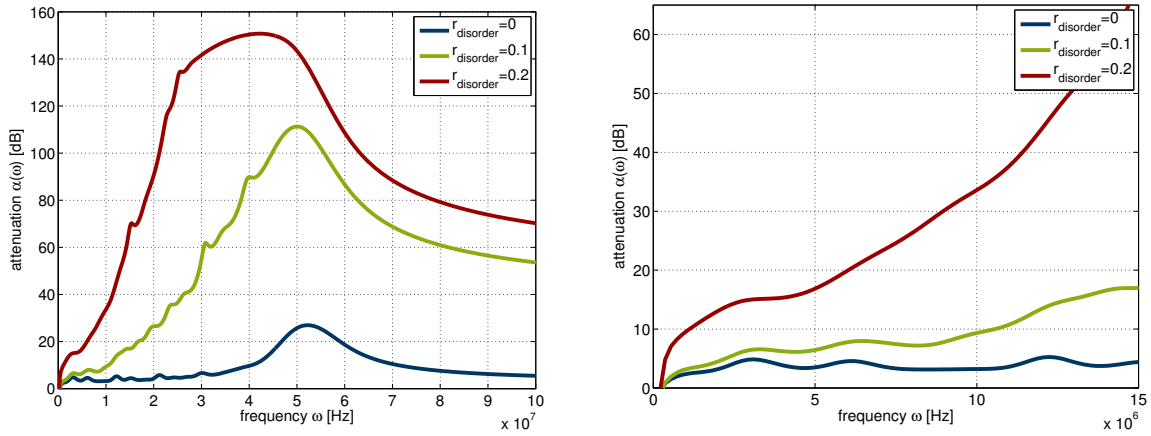

Figure 7.15: Attenuation dependent on the frequency for scaffold chains comparing a non random model with two disordered models with disorder parameters 0.2 and 0.1

observations are made as for the frequency spectra. The higher the disorder parameter, the smaller is the frequency at which the filter out of the frequencies starts. Therefore, some kind of diffraction can be placed in a one dimensional chain by only introducing a distribution of the particle sizes.

7.3.2 Sine excitation

Here, one chain excited by a sine is analyzed. The disorder parameter is 0.2.

7.3.2.1 Sample wave velocity

Here, the sample wave velocity is examined with respect to the number of interfaces and the porosity. The used mean particle radius is 0.01 mm. In table 7.4 the wave velocity

is shown for the sample, calculated the experimental way. The wave velocity decreases

	c_p [m/s] (sample)
Original sample	1310.4
Disordered sample	1279.3

Table 7.4: Wave velocities obtained from the sine excited chains simulating the regular and the disordered scaffold

distinctly with the introduction of the disorder, as seen for the pulse excitation.

7.3.2.2 Frequency spectra

The frequency spectrum of the disordered chain is compared with the non disordered chain and the effect of disorder is investigated. The time signal of the last particle is cut using the Hanning window, as described in chapter 5. The comparison is shown in figure 7.16. In the left a more wider frequency spectrum is shown as in the right. It is found

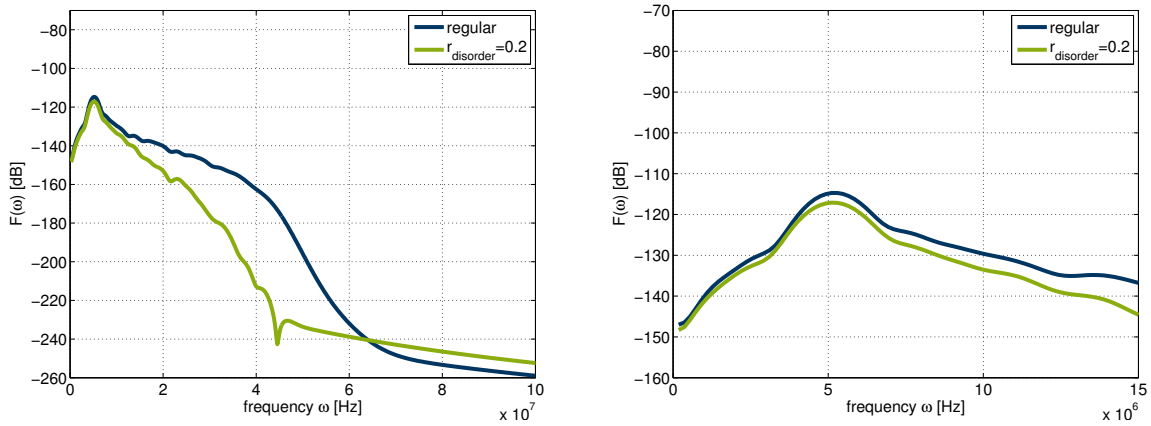

Figure 7.16: Frequency spectra for scaffold chains comparing a non random model with a disordered model of disorder parameter 0.2, two different scales

that the high frequencies are filtered out, as seen in the results of the pulse excitation before. But, looking at the right, the lower frequencies are nearly not affected. The shape in the frequency range smaller than about 12 MHz is nearly the same. The difference is that the amplitudes are just slightly smaller. It can be supposed, that the excitation of a special frequency is not as much affected by the filtering as the excitation without any

special frequency.

7.3.2.3 Attenuation

The attenuation values dependent on the frequencies are shown in figure 7.17. In the left,

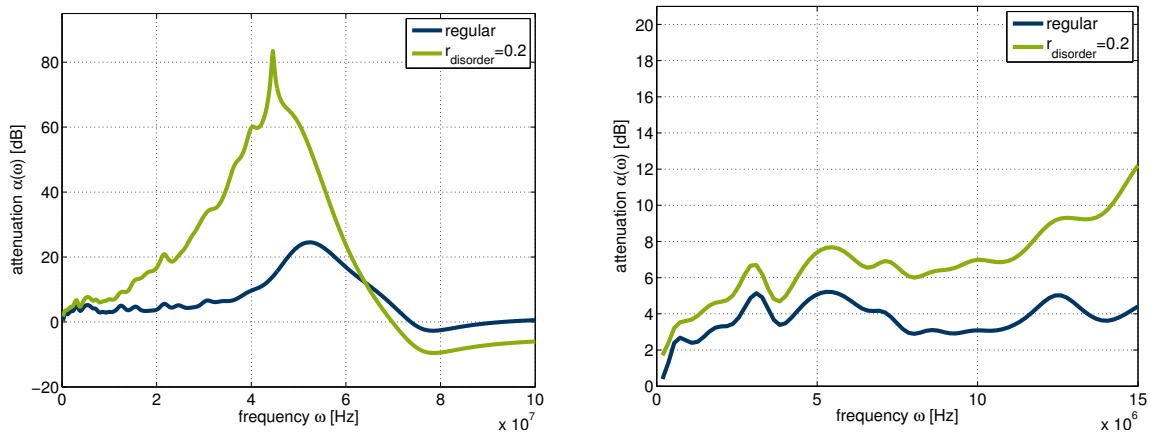

Figure 7.17: Attenuation for scaffold chains comparing a non random model with a disordered model of disorder parameters 0.2, two different scales

a wider range of frequencies is shown. Because the higher frequencies of the disordered chains are filtered out more strongly, the attenuation values are higher than these of the regular chain. The attenuation values are increasing to that point, at which the cut off of the water chain highly damps the amplitudes. In the right, the range of interest is shown. Here, the curves have the same shape and they differ only in the amplitude. Of course, here is seen that the disordered chain is attenuated more.

7.4 Conclusion and summary

In this chapter a regular structured specimen was investigated, as a start. The porous three dimensional media was reduced to a one dimensional model using the assumptions of the stratified model (cf. 2.4). Different number of interfaces in the sample and different porosities are investigated for the regular model. The wave velocity is calculated for the

complete chain and the sample and is found for both excitation methods dependent on the porosity. However, no influence of a different number of interfaces is investigated. Maybe the difference of the wave velocities in the materials is too small to obtain a relation. The influence on the frequency spectrum of the number of interfaces is visible. The higher the number of interfaces, the more and higher frequency peaks occurred. The porosity does not change the shape of the spectrum, but shifted the spectrum to higher amplitudes. Looking at the attenuation spectra, the same statements are valid as claimed for the frequency spectra.

Regarding the particle disordered chains, the wave velocity decreases with increasing disorder. The higher frequencies were filtered out, as described in [21]. The filtering effect is more strongly for an excitation of many frequencies. The frequencies around the excitation frequency of the sine method were not that much effected. Attenuation values for small frequencies for the sine excitation are shifted upwards, but the shape does not change, comparing to a none disordered chain. For the pulse excitation the amplitudes are decreasing and the cut off happens at smaller frequencies, when the disorder is increased.

Chapter 8

Conclusion and Outlook

This last chapter summarizes what has been investigated in this thesis and what is observed during the analysis. For this, the relation between the results of the validation experiments and simulations is of high importance. Upcoming questions are presented. Ideas and proposals for further investigations to find answers to get unsolved problems are stated.

8.1 Summary

In this thesis, simulations and experiments are used to investigate media properties. A one-dimensional particle chain is used to simulate wave propagation and compared with through transmission experiments. The simulation method is explained and how it is calibrated with experimental results. Before that, an analysis of some techniques to obtain the wave velocity and the frequency spectrum is done and the best is chosen for further investigations. Experiments conducted on solid aluminium samples are simulated and the wave characteristics wave velocity, frequency spectrum and attenuation are investigated. The method is additionally applied to a bone like, or porous media, a polymer scaffold.

Randomization is furthermore applied to simulate real bone structure.

8.1.1 Experimental results

With through transmission experiments a solid sample is investigated with respect to the wave velocity, frequency spectrum and attenuation. Wave velocity and attenuation are compared with literature values to validate the experimental setup. The results are further on used as input for the simulations.

8.1.2 Analysis techniques for model investigations

A reference chain of pure water is used to choose the most precise methods to detect the overall wave velocity and the frequency spectrum. The investigated techniques are a threshold method, a peak method, two peak finding algorithms and cross correlation. For both excitation methods the peak method was found as most accurate. To obtain the sample wave velocity, the time difference between a reference and a sample measurement is used, which is found as most precise. The frequency spectrum is obtained by the application of the FFT-algorithm to a time displacement signal of a specific length. It is applied to the full time signal, a time signal cut by a rectangular window and by a Hanning window. It is found, that the cut of the signal is necessary and the use of a Hanning window leads to the smoothest window. The cut is also needful, since the reflections at the boundaries have to be cut off.

8.1.3 Solid sample investigation, experiments and simulations

Two solid samples (aluminium and PMMA) are investigated with through transmission experiments. The model is build with respect to the distance between the transducers,

the sample length and the physical properties of the media water and sample. The experiments with the aluminium sample are modeled here only. For a specific range of particle radii the relative error between the from the simulations back calculated wave velocity and the experimental wave velocity is smaller than 1% for uniform particle radii and sine and pulse excitation. Therefore, a discretization range for the particle radii is found, that leads to reliable wave velocities. Out of the specified range, the wave velocities are influenced by the dispersion relation determined by the particle radii. Regarding the Fourier spectra, no match with the experimental results are found for all case studies. Therefore, no matches in attenuation are found, too. One reason can be found in the different wave excitation. In the experiments the waves are excited with a pulse of a central frequency. In the simulations a pulse of undefined central frequency and a sine excitation are used, that lead to different time-displacement signals. The oscillations created by the interfaces of the sample, the interface effects, are also responsible for the mismatch. The time window is in this thesis chosen arbitrary and could include the two times reflected wave.

8.1.4 Porous and regular scaffold investigation, simulations

A PCL scaffold is modeled with the one-dimensional particle chain, on which the stratified model is applied. This divides the model in layers of water and PCL. The porosity is used to determine the length of each material layer. A solid model is simulated as a comparison for the porous models. The wave velocity of PCL was calculated with the help of elastic parameters. The influence of different number of layers and different porosity are investigated for pulse and sine excited waves.

A linear dependency of the overall and sample wave velocity on the porosity is found. The linear relation can not be further specified, because more simulations are needed. A dependency of the wave velocity on the number of interfaces is not found.

The frequency spectrum is found to be influenced by the porosity. The main effect that

determines the height and the slope of the frequency spectrum is the common cut-off frequency of water and PCL. The higher the porosity, the later the cut off in the frequency spectrum. Regarding the number of interfaces, the frequency spectra are similar in shape, but additional oscillations are found till the spectra are beginning to cut off due to the mixed cut-off frequency. These oscillations are independent on the wave excitation method, but dependent on the number of interfaces. The creation of oscillations can be recognized in the attenuation spectra, too. The attenuation spectra of sine and pulse excited waves have approximately the same shapes of the frequency spectra. Comparing with the theoretical acoustic interface reflection, the obtained attenuation magnitudes are too high.

8.1.5 Porous and disordered scaffold investigation, simulations

The regular porous scaffold model was changed form the regular scaffold model by introducing disorder to mimic a real bone, which is not a regular, but a random, natural grown structure. Here, the particle size was randomized around the mean value using a normal distribution. The disorder parameter is the standard deviation. A linear relation between the wave velocity and the disorder parameter is found for pulse excited waves. For the sine excited waves, a decrease with introducing disorder is found, which is consistent with the results of the sine excited waves. Disorder leads to frequency filtering of the high frequencies. It is found, that the former present oscillations are not visible anymore. Thus, the randomization of the particle sizes has two effects: Frequency filtering and 'weakening' of the interfaces. The attenuation spectra are related to regular water chains. For both excitation attenuation increases with disorder. For small disorder and pulse and sine excitation, the oscillations are again slightly visible. However, they do not dominate the spectra.

8.2 Recommendations

Open questions and suggestions of the previous section are in this section are here answered. This should give some impulses for further work. Regarding the wave velocity, for a specified range the wave velocity is found to be very accurate (relative error smaller than 1%) with comparison to the experimental results. Since no experimental results are available yet for the PCL samples, it would be very interesting to validate the investigations with experimental wave velocities for the solid and the scaffold PCL media.
The difference in the excitation of the waves can be either matched by using a wave generator for the experimental setup, or by using a numerical investigation method, e.g. the discrete element method (DEM). In the DEM, a negative square pulse excitation could be inserted.
For the calculation of the Fourier spectra, it could be investigated how the frequency peaks are created. The oscillations were first found for the model of the experimental setup. For this, the time range could be calculated to be so long, that:

- the two times reflected wave is included in the transformation to the frequency range
- the two times reflected wave is not included in the transformation to the frequency range

This would reveal, if the interface creates the peaks on the propagating wave itself or if the reflections are responsible for the oscillations at peaks related to the wavelength. With a match of the shape of the Fourier spectra, also a better match of the attenuation shape is expected. It has to be further investigated, how the interfaces have to be modeled, because no match to the theoretical interface loss calculation has found yet. For example, the spring stiffness between the material layers can be changed to create softer or harder interfaces. Another possibility is to change the particle radii around the interfaces. The

interface effects can be also studied by the observation of the wavenumber. For example the time can be plotted over the wavenumber to reveal the change. Then, also effects like the peaks in the frequency spectra can hopefully be better understand. Other effects can also be studied dependent on the wavenumber.

In this thesis, simulations based on elastic connected particles are made. However, it can be interesting to change the time displacement signal by the introduction of viscosity. A time signal with a clear start and a clear end is expected. With the time signal the frequency spectrum changes, too. Viscosity would probably change the attenuation, too, because it can be used to simulate absorption of the material. A dependence on the wave velocity is not expected, because the wave velocity is mainly dependent on the elastic properties of the material. Apart from the effects, the introduction of viscosity can not be done in the here presented model, but it can easily done by using the DEM. Before introducing the viscosity to the DEM, the analytic solution could be compared with the numerical DEM, to validate the model.

To include scattering, for example a two dimensional or three dimensional DEM model can be used.

The mass disordered chain could be also use to simulate a solid sample, because it was found that the qualitative shape of the frequency spectrum of the disordered simulation was similar to these of the experimental result (cf. fig. 7.14 and 3.4).

In the last step towards simulation of bone, a real bone experiment can be conducted. The obtained experimental results can then be used to build up a simulation model, specific, the here used one-dimensional chain. The disorder can then be used together with the stratified model to mimic the experiments. Experimental results conducted on a chicken bone are shown in figure 8.1, as an exemplary and outlook. With this figure, this section is closed.

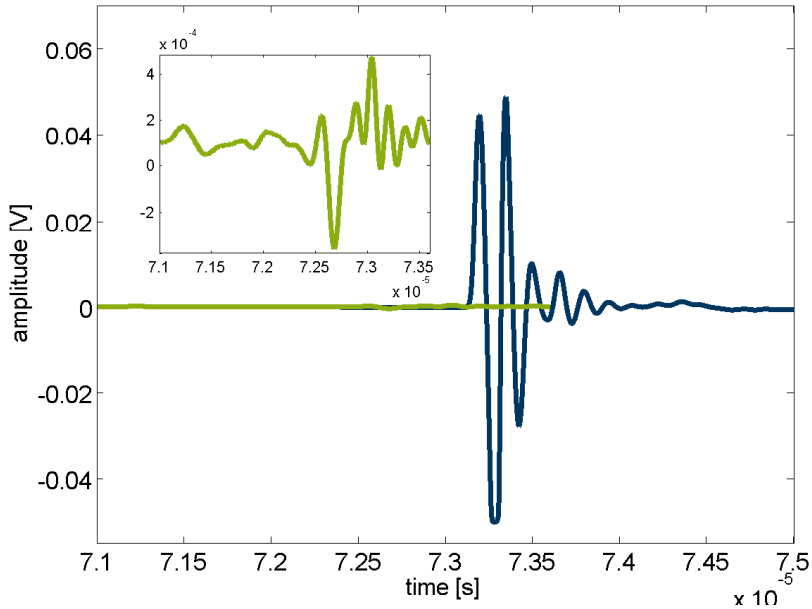

Figure 8.1: Experimental obtained reference (blue) and sample (green) signal, chicken bone, long bone

8.3 Final remarks

This thesis gives an overview of the simulation of wave propagation with a one-dimensional particle chain with comparison to experimental results. The one dimensional chain was found as a very accurate method to simulate wave propagation with respect to the wave velocity. The chain has to be adjusted further on to match frequency spectrum and attenuation spectrum, e.g. the excitation and the interfaces can be changed. As comparison and calibration, experimental results are very useful, because then the simulation results can be validated. From the simulation technique applied to a bone-like structure, differences are found in comparison to a solid sample. The simulations reveal the dependency of the structure and the material properties very clearly. Since easy parameter studies can be made with just a small effort, they are useful to help to develop a better understanding of wave propagation. This can not be as easily done with experiments. Concluding, this thesis showed that the one dimensional chain is useful to reveal influences on the wave propagation using an adjusted particle chain by experiments, but it has be further adjusted so that it is useful for all wave characteristics.

Appendix A

Parameter study regarding porosity and number of interfaces

Another study, independent from the previous presented, is based on the analytical solution of the one dimensional particle. For this, bone properties are used to model a regular structured bone model (cf. e.g. [16]). The investigation target is the number of interfaces with respect to the wave velocity. The wave velocity is plotted over the number of interfaces in figure A.1. A linear relation is found for the dependence of the wave velocity on

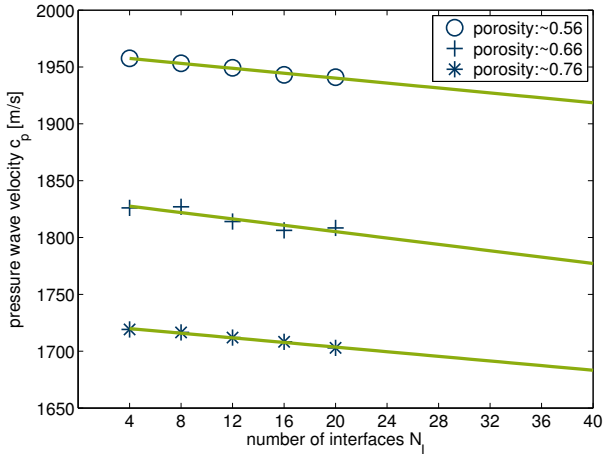

Figure A.1: Wave velocities obtained from simulations modeling bone propagation for a regular structured system

the number of interfaces. The porosity value influences the wave velocity crucially, too.

ï»¿

Bibliography

[1] Saiful Izwan Abd Razak & Noor Fadzliana Ahmad Sharif & Wan Aizan Wan Abdul Rahman [February 2012]. 'Biodegradable Polymers and their Bone Applications: A Review.' *International Journal of Basic & Applied Sciences IJBAS-IJENS*, **12**(1), pp. 31++

[2] [February 2012]. *Phased Array Testing: Basic Theory for Industrial Application*, second edition.

[3] Mace, Brian R. & Manconi, Elisabetta [December 2008]. 'Modelling wave propagation in two-dimensional structures using finite element analysis.' *Journal of Sound and Vibration*, **318**(1), pp. 884–902

[4] Bassi, A. K., J. E. Gough, M. Zakikhani & S. Downes [December 2011]. 'The Chemical and Physical Properties of Poly(ϵ-Caprolactone) Scaffolds Functionalised with Poly(vinyl phosphonic acid-co-acrylic acid).' *Journal of Tissue Engineering*, **2**(1), pp. 2011_615328+.

[5] Bathe, K.-J. [June 1995]. *Finite Element Procedures*. Prentice Hall, first edition. ISBN 0133014584.

[6] Benesty, J., J. Chen & Y. Huang [August 2004]. 'Time-delay estimation via linear interpolation and cross correlation.' *Speech and Audio Processing, IEEE Transactions on*, **12**(5), pp. 509–519.

[7] Bui, T. D. & V. N. Hanh [1990]. 'Automatic mesh generation for finite element analysis.' **44**(4), pp. 305–329.

[8] Cheeke, J. D. N. [April 2002]. *Fundamentals and Applications of Ultrasonic Waves (CRC Series in Pure and Applied Physics)*. CRC Press, first edition. ISBN 0849301300.

[9] Chen, Y.-J. [August 2009]. 'Relationship between Ultrasonic Characteristics and Relative Porosity in Al and Al-XSi Alloys.' *Materials Transactions*, **50**(9), pp. 2308–2313.

[10] Cundall, P. A. & O. D. L. Strack [January 1979]. 'A discrete numerical model for granular assemblies.' *Géotechnique*, **29**(1), pp. 47–65.

[11] Eshraghi, S. & S. Das [July 2010]. 'Mechanical and microstructural properties of polycaprolactone scaffolds with one-dimensional, two-dimensional, and three-dimensional orthogonally oriented porous architectures produced by selective laser sintering.' *Acta Biomaterialia*, **6**(7), pp. 2467–2476.

[12] Grafakos, L. [2009]. *Modern Fourier Analysis*, volume 250. Springer New York, New York, NY. ISBN 978-0-387-09433-5.

[13] Haire, T. J. & C. M. Langton [April 1999]. 'Biot Theory: A Review of Its Application to Ultrasound Propagation Through Cancellous Bone.' *The BoneJournal*, **24**(4), pp. 291–295.

[14] Ham, S. & K.-J. Bathe [March 2012]. 'A finite element method enriched for wave propagation problems.' *Computers & Structures*, **94-95**, pp. 1–12.

[15] Hamed, E., Y. Lee & I. Jasiuk [May 2010]. 'Multiscale modeling of elastic properties of cortical bone.' *Acta Mechanica*.

[16] Hughes, E. R., T. G. Leighton, G. W. Petley & P. R. White [June 1999]. 'Ultrasonic propagation in cancellous bone: a new stratified model.' *Ultrasound in medicine & biology*, **25**(5), pp. 811–821.

[17] Hughes, E. R., T. G. Leighton, G. W. Petley, P. R. White & R. C. Chivers [July 2003]. 'Estimation of critical and viscous frequencies for Biot theory in cancellous bone.' *Ultrasonics*, **41**(5), pp. 365–368.

[18] Kaczmarek, M., J. Kubik & M. Pakula [May 2002]. 'Short ultrasonic waves in cancellous bone.' *Ultrasonics*, **40**(1-8), pp. 95–100.

[19] Knuth, M., H. Tobin & C. Marone [2013]. 'Evolution of ultrasonic velocity and dynamic elastic moduli with shear strain in granular layers.' **15**(5), pp. 499–515.

[20] Laugier, P. & G. Haïat, editors [2011]. *Bone Quantitative Ultrasound*. Springer Netherlands, Dordrecht. ISBN 978-94-007-0016-1.

[21] Lawney, B. P. & S. Luding [2014]. 'Mass-disorder effects on the frequency filtering in one-dimensional discrete particle systems.' *Acta Mechanica*, **to be published**.

[22] Le, K. C. [September 2011]. *Energy Methods in Dynamics (Interaction of Mechanics and Mathematics)*. Springer, 2012th edition. ISBN 3642224032.

[23] Lee, K. I., V. F. Humphrey, T. G. Leighton & S. W. Yoon [November 2007]. 'Predictions of the modified Biot-Attenborough model for the dependence of phase velocity on porosity in cancellous bone.' *Ultrasonics*, **46**(4), pp. 323–330.

[24] Leighton, T. [January 2007]. 'What is ultrasound?' *Progress in Biophysics and Molecular Biology*, **93**(1-3), pp. 3–83.

[25] Leighton, T. G. [1998]. 'Fundamentals of underwater acoustics and ultrasound.' *Noise and Vibration*, pp. 373–444.

[26] Luding, S. [2008]. 'Cohesive, frictional powders: contact models for tension.' *Granular Matter*, **10**, pp. 235–246. 10.1007/s10035-008-0099-x.

[27] Madeo, A. & S. Gavrilyuk [September 2010]. 'Propagation of acoustic waves in porous media and their reflection and transmission at a pure-fluid/porous-medium permeable interface.' *European Journal of Mechanics - A/Solids*, **29**(5), pp. 897–910.

[28] Musielak, Z., D. Musielak & H. Mobashi [March 2006]. 'Method to determine cutoff frequencies for acoustic waves propagating in nonisothermal media.' *Physical Review E*, **73**(3).

[29] Njeh, C. F., C. M. Boivin & C. M. Langton [1997]. 'The role of ultrasound in the assessment of osteoporosis: a review.' *Osteoporosis international : a journal established as result of cooperation between the European Foundation for Osteoporosis and the National Osteoporosis Foundation of the USA*, **7**(1), pp. 7–22.

[30] Ogi, H., T. Hamaguchi & M. Hirao [2000]. 'Ultrasonic attenuation peak in steel and aluminum alloy during rotating bending fatigue.' **31**(4), pp. 1121–1128.

[31] Padilla, F. & P. Laugier [October 2000]. 'Phase and group velocities of fast and slow compressional waves in trabecular bone.' *The Journal of the Acoustical Society of America*, **108**(4), pp. 1949–1952.

[32] Qin, Y.-X., Y. Xia, W. Lin, E. Mittra, C. Rubin & B. Gruber [2007]. 'Non-invasive Ultrasound Imaging for Bone Quality Assessment Using Scanning Confocal Acoustic Diagnosis, $\hat{\text{I}}\frac{1}{4}$CT, DXA Measurements, and Mechanical Testing.' In *Medical Biometrics*, edited by D. Zhang, volume 4901 of *Lecture Notes in Computer Science*, pp. 216–223. Springer Berlin Heidelberg.

[33] Rezgui, F., M. Swistek, J. M. Hiver, C. G'Sell & T. Sadoun [August 2005]. 'Deformation and damage upon stretching of degradable polymers (PLA and PCL).' *Polymer*, **46**(18), pp. 7370–7385.

[34] Rho, J.-Y., L. Kuhn-Spearing & P. Zioupos [March 1988]. 'Mechanical properties and the hierarchical structure of bone.' *Medical Engineering & Physics*, **20**(2), pp. 92–102.

[35] Richards, A. M., N. W. Coleman, T. A. Knight, S. M. Belkoff & S. C. Mears [2010]. 'Bone Density and Cortical Thickness in Normal, Osteopenic, and Osteoporotic Sacra.' *Journal of Osteoporosis*, **2010**, pp. 1–5.

[36] Steeb, H. [2010]. 'Ultrasound propagation in cancellous bone.' *Archive of Applied Mechanics*, **80**(5), pp. 489–502.

[37] Strelitzki, R. & J. A. Evans [May 1998]. 'Diffraction and interface losses in broadband ultrasound attenuation measurements of the calcaneum.' *Physiological measurement*, **19**(2), pp. 197–204.

[38] Tamim, N. S. M. & F. Ghani [April 2010]. 'Techniques for Optimization in Time Delay Estimation from Cross Correlation Function.' *International Journal of Engineering & Technology*, **10**(2).

[39] Umchid, S. [2008]. 'Frequency dependent ultrasonic attenuation coefficient measurement.' In *The 3rd International Symposium on Biomedical Engineering (ISBME)*, pp. 234–238.

[40] Vazquez, M., L. Leija, A. Vera, A. Ramos & E. Moreno [2005]. 'Experimental estimation of acoustic attenuation and dispersion.' In *Electrical and Electronics Engineering, 2005 2nd International Conference on*, pp. 156–159. IEEE. ISBN 0-7803-9230-2.

[41] Wang, X. & Q. Ni [March 2003]. 'Determination of cortical bone porosity and pore size distribution using a low field pulsed NMR approach.' *Journal of Orthopaedic Research*, **21**(2), pp. 312–319.

[42] Xia, W., D. Piras, M. Heijblom, W. Steenbergen, T. G. van Leeuwen & S. Manohar [July 2011]. 'Poly(vinyl alcohol) gels as photoacoustic breast phantoms revisited.' *Journal of biomedical optics*, **16**(7).

[43] Zhang, C., L. H. Le, R. Zheng, D. Ta & E. Lou [2011]. 'Measurements of ultrasonic phase velocities and attenuation of slow waves in cellular aluminum foams as cancellous bone-mimicking phantoms.' *The Journal of the Acoustical Society of America*, **129**(5), pp. 3317+.

[44] Zioupos, P., R. B. Cook & J. R. Hutchinson [January 2008]. 'Some basic relationships between density values in cancellous and cortical bone.' *Journal of Biomechanics*, **41**(9), pp. 1961–1968.